DESIGN OF ALL-OPTICAL ADDER/SUBTRACTOR CIRCUITS BASED ON MICRORING RESONATORS

SAYSAMONE SOYSOUVANH

A THESIS SUBMITTED IN PARTIAL FULFILLMENT
OF THE REQUIREMENT FOR THE DEGREE OF
DOCTOR OF ENGINEERING IN ELECTRICAL ENGINEERING
FACULTY OF ENGINEERING
KING MONGKUT'S INSTITUTE OF TECHNOLOGY LADKRABANG
2020

KMITL-2020-EN-D-018-020

DESIGN OF ALL-OPTICAL ADDER/SUBTRACTOR CIRCUITS BASED ON MICRORING RESONATORS

SAYSAMONE SOYSOUVANH

A THESIS SUBMITTED IN PARTIAL FULFILLMENT
OF THE REQUIREMENT FOR THE DEGREE OF
DOCTOR OF ENGINEERING IN ELECTRICAL ENGINEERING
FACULTY OF ENGINEERING
KING MONGKUT'S INSTITUTE OF TECHNOLOGY LADKRABANG
2020

KMITL-2020-EN-D-018-020

Thesis Title	Design of All-optical Adder/Subtractor Circuits based on Microring Resonators
Student	Mr. Saysamone Soysouvanh
Student ID.	56601359
Degree	Doctor of Engineering
Program	Electrical Engineering
Year	2020
Thesis Advisor	Assoc. Prof. Dr. Somsak Mitatha

ABSTRACT

This thesis proposes the designed circuits of all-optical full adder/subtractor, optical logic AND gate, OR gate, and optical multiplexers based on optical switching within nonlinear microring resonators. The switching scheme caused by nonlinear effects in the medium such as cross-phase modulation (XPM) and carrier injection pumping to induce the change of the refractive index of the material, which causes the MRRs resonant wavelength shifted. Therefore, optical switching performed and applied to the design circuit of all-optical 1-bit arithmetic and logic unit (ALU). In this method, the advantage of the system, such as power stability, non-dispersion, and the dark-bright soliton phase conversion control, can be obtained. The input source into the circuit is the bright soliton pulse, with the pulse width of 35 ps, the peak power at 1.55 μm is 1 mW.

The simulation result using MATLAB shows the output signal with a minimum loss of only 0.1% for a low input power of 1 mW and an ultra-fast response time of approximately 1 ps. It gives the ultra-high bandwidth of more than 40 $Gbits^{-1}$. The circuit composes of 14 microring resonators made of InGaAsP/InP material with smaller ring radii of 1.5 μm, and the total physical scale of the circuit less than 100 μm^2. The designed circuits are compact, simple, and flexible, which is suitable for more development in terms of substituting the electronic circuitry in the future.

กิตติกรรมประกาศ

คุณความดีอันใดที่เกิดจากดุษฎีนิพนธ์ฉบับนี้ข้าพเจ้าขอมอบแด่ผู้มีอุปการะและผู้ทรงคุณทุกๆ ท่านที่มีส่วนช่วยเหลือในการงานต่างๆ จนดุษฎีนิพนธ์สำเร็จลุล่วงไปด้วยดี

ขอขอบคุณเจ้าหน้าที่บัณฑิตศึกษาคณะวิศวกรรมศาสตร์และเจ้าหน้าที่ส่วนงานอื่นๆ ของสถาบันเทคโนโลยีพระจอมเกล้าเจ้าคุณทหารลาดกระบังทุกๆ ท่าน ที่ช่วยเหลือติดต่อประสานงานและงานด้านเอกสารต่างๆ เสมอมา

ขอขอบคุณพี่ๆ ศิษย์เก่าห้องวิจัย Hybrid Computing Research Laboratory (ECC 607/1) ทุกๆ ท่านที่เป็นกันเองคอยห่วงใยเอาใจใส่ ให้กำลังใจ ช่วยเหลือ ให้คำแนะนำทั้งด้านวิชาการและการใช้ชีวิตในไทยเสมอมา

ขอขอบพระคุณกรรมการสอบดุษฎีนิพนธ์ทุกๆ ท่านที่เมตตา กรุณา ติติง ให้คำแนะนำในการปรับปรุงแก้ไขงานวิจัยและดุษฎีนิพนธ์จนกระทั่งเสร็จสิ้นสมบูรณ์ลุล่วงไปด้วยดี

ขอขอบพระคุณอาจารย์ที่ปรึกษาร่วม Prof. Noriyuki Komine และคณาจารย์ชาวญี่ปุ่นที่ Tokai University ที่ดูแลอนุเคราะห์ข้าพเจ้าเสมอมาทั้งในตอนพำนักวิจัยแลกเปลี่ยนอยู่ที่ประเทศญี่ปุ่นและอยู่ในไทย

ขอขอบคุณทุน AUN/SEED-Net ที่ให้ทุนสนับสนุนการศึกษาระดับดุษฎีบัณฑิตของข้าพเจ้าตลอดหลักสูตรด้วยดีเสมอมา ขอขอบคุณเจ้าหน้าที่ประสานงานของทุน AUN/SEED-Net ทุกๆ ท่าน

ขอขอบพระคุณ รศ.ดร.จงกล งามวิทย์ และ รศ.ดร. ปรีชา ยุพาพิน และคณาจารย์ท่านอื่นๆ ที่เมตตา กรุณา ช่วยเหลือ และอนุเคราะห์ข้าพเจ้าจนดุษฎีนิพนธ์สำเร็จลุล่วงดังข้าพเจ้าปราถนาตั้งใจ

ดุษฎีนิพนธ์ครั้งนี้จะสำเร็จลุล่วงไปมิได้ หากปราศจากความช่วยเหลือ อนุเคราะห์ อบรมสั่งสอน ชี้แนะแนวทางจาก รศ. ดร. สมศักดิ์ มิตะถา อาจารย์ที่ปรึกษาดุษฎีนิพนธ์ ข้าพเจ้าขอสำนึกในพระคุณและขอกราบขอบพระคุณมา ณ โอกาสนี้

สุดท้ายขอขอบพระคุณบิดา มารดา และน้องชาย ที่คอยส่งเสริม สนับสนุนการศึกษาในครั้งนี้ของข้าพเจ้าเสมอมา

สายสมร สร้อยสุวรรณ

TABLE OF CONTENTS

CONTENTS (Cont.)

CONTENTS (Cont.)

LIST OF FIGURES

LIST OF FIGURES (Cont.)

LIST OF FIGURES (Cont.)

LIST OF TABLES

Chapter 1
INTRODUCTION

This chapter presents the history and significance of the problem, objectives, and goals of the research, scope, and structure of the thesis as the following details.

1.1 Motivation

Nowadays, fiber-optic technology has been developed and widely used in the field of communication and measurement equipment due to the effectiveness of ultra-high data transmission bandwidth. The demand for bandwidth in data processing and communication is still dramatically increasing. As a result, the development of electronic technologies for data processing has been continuously improved, such as reducing the size of the device so that it can increase the number of parts; thus, the electrons can reduce the distance and travel time, and the system efficiency increases. Among the development of electronic technologies to enhance the efficiency of electronic signal processing from past to present is likely to encounter the limit of bandwidth and processing speed [1], [2]. Therefore, photonic technologies have been applied.

Since the photon is the particle that has no mass, it can perform at higher speeds than that electron does (where the mass of an electron is $9.10938291 \times 10^{-31}$ kg). In terms of computation and communication, the electron can control easier than a photon. Therefore, new disciplines have developed to utilize photonics or light, and this brings to a high-speed data transmission rate where specific devices are used to convert from electrical signals to optical signals (electrical-to-optical converter: EOC) or reconvert from optical signals to electrical signals (optical-to-electrical converter: OEC). However, two of the most critical issues in converting the signals for high-speed data processors are the power consumption and the delay of the EOC/OEC devices [3], [4]. All-optical technologies have proposed to solve the problem [5], [6], and increase efficiency.

In all-optical signal processing, it is the same as electronic. It can produce a bit of information and can verify the data as well as can send bits of information from one place to another. It can also use to obtain data in logical and arithmetic forms [7]–[11]. In general, photonic circuit design is still costly and limited in use because of its limitations in terms of connectivity, device size, design, and fabrication. The photonic circuit can be made more inexpensive and more efficient, it is important to keep researching in the photonic field, especially in optical data processing, logical operation, and computation.

Therefore, in this thesis, the photonic circuit is designed for performing the logical and arithmetical operators based on the nonlinear effect within the microring resonator system. All operations can be controlled by a nonlinear pulse applying for switching the optical logic signal with high flexibility in design, compact in scale, simple in fabrication, and can be used extensively [12]–[14]. By the effect of increasingly researching development in photonic technology and many advantages of nonlinear ring resonator [4] will lead to all-optically computation, as well as quantum computing that can perform at even more ultra-fast speed data transmission soon.

1.2 Goal of the Thesis

- To study the characteristics of the microring resonator.
- To study the nonlinear phenomena in the microring.
- To derive the mathematical model of nonlinear ring resonator as the transfer function and to understand the ring resonator characteristic.
- To study the applications of nonlinear ring resonator for optical logic and arithmetic operations.
- To design the photonic circuits based on a nonlinear ring resonator system for performing all-optical logic and arithmetic operations using for all-optical ALU.
- To analysis the efficiency and effect of parameters in a nonlinear ring resonator.
- To publish the researches on all-optical data processing, so that inspires the awareness of the development in all-optical logic and arithmetic devices.

1.3 Concept used in the Research

Changing properties in linear optical semiconductor material will not depend on the intensity of the light. In contrast, nonlinear optical semiconductor materials will be able to change its properties from changing the intensity of light that travels through it. The intensity of light will cause various property changes such as refractive index, transparency, light absorption, etc., in which the evolution of some properties using the intensity of light can be used to perform as an optical processing device. Microring resonator is one of the most popular devices for optical applications, as the ring resonator has many advantages compared to other devices such as durability, small scale, high efficiency, uncomplicated design, and high flexibility. Besides, the price and the size of the ring resonator are reducing continuously [15]. From such advantages of the microring resonator, it is appropriate to apply in various optical applications.

Nonlinear light pulses or solitons are other types of waves that can be found naturally, such as the Tsunami. The advantage is that soliton can maintain the shape of its waveform when a pulse travels in the long distance at high speed. Light is a type

of transverse wave that can transform as a soliton (solitary wave). Also, the soliton wave can generate in wavelengths with a minimum loss length between (1.3 to 1.6) micrometers. When applying optical soliton into optical data signals processing and communication, it allows the overall efficiency of the system to be increased.

Optical tree architecture [16] is one of the structures integrating with high-speed photonic circuits in optical data processing and computing systems. Optical tree architecture and nonlinear materials play an important role in optical data signals processing with the ability to be controlled the entire system with light. Therefore, it is one of the alternatives that has designed and applied to process optical data such as in a logical-integrated circuit [17], arithmetic circuit [7], and other operations.

Therefore, this research relies on the changing properties in nonlinear material, the effectiveness of nonlinear light pulses and nonlinear ring resonator, and the flexible design of optical tree architecture scheme, the design of all-optically switching, multiplexing, and arithmetic operation such as full-adder/full-subtractor using for all-optical further ALU design are proposed.

1.4 Scope of Research

This thesis focuses on the study of theory and principles of nonlinear microring resonator devices in terms of logical processing and optical computation in order to design and propose photonic circuits using the nonlinear ring resonator such as all-optical switching, multiplexing and all-optical full-adder/full-subtractor operations which are the necessary components in all-optical ALU design. The simulation result of mathematical models of the systems is obtained by using MATLAB.

1.5 Expectation

To understand the ring resonator characteristics and to realize the mathematical models of nonlinear ring resonator circuits as the transfer functions (transmission equations) and to design the ultra-high-speed photonic circuit using the nonlinear ring resonator for logic and arithmetic operations which the optical logic "0" and logic "1" are performed by the nonlinear optical dark and bright soliton pulses. The design system is suitable to be applied in more advanced techniques as well as to inspire the research and development of optical signal processing consistently.

1.6 Structure of the Thesis

Chapter 1: This chapter describes the history and importance of problems, basic principles, and the structure of the thesis.

Chapter 2: This chapter explains the properties of light, a ring resonator, and optical semiconductor properties, which is necessary for the system design.

Chapter 3: This chapter describes the reported relating researches, research method, principle, and the concept for designing optical arithmetic and logic operators.

Chapter 4: This chapter describes the principles, concepts of proposed methods as well as the simulation results of the system.

Chapter 5: This chapter is a summary of research results, discussion, and future research guidelines

Chapter 2
THEORETICAL BACKGROUND

This section discusses the essential theories and fundamentals of light as a basis for studying and understanding light for further research, starting with the nature of light, the optical phenomena occurring in both linear and nonlinear media, optical soliton, nonlinear ring resonator and the reaction of radiation with the material.

2.1 Electromagnetic Spectrum

The electromagnetic spectrum is the collective term for all possible frequencies of electromagnetic radiation, where the polarization characterizes the medium, and it is a function of the electrical field in the case of weak nonlinear behavior of the medium. Light is an electromagnetic wave. By the nature of light, it can determine in two ways, in the form of photons or waves, where the motion of light (c) moves at a speed of about 300,000 km/s, or 180,000 mi/s. In each of the electromagnetic spectrum, the wave has different properties such as wavelength, photon energy, and frequency of electromagnetic vibration, as shown in Figure 2.1.

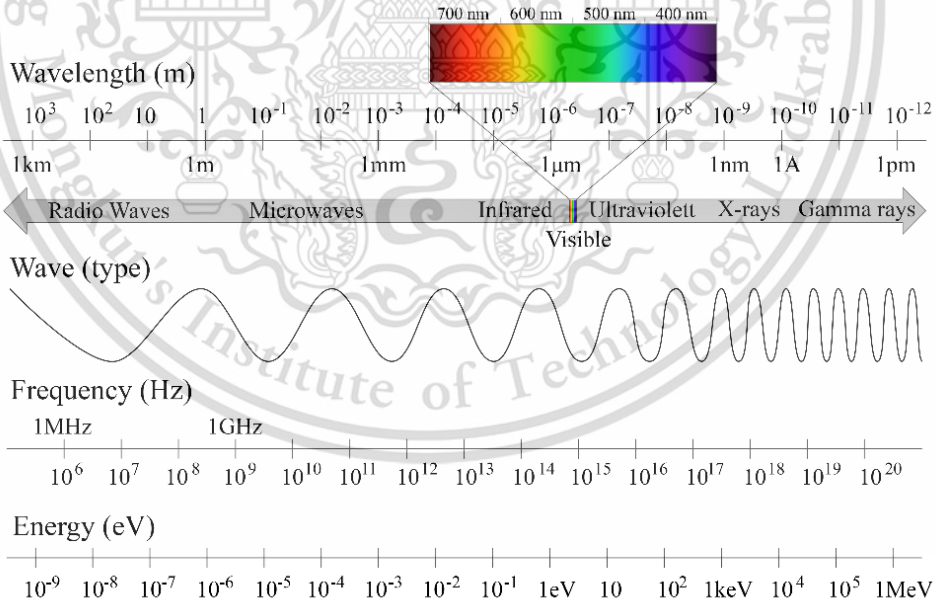

Figure 2.1 The electromagnetic spectrum

In each of the electromagnetic spectrum, as shown in Figure 2.1, Hertz (Hz) is the most used to measure frequency. The wavelength measure in meter (m). The equation used to calculate wavelength and frequency is derived from (2.1).

$$\lambda = \frac{c}{f} \tag{2.1}$$

Where λ is the wavelength (m), f is the frequency (cycles per times or Hz), and c is the speed of light in a vacuum (299,792,458 m/s $\approx 3\times10^8$ m/s). Moreover, the photon energy is given by (2.2).

$$Energy\,(eV) = hf \tag{2.2}$$

Where h is the Plank's constant (6.63×10^{-34} J s or 4.14×10^{-15} eV s).

2.1.1 Electromagnetic Radiation

Traditionally, an electromagnetic wave comprises the synchronized oscillations of electrical and magnetic fields that propagate at the speed of daylight through a vacuum (approximately 3×10^8 m/s).

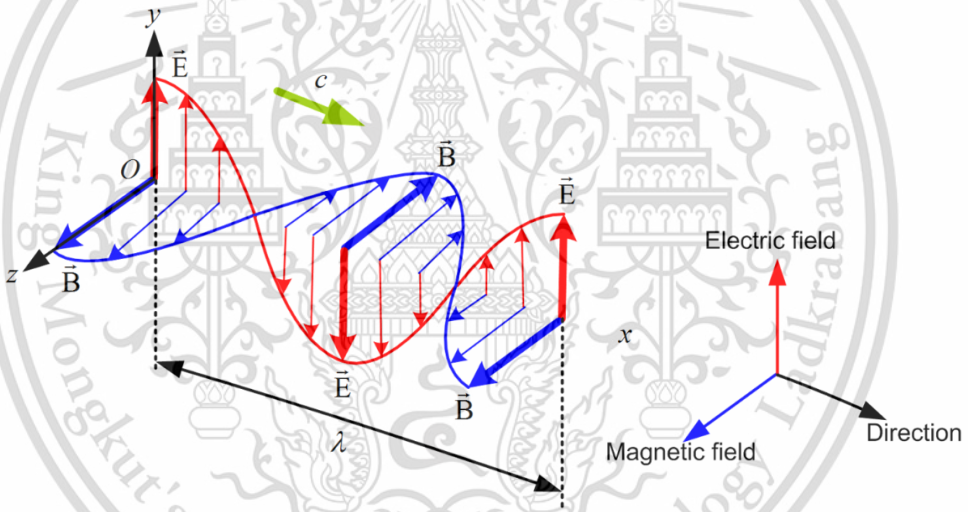

Figure 2.2 Electromagnetic wave radiation

Maxwell's equations can express the radiation of electromagnetic radiation as in (2.3) – (2.6), which is a series of partial differential equations explaining how charges and currents induce electric fields and magnetic fields [18].

Gauss's law for electric: $$\oint_s \vec{E}d\vec{A} = \frac{Q}{\varepsilon_0} \tag{2.3}$$

Gauss's law for magnetism: $$\oint_s \vec{E}d\vec{A} = 0 \tag{2.4}$$

Faraday's law: $$\oint \vec{E}d\vec{s} = -\frac{d\varphi_B}{dt} \tag{2.5}$$

Ampere's law with Maxwell's addition: $$\oint \vec{B}d\vec{s} = \mu_0 I + \mu_0\varepsilon_0\frac{d\varphi_E}{dt} \tag{2.6}$$

2.2 Properties of Lightwave and total Internal Reflection

Light is an electromagnetic wave, which is due to the movement of the photon particles into every wavelength of light. The basic properties of light waves described as follows.

In the medium with the same refractive index (n), light travels in a straight line. The refractive index is the ratio at which the speed of light decreases in that material (compared to the speed of light in the vacuum). The refractive index of the material can obtain from $n=c/v$, where n is the refractive index of the material, c is the speed of light in vacuum, and v is the speed of light in the material. Therefore, the shorter wavelength (blue light) has a higher index of refraction, casing more reduction in speed. The refractive index is generally more than one. If the material has high dense, light travels more slowly.

Table 2.1 Some examples of refractive indices of common materials

Material	Refractive index
Vacuum	1
Air	1.000293
Air (at standard atmosphere)	1.000277
Water	1.333
Diamond	2.419
Indium phosphide (InP)	3.21
Gallium arsenide (GaAs)	3.35
Silicon (Si)	3.48
Indium gallium arsenide phosphide (InGaAsP)	3.51
Aluminum gallium arsenide (AlGaAs)	3.6

**Note: The refractive index of each material might vary depending on many factors such as temperature, wavelength, density, ingredient ratio, the process of mixing, etc.

The refraction of light follows the Snell's law as in (2.7), when light passing through the two distinct material with different refractive indexes when the light hits the object, the reflection will follow the law of reflection of light that "The angle of incidence is always equal to the angle of reflection."

$$\frac{sin\theta_1}{sin\theta_2} = \frac{n_2}{n_1} \tag{2.7}$$

Here θ_1 is the angle of incidence, and θ_2 is the angle of refraction where n_1 and n_2 are refractive indexes of first and second mediums, respectively.

The reflection of light can be divided into two characteristics such as regular reflection which occurs when the light hits a shiny surface object (mirror-like), and diffuse reflection which occurs when the light hits a rough surface object (retaining the energy, but losing the image), depending on the nature of the interface.

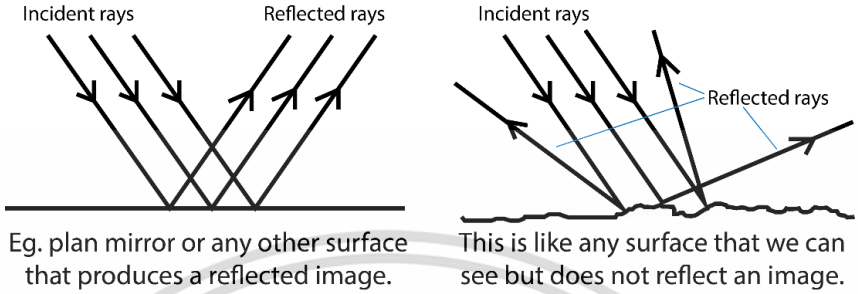

Figure 2.3 Regular reflection and diffuse reflection

Total internal refraction is a phenomenon happening once a propagating wave strikes a medium boundary at a greater angle than the critical angle (θ_c) respected to the normal line of the surface. If the index of refraction is lower than the opposite aspect of the boundary, and the angle of incidence (θ_1) is larger than the critical angle, the lightwave, therefore, cannot pass through and is totally reflected as shown in Figure 2.4. Hence, the light wave can travel along with the medium, and optical data can be transmitted. Underneath this case, the angle of incidence referred to as the critical angle (θ_c) is given by (2.8). Once the angle of incidence is larger than the critical angle, the ray originating in medium one is completely reflected in the same medium. This phenomenon is termed total internal reflection. The optical fiber uses this principle of total internal reflection to guide the light wave, and the mirage on a hot summer day is a phenomenon caused by the same principle [19].

$$sin\theta_c = \frac{n_2}{n_1} \tag{2.8}$$

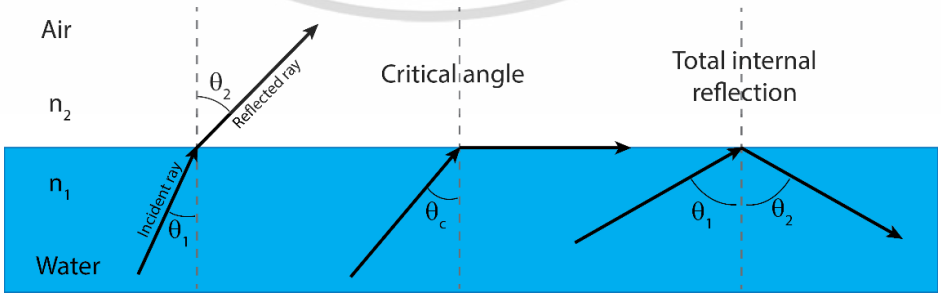

Figure 2.4 Critical angle and total internal reflection of light

Here θ_1 is the incident angle, θ_2 is the refracted angle, and θ_c is the critical angle. n_1 is the incident index, and n_2 is the refractive index of the second medium.

2.3 Loss in Optical Fiber

The steady reduction or loss of signal power in an optical fiber mainly a result of absorption and dispersion. Attenuation is wavelength-dependent and can be converted to decibels per kilometer (dB/km). A combination of material absorption, Rayleigh scattering, Mie scattering, and connecting losses induces fiber attenuation, which includes the use of amplification systems.

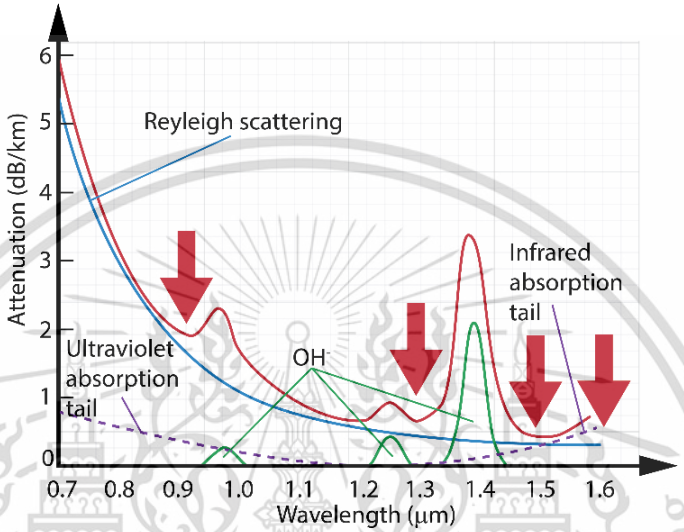

Figure 2.5 Losses occurring in optical fiber.

Figure 2.5 shows the losses in fiber such as Rayleigh scattering (gives the atmosphere its blue color), with different wavelength, and the most widely used center wavelength for communication is 900 nm, 1300 nm, 1500 nm, and 1600 nm due to these wavelength bands caused the weakest of the attenuation losses. The other common wavelengths used are O-band (1260 to 1360) nm, E-band (1360 to 1460) nm, S-band (1460 to 1530) nm, C-band (1530 to 1565) nm, L-band (1565 to 1625) nm, U-band (1625 to 1675) nm, etc.

2.4 Nonlinear Optics

Nonlinear optics is about the phenomenon that occurs in the optical conductor. The nonlinear optic has been studied since 1961 when Ruby Laser is used to creating the second harmonic in the crystal [20]. After that, in 1970, the development of optical fiber generated from nonlinear medium until the loss value was reduced to less than 20 dB/km [21]. Therefore, the nonlinear optical fiber was introduced. In 1972 [22], [23], there were studies of stimulated Raman and Brillouin scatterings in single-mode optical fiber, which was affected by the nonlinear properties caused by energy accumulation when light travels in various devices, and later, other nonlinear phenomena such as Cross-Phase Modulation (XPM), Self-Phase Modulation

(SPM), Four-Wave Mixing (FWM) [24], etc. The research on nonlinear phenomena has been studied and researched continuously until 1989; there have been written advanced nonlinear fiber-optic books [25]. Until in the 1990s, the study of the research and development of lightwave technology has continued to grow rapidly and continuously as never before.

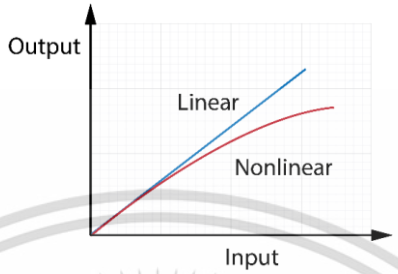

Figure 2.6 Linear and nonlinear actions

A variety of nonlinear phenomena arising from the Kerr effect phenomenon [26], such as Nonlinear Phase Shift, Cross-Phase Modulation, Self-Phase Modulation, Optical Bistability, Optical Bifurcation, Optical Soliton, etc. There are also other phenomena that occur due to the third order susceptibility of the medium (χ^3), such as two-photon absorption, four-wave mixing generation, optical phase conjugation [27], in which only some aspects will be explained and studied in this thesis.

2.4.1 Nonlinear Effects

The significant light phenomena that when light pulses travel on a nonlinear medium are able to group vital nonlinear phenomena as follows [15], [28]–[30].

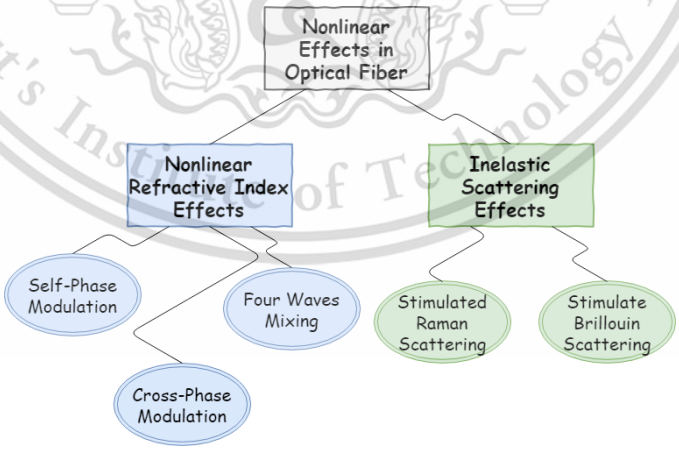

Figure 2.7 Nonlinear phenomena in optical fiber

The first group is the phenomenon that occurs without the energy exchange between the medium and the electric field.

2.4.2 Nonlinear Refraction

The result of the third-order nonlinear susceptibility (χ^3) is the optical Kerr effect or nonlinear refraction. It is a nonlinear optical phenomenon that occurs in crystals and glasses as intense light propagates, as well as other media such as gases. This phenomenon is the effect of a nonlinear response that occurs instantly and can describe as modifying the refractive index. Especially the refractive index of the high-intensity light beam itself is adjusted according to (2.9). The intensity-dependent refractive index for a nonlinear material is given by

$$n=n_0+n_2I=n_0+\frac{n_2P}{A_{eff}} \tag{2.9}$$

Where n_0 is linear index of refraction, n_2 is nonlinear refractive index, P is the optical power, I is the optical intensity, and A_{eff} is the effective mode core area of the system device, for micro/nanometer ring resonators, the value of A_{eff} is in the range of 0.1 μm^2 to 0.5 μm^2 [15], for silica $n_2=3\times10^{-16}$ cm^2/W [28], where the relationship between nonlinearity and the third-order susceptibility value is determined by (2.10).

$$n_2=\frac{3}{8nc\varepsilon_0}\chi^3 \tag{2.10}$$

Optical Kerr nonlinearity is a phenomenon that occurs from a third-order susceptibility (χ^3) without the energy exchange between the electric field and the medium. Kerr phenomenon explains the change in the refractive index of the medium when the electric field moves in the medium, where the wave in the medium depends on the phase velocity of the wave and the intensity of the electric field. The changing of the refractive index based on the intensity of the electric field, according to (2.10). The change in the refractive index of the media material, which depends on the intensity of light, is applied in a wide range of applications such as squeezing, solitons, wavelength conversion, pulse compression, optical switching, which are significant phenomena as follows.

- Self-Phase Modulation (SPM) is a phenomenon that changes the refractive index of a medium resulting from the intensity of light pulses moving through the medium [31].
- Cross-Phase Modulation (XPM) is a phenomenon that occurs when the light waves are ranging from two different wavelengths, which travel in the same medium at the same time and resulting in one light wave able to induce the

phase change of another one light wave with a different wavelength. This effect will cause the spectrum to broaden (spectral broadening).

- Four-Wave Mixing (FWM) is a phenomenon caused by transmitting multiple wavelengths of light into the same medium at the same time, where the signal is combined; it creates a new frequency to occur, as shown in Figure 2.8. This new frequency might be overlapped or induced by the original signal resulting in the reduction of the initial signal.

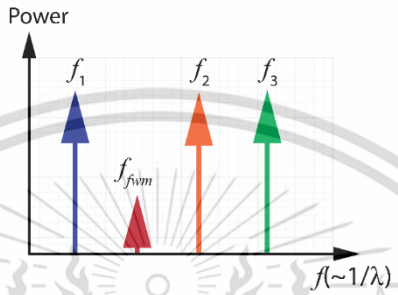

Figure 2.8 The formation of a four-wave mixing when entering frequencies f_1, f_2, f_3 into the system causes f_{fwm}, where $f_{fwm} = f_1 + f_2 - f_3$.

The second group of nonlinear phenomena that result from an electric field transfers some energy to a nonlinear medium, causing scattering nonlinearity. This phenomenon is caused by the instability of the energy level, which causes the transfer of photon energy to photons with lower energy levels, which consists of

- Stimulated Brillouin Scattering (SBS) occurs when the energy level of light is enough to cause scattering in the medium.
- Stimulated Raman Scattering (SRS) is the impact caused by the variance of light waves affecting other waves when the intensity of light reaches a certain level.

2.4.3 Nonlinear Phase Shift

When the light wave moves through a non-linear optical medium with length (L), the amplitude and phase change occurs [32], as shown in (2.11).

$$E_{out} = ae^{+i\phi}E_{in} \tag{2.11}$$

Here, E_{out} is an output electric field, and E_{in} is the input electric field. Where the amplitude change value (a) can be obtained from (2.12).

$$a = e^{-\alpha L} \tag{2.12}$$

The sum of the phase changes (ϕ) caused by linear phase change (ϕ_L) and non-linear phase change (ϕ_{NL}) according to the following equations.

$$\phi=\phi_L+\phi_{NL}=n_0k_nL+n_2Ik_nL_{eff} \quad (2.13)$$

$$k_n=\frac{2\pi}{\lambda} \quad (2.14)$$

$$L_{eff}=\frac{1-e^{-\alpha L}}{\alpha} \quad (2.15)$$

The length of the medium that causes effective depends on the linear absorption (α) of the medium. If the absorption value of the medium is very high, it will cause L_{eff} to below. In which the optical switching is needed at least pi phase shift for nonlinear phase shift, where, if the n_2 of material has a greater value and less loss, it will make the photon circuit are small and use less energy in the work process.

2.4.4 Optical Bistability

The Optical Bistability (OB) phenomenon occurs from a combination of nonlinearity in the interaction between radiation and matter and a feedback mechanism [33]. There are generally two OB classes: absorptive and dispersive OB. An increase in input power increases saturation, i.e., the degree of media transparency. This allows the intensity cavity field to increase, which in return increases the saturation. InGaAsP can be designed to have the band edge around 1.45 μm and thus can show absorptive OB when pumped at 1.55 μm [34]. Since the refractive index is a function of intensity, it shifts the optical length of the medium so that the resonance of the cavity is moved closer to the input frequency.

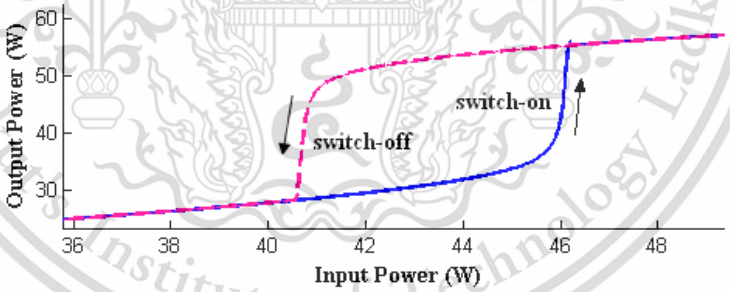

Figure 2.9 Optical Bistability of nonlinearity switch on/off within ring resonator.

2.4.5 Optical Bifurcation

Bifurcations can be occurred in continuous systems and also in discrete systems [35]–[37]. The study of how the character of fixed points changes as parameters of the system change is called bifurcation theory. Recall that the term bifurcation is used to describe any sudden change in the dynamics of the system. When a fixed-point changes character as parameter values change, the behavior of trajectories about that fixed point will change.

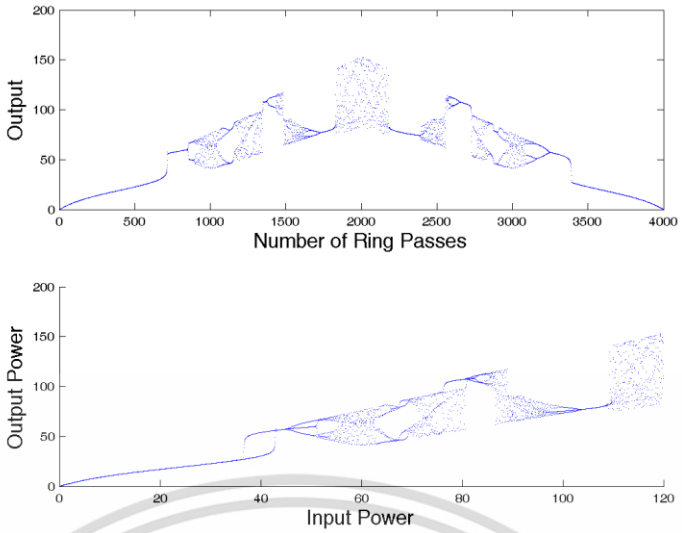

Figure 2.10 Optical Bifurcation occurring within ring resonator

2.4.6 Optical Chaos

The theory of chaos explains the behavior in mathematics and physics of certain nonlinear dynamical systems that exhibit dynamics that are sensitive to initial conditions under specific conditions (popularly referred to as the butterfly effect) [38]. Optical Chaos is observed in many non-linear optical systems. A ring resonator is one of the most common examples. As a result of this sensitivity, the behavior of chaotic systems seems to be unpredictable due to an exponential increase in errors in the initial conditions.

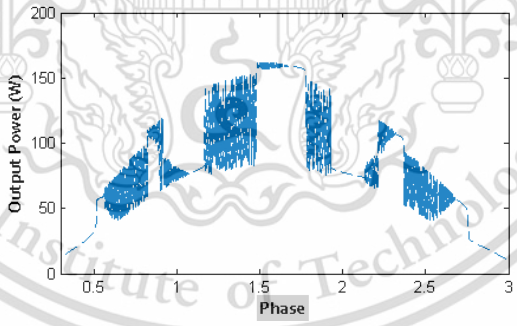

Figure 2.11 Chaotic signal generated by microring resonator

- In general, these three ingredients, such as the time-evolution equations; the values of the parameters describing the system; and the initial conditions, are needed to define the behavior of a system.

2.4.7 Optical Solitons

Soliton [39]is one type of wave that was recorded for the first time in 1834 [40] by John Scott Russell, a Scottish mathematician. This solitary wave can propagate for several distances without changing its shape and has a constant speed. Soliton waves

can be seen in nature, such as the tsunami, sound waves, and can also be found in the light waves. According to the soliton is a short pulse and can be generated within the wavelength of 1.55 μm. It can be propagated for long distances, and when the collision of a soliton within the medium occurs, it remains their pulse shape (no dispersion-induced pulse broadening). Soliton has a low loss while propagating in long-distance; therefore, the Soliton's applications have been widely reported.

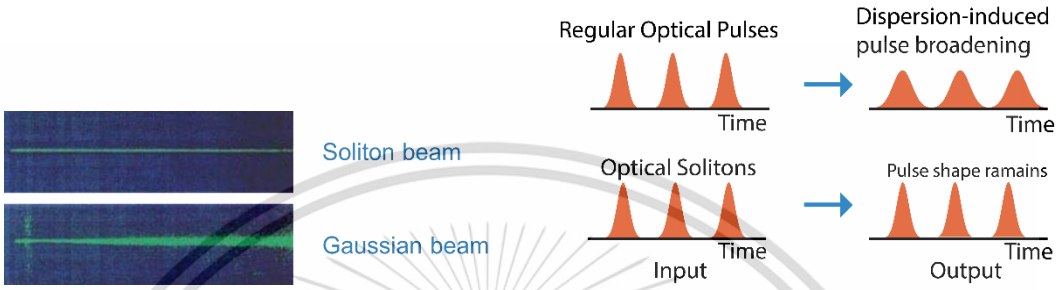

(a) Soliton vs. Gaussian beams (b) Soliton vs. Gaussian pulses

Figure 2.12 Difference of Soliton and Gaussian.

When light signals propagate within the medium for a distance, unavoidably loss and pulse distribution occur. However, a soliton is possible to utilize the nonlinear properties of the medium to compensate for the distribution of waveforms while the waves are propagating. Another advantage of using soliton is the power is gained and used for non-dispersion propagation is a long-distance communication link.

(a) Dark Soliton (b) Bright Soliton

Figure 2.13 The shapes of dark and bright soliton pulses.

Optical dark and bright Soliton pulses can be represented by the hyperbolic secant and tangent as in (2.16) and (2.17), respectively.

$$E_{Dark}(t)=A.tanh\left[\frac{T}{T_0}\right]exp\left[\left(\frac{x}{2L_D}\right)-i\phi(t)\right] \quad (2.16)$$

$$E_{Bright}(t)=A.sech\left[\frac{T}{T_0}\right]exp\left[\left(\frac{x}{2L_D}\right)-i\phi(t)\right] \quad (2.17)$$

Soliton signals are suitable to be used in logic. If comparing the soliton signal with the digital signal level, the logic signal can be shown as in Figure 2.14. In addition, the soliton signal can be interfered with to construct or destruct each other according to the endless wave characteristics. However, the introduction of dark and bright solitons to be used in optical logic is still minor and can be developed to improve system performance and system security.

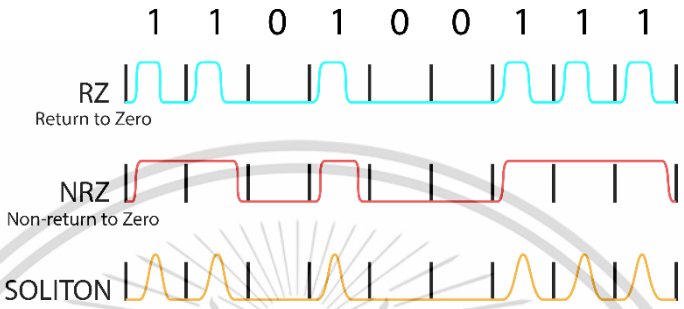

Figure 2.14 Digital signal RZ, NRZ and Soliton comparison.

Even if soliton is a pulse that can maintain the pulse properties when the pulse travels in a nonlinear medium. But soliton has the property of inducing the side soliton pulses that cause the gravitational attraction between the masses, which can only be found in nonlinear pulses. From this feature, the adjacent pulses might be induced to move out of the bit slot.

In the synchronization control process, many techniques can be performed [41]–[43]. In general, it requires an independent laser that can determine the mode-locked that can control the same repetition rate, which the process is based on the linear of effective cavity length (L_{eff}), which is derived from $f_r=c/L_{eff}$, (c is the speed of light in vacuum). In particular, the feedback system, which in the process of controlling the synchronization of the laser, is necessary to use to compensate for the instability of the resonant cavity. In the feedback control process, it can be divided into Active, Passive, and Hybrid Synchronization, where the stability of each synchronization technique is still being improved and developed continuously, which will lead to a system that can control the unison synchronization. In this thesis, the signal can be controlled by the unison.

2.5 Transfer Function Theory of Ring Resonators

The waveguide is an essential device in the photonic circuit, in which each waveguide has different characteristics of filtering and wave distribution, as shown in Figure 2.15. In the design of the photonic circuit, it is important to understand the properties of each device to be able to choose the appropriate utilization and to

achieve optimum performance. This section discusses the transfer function theory of the ring resonators.

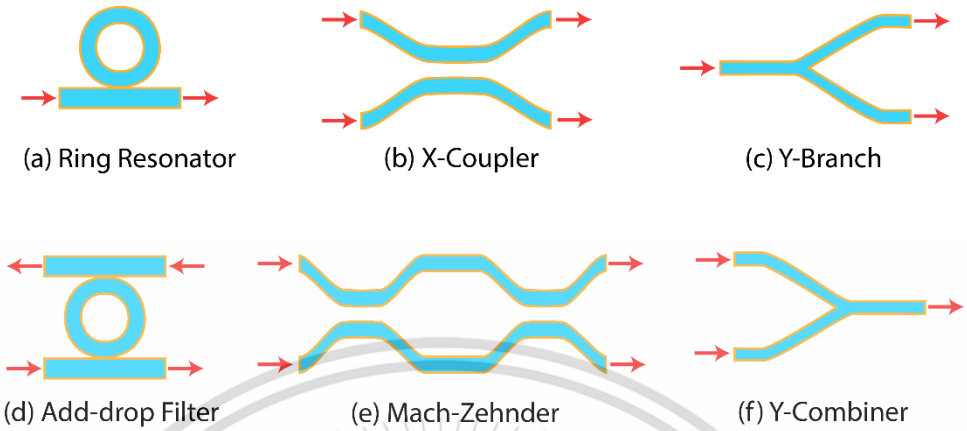

Figure 2.15 Waveguide structures.

2.5.1 Directional Coupler Theory

In analyzing the delay and the coupling direction when the signal moving through the waveguide in which the signal platforms with separated and combined signals can be analyzed by using Z-Transforms. The diagram of the coupling direction is shown in Figure 2.16. The line in the figure represents the waveguide, which will have a curve to each other and separated, where the ratio of energy transferred to each direction is determined by κ. This parameter indicates the level of imported energy that will be transferred to the waveguide on the opposite side (cross-port), where the relationship of import and export energy can be written as in (2.18) - (2.19).

$$c=cos\theta=\sqrt{(1-\gamma)(1-\kappa)} \quad (2.18)$$

$$-js=-jsin\theta=-j\sqrt{(1-\gamma)\kappa} \quad (2.19)$$

Where γ is the loss coefficient when the signal passed through the coupler and θ refers to the signal strength, including the length of the coupling section, complex number $-j$ means phase shift ($\pi/2$) when the optical signal crosses the waveguide to the opposite side.

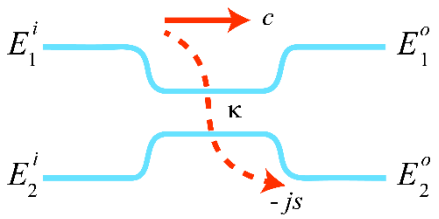

Figure 2.16 The coupling direction of the coupler and the I/O relationship.

2.5.2 Single Coupling Ring Resonator

From the theory of light transmission in linear systems, the electric field of light waves moving in each segment can be determined by (2.20).

$$E_{Segment}=E_A exp\left(\frac{\alpha_{Segment}}{2}L\text{-}jk_{n(Segment)}L_{Segment}\right) \quad (2.20)$$

Where E_A is the amplitude of the electric field, $L_{Segment}$ is the optical path length in each segment, $\alpha_{Segment}$ is the intensity attenuation coefficient of light according to distance and $k_{n(Segment)}$ is the wave propagation of each segment.

A simple structure of a single coupling ring resonator [44]–[46] is shown in Figure 2.17. From the figure, the ring with a radius of R, the length of the circumference of the ring is $L=2\pi R$, where κ is defined as the coupling coefficient of power, α is the attenuation coefficient, the intensity of light according to distance and k_n is the wave propagation constant.

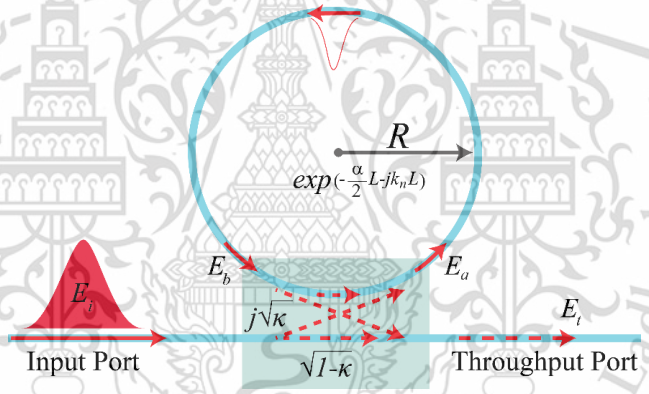

Figure 2.17 Single coupling ring resonator

In the mobility of the electric field of light, when light moving through the coupling area, it can express the equation according to the direction of movement as follows: when the light travels in a straight line (bar state) instead of $\sqrt{1\text{-}\kappa}$ and when the light travels in a cross-state instead of $j\sqrt{\kappa}$. Therefore, from Figure 2.17, the relationship between the throughput electric field (E_t) and the input electric field (E_i) can be determined as follows.

$$E_t=\sqrt{1\text{-}\gamma}\left[\sqrt{1\text{-}\kappa}E_i+j\sqrt{\kappa}E_b\right] \quad (2.21)$$

$$E_a=\sqrt{1\text{-}\gamma}\left[\sqrt{1\text{-}\kappa}E_b+j\sqrt{\kappa}E_i\right] \quad (2.22)$$

$$E_b=E_a exp\left(\frac{\text{-}\alpha L}{2}\text{-}jk_nL\right) \quad (2.23)$$

Herein, defined as $k_n=2\pi n_{eff}/\lambda$, γ represents the intensity coupling loss coefficient, and n_{eff} is the effective refractive index. From (2.21) – (2.23), the transfer function (E_t/E_i) can be derived as follows.

$$\frac{E_t}{E_i}=\sqrt{1-\gamma}\left[\frac{\sqrt{1-\kappa}-\sqrt{1-\gamma}exp\left(\frac{-\alpha L}{2}-jk_nL\right)}{1-\sqrt{1-\gamma}\sqrt{1-\kappa}exp\left(\frac{-\alpha L}{2}-jk_nL\right)}\right] \tag{2.24}$$

For better understanding, new parameters are defined as follows: $D=\sqrt{1-\gamma}$, $x=De^{\frac{-\alpha L}{2}}$, $y=\sqrt{1-\kappa}$, and $\phi=k_nL$. The relationship of the intensity of the output port compared to the input port is as in (2.25) [45].

$$\frac{I_t}{I_i}=\left|\frac{E_t}{E_i}\right|^2=D^2\left[1-\frac{(1-x^2)(1-y^2)}{(1-xy)^2+4xysin\left(\frac{\phi}{2}\right)}\right] \tag{2.25}$$

2.5.3 Double Coupling Ring Resonator

Double coupling ring resonator, as shown in Figure 2.18, in calculating the relationship of signal intensity [40] of the double coupling ring resonator, the loss coefficient caused by coupling ($D^2=1$) can be calculated as follows.

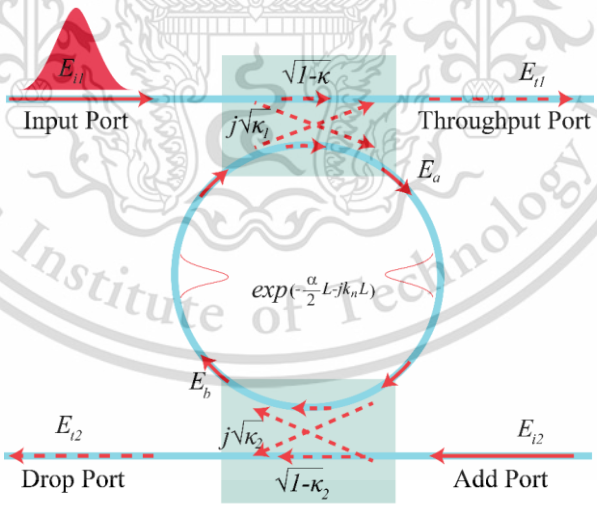

Figure 2.18 Double coupling ring resonator

$$E_a=j\sqrt{\kappa_1}E_{i1}+\sqrt{1-\kappa_1}exp\left(\frac{-\alpha}{4}L-jk_n\frac{L}{2}\right)E_b \tag{2.26}$$

$$E_b=\sqrt{1-\kappa_2}exp\left(\frac{-\alpha}{4}L-jk_n\frac{L}{2}\right)E_a, \text{ when } (E_{i2}=0) \tag{2.27}$$

Substitute (2.27) into (2.26), therefore

$$E_a = j\sqrt{\kappa_1}E_{i1} + \sqrt{1-\kappa_1}e^{\left(\frac{-\alpha}{4}L - jk_n\frac{L}{2}\right)}\left[\sqrt{1-\kappa_2}e^{\left(\frac{-\alpha}{4}L - jk_n\frac{L}{2}\right)}E_a\right]$$

$$E_a = \frac{j\sqrt{\kappa_1}E_{i1}}{1-\sqrt{1-\kappa_1}\sqrt{1-\kappa_2}e^{\left(\frac{-\alpha}{2}L - jk_nL\right)}} \quad (2.28)$$

Substitute (2.28) into (2.27), therefore

$$E_b = \sqrt{1-\kappa_2}e^{\left(\frac{-\alpha}{4}L - jk_n\frac{L}{2}\right)}\left[\frac{j\sqrt{\kappa_1}E_{i1}}{1-\sqrt{1-\kappa_1}\sqrt{1-\kappa_2}e^{\left(\frac{-\alpha}{2}L - jk_nL\right)}}\right]$$

$$E_b = \frac{j\sqrt{\kappa_1}\sqrt{1-\kappa_2}e^{\left(\frac{-\alpha}{4}L - jk_n\frac{L}{2}\right)}E_{i1}}{1-\sqrt{1-\kappa_1}\sqrt{1-\kappa_2}e^{\left(\frac{-\alpha}{2}L - jk_nL\right)}} \quad (2.29)$$

From Figure 2.18, therefore

$$E_{t1} = j\sqrt{\kappa_1}e^{\left(\frac{-\alpha}{4}L - jk_n\frac{L}{2}\right)}E_b + \sqrt{1-\kappa_1}E_{i1} \quad (2.30)$$

Substitute (2.29) into (2.30), therefore

$$E_{t1} = j\sqrt{\kappa_1}e^{\left(\frac{-\alpha}{4}L - jk_n\frac{L}{2}\right)}\left[\frac{j\sqrt{\kappa_1}\sqrt{1-\kappa_2}e^{\left(\frac{-\alpha}{4}L - jk_n\frac{L}{2}\right)}E_{i1}}{1-\sqrt{1-\kappa_1}\sqrt{1-\kappa_2}e^{\left(\frac{-\alpha}{2}L - jk_nL\right)}}\right] + \sqrt{1-\kappa_1}E_{i1}$$

$$\frac{E_{t1}}{E_{i1}} = \left[\frac{\sqrt{1-\kappa_1} - \sqrt{1-\kappa_2}e^{\left(\frac{-\alpha}{2}L - jk_nL\right)}}{1-\sqrt{1-\kappa_1}\sqrt{1-\kappa_2}e^{\left(\frac{-\alpha}{2}L - jk_nL\right)}}\right]$$

$$\frac{I_{t1}}{I_{i1}} = \left|\frac{E_{t1}}{E_{i1}}\right|^2 = \left[\frac{1-\kappa_1-2\sqrt{1-\kappa_1}\sqrt{1-\kappa_2}e^{\frac{-\alpha}{2}L}\cos(k_nL)+(1-\kappa_2)e^{-\alpha L}}{1+(1-\kappa_1)(1-\kappa_2)e^{-\alpha L}-2\sqrt{1-\kappa_1}\sqrt{1-\kappa_2}e^{\frac{-\alpha}{2}L}\cos(k_nL)}\right] \quad (2.31)$$

$E_{t2} j\sqrt{\kappa_2}e^{\frac{-\alpha}{4}L - jk_n\frac{L}{2}}E_a$, when $(E_{i2}=0)$ (2.32)

Substitute (2.28) into (2.32), therefore

$$E_{t2} = j\sqrt{\kappa_2}e^{\left(\frac{-\alpha}{4}L - jk_n\frac{L}{2}\right)}\left[\frac{j\sqrt{\kappa_1}E_{i1}}{1-\sqrt{1-\kappa_1}\sqrt{1-\kappa_2}e^{\left(\frac{-\alpha}{2}L - jk_nL\right)}}\right]$$

$$\frac{E_{t2}}{E_{i1}} = \left[\frac{\sqrt{\kappa_1}\sqrt{\kappa_2}e^{\left(\frac{-\alpha}{4}L - jk_n\frac{L}{2}\right)}}{1-\sqrt{1-\kappa_1}\sqrt{1-\kappa_2}e^{\left(\frac{-\alpha}{2}L - jk_nL\right)}}\right]$$

$$\frac{I_{t2}}{I_{i1}} = \left|\frac{E_{t2}}{E_{i1}}\right|^2 = \left[\frac{\kappa_1\kappa_2 e^{\frac{-\alpha}{2}L}}{1+(1-\kappa_1)(1-\kappa_2)e^{-\alpha L}-2\sqrt{1-\kappa_1}\sqrt{1-\kappa_2}e^{\frac{-\alpha}{2}L}\cos(k_nL)}\right] \quad (2.33)$$

2.5.4 Measurement of The Ring Resonator Efficiency

The measurement of the ring resonator circuit efficiency has important parameters that indicate the efficiency of the ring resonator, consisting of Q factor, free spectral range (FSR), finesse, and photon lifetime, in which each parameter can be found as follows.

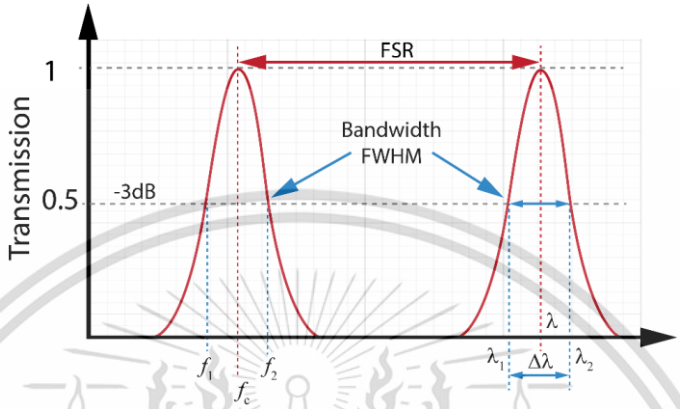

Figure 2.19 Measuring the various efficiencies of the waveforms.

- **Quality factor (Q)**

The Q factor is the parameter value of the ring resonator circuit that indicates the sharpness of the resonant output signal. In the electrical field, the Q value of the light waveguide refers to the accumulation of energy and the rate of energy loss of the light each round-trip in the ring resonator, where the Q value can be determined.

$$\frac{Q}{F}=\frac{f_0}{\Delta f}=\frac{\lambda_0}{\Delta\lambda} \tag{2.34}$$

Where $\Delta\lambda$ is Full Width at Half Maximum (FWHM), and λ_0 is the resonant wavelength of the ring resonator.

- **Free Spectral Range (FSR)**

The gap between the resonant frequencies is called the free spectral range, when determining the constant phase value and corresponds to $\phi=2m\pi$, which is defined as$k$. Therefore, when the phase has a constant change, $\phi=2(m+1)\pi$, it is defined as $k+\Delta k$.

The frequency shift (Δf) and wavelength shift ($\Delta\lambda$) is corresponding to the phase constant value (Δk) according to $\Delta f=c\Delta k/2\pi$ and $\Delta\lambda=\lambda^2\Delta k/2\pi$ equations. Therefore we can find the gap between the resonant frequency (f) and wavelength (λ) are given by (2.35) and (2.36).

$$\Delta f = \frac{c}{n_{gr}L} \tag{2.35}$$

$$\Delta\lambda = \left|\frac{-\lambda^2}{n_{gr}L}\right| \tag{2.36}$$

Where n_{gr} is the group refractive index determined as follows

$$n_{gr} \equiv n_{eff} - \lambda\frac{dn_{eff}}{d\lambda} \tag{2.37}$$

- **Resonance Bandwidth**

Resonance bandwidth determines how fast the ring resonator can process optical data. The bandwidth of the ring resonator is given by the resonator's finesse (F) and the full width at half-maximum (FWHM or 3 dB bandwidth). In order to understand how the coupling coefficient (κ) affects the resonator bandwidth, we will consider critically coupled ring resonator in the case of $\delta\phi = 2\kappa/\sqrt{1-\kappa}$. Therefore, the lower coefficient of coupling, the larger bandwidth of resonance is obtained.

When using $\delta\phi = \delta(k_n L) = 2\pi/F$, therefore FWHM ($\delta\phi$) in terms of frequency and wavelength at the resonant point can be determined by (2.38) - (2.39).

$$\delta f = \frac{c}{Fn_{gr}L} \tag{2.38}$$

$$\delta\lambda = \frac{\lambda^2}{Fn_{gr}L} \tag{2.39}$$

- **Finesse (F)**

The finesse value of the resonator is the parameter determined by the ratio of the full-width at half-maximum (FWHM of the waveform) and the free spectral range and (FSR) of the resonant frequency, can be calculated using FSR (Δf or $\Delta\lambda$) and FWHM (δf or $\delta\lambda$) of the filter by (2.40) – (2.42).

$$F = \frac{\Delta f}{\delta f} = \frac{\frac{c}{n_{gr}L}}{\frac{c}{Fn_{gr}L}} \tag{2.40}$$

$$F = \frac{\Delta\lambda}{\delta\lambda} = \frac{\frac{\lambda^2}{n_{gr}L}}{\frac{\lambda^2}{Fn_{gr}L}} \tag{2.41}$$

$$F = \frac{FSR}{\delta\lambda} \approx \frac{1}{\alpha L} \tag{2.42}$$

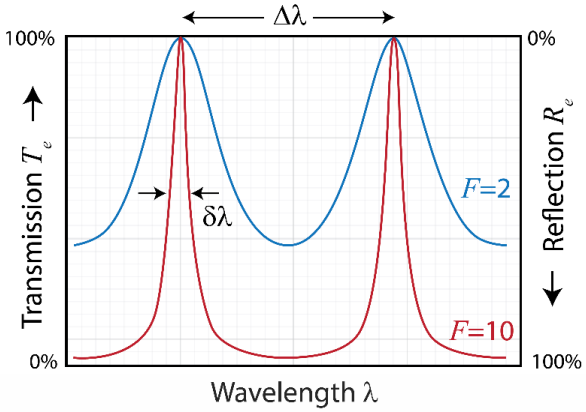

Figure 2.20 The sharpness level of the signal at various F values.

- **Photon lifetime (τ_{cav})**

The photon lifetime (τ_{cav}) is the period that indicates the degradation of energy or the increased duration of energy in the ring resonator. In the ring resonator, the photon lifetime value is corresponding to the coupling value between the waveguide and the ring resonator, including with various loss values that occur within the ring resonator, where the photon lifetime is typically very small compared to the carrier lifetime, which is about 10×10^{-12} s. The photon lifetime in the ring resonator can be calculated from (2.44).

$$\tau_{cav}=\frac{Q\lambda}{2\pi c}=\frac{\lambda^2}{2\pi c\Delta\lambda} \tag{2.43}$$

Where τ_{cav} is the photon lifetime, Q is the Q-factor of the ring resonator, λ is the resonant wavelength, and c is the velocity of light in the vacuum.

- **Switching Time (τ_{sw})**

The time for the switching of the optical resonator device can be used to shift the resonant frequency into and out of λ_0 [47]–[49] from the desired resonant frequency by using signal controlling the resonant frequency change as shown in Figure 2.20. The fastest time that device achieved can be obtained from (2.44).

$$\tau_{sw}=\frac{Q}{\delta v}=\frac{Q}{f_R}=\frac{Q\lambda_R}{c} \tag{2.44}$$

Where Q is the quality factor, δv is the full width at half maximum (FWHM), f_R is the resonant frequency, λ_R is the resonant wavelength, and c is the speed of light in the vacuum (3×10^8 m/s).

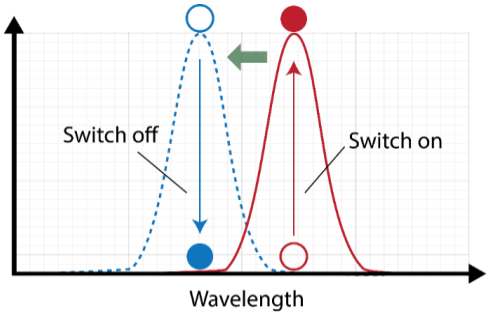

Figure 2.21 Pulse switching.

2.6 Interaction of Radiation with Matter

The electromagnetic spectrum consists of numerous types of radiation, each with a different energy, causing the reaction with different objects, where each part of the electromagnetic wave consists of quantum energy, which is high enough to cause an excitation. Energy levels of atoms and molecules characterize in periodic or quantum. If the energy does not reach or does not fit the quantum energy level, the radiation passes through the object without reaction. The radiation in each range of the electromagnetic wave spectrum interacts with objects differently depending on the type of material by transmitting energy between the quantized states generated by the photons, consisting of absorption, emission and stimulated emission, in which every process requires photon energy according to the Planck's relationship principle. By the nature of the semiconductor, there will be a bandgap that is less than the insulator, but more than the conductor, as shown in Figure 2.22.

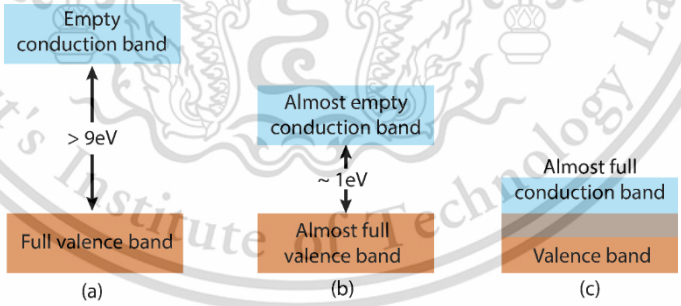

Figure 2.22 The gap between the energy band of (a) insulator (b) semiconductor and (c) electrical conductor.

2.6.1 Absorption

According to the quantum theory, particles (atoms, molecules, or ions) have energy levels that are specific to each particle type. At room temperature, most particles are in the state with the lowest energy, which is called the ground state, but when providing energy to the particles in the form of electromagnetic radiation, if the photon energy is given to fit the difference between the energy levels of the particles

will absorb energy, causing the particles to move in a higher energy state called excited state. The process by which particles absorb energy (heat, electricity, or radiation) causes higher energy levels, called excitation, in which energy absorption can be written as in (2.45).

$$M+h\nu \rightarrow M^{*} \tag{2.45}$$

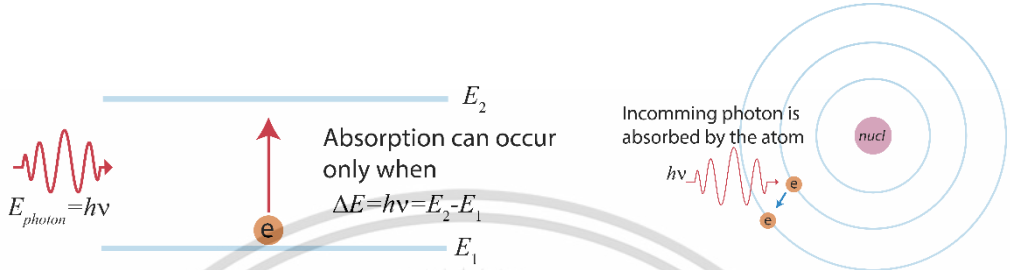

Figure 2.23 Energy absorption.

2.6.2 Emission

After the particles receive energy (heat, electricity, or radiation) stimulated higher energy, particles that are in the excited state are unstable. After a short period of time (about 10^{-6} s to 10^{-9} s) will cause energy emission and reduce the energy level, as shown in Figure 2.24. The process in which the particles that are in the state of stimulating the release of excess energy return to the ground state or have a lower energy level is called relaxation, which electromagnetic radiation emitting can be written as in (2.46).

$$M^{*} \rightarrow M+h\nu \tag{2.46}$$

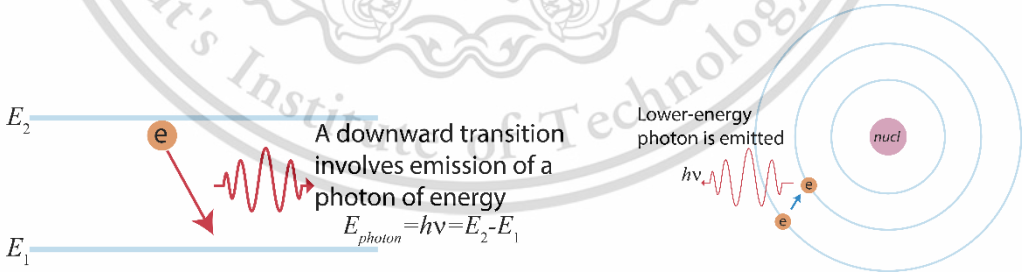

Figure 2.24 Energy emission.

2.6.3 Stimulated Emission

When the electrons are in the excited state, into the level of power that is higher than the ground state. At the same time, the giving of photon energy, which has quantum energy equivalent to the difference of the energy level between the current levels, where this energy is not absorbed by the system, but will make atoms or molecules emit the energy before time. The emitted light and the stimulating light,

therefore, comes out of the system at the same time, the same energy, and in unison, both the direction of mobility and phase of the light wave, as shown in Figure 2.25.

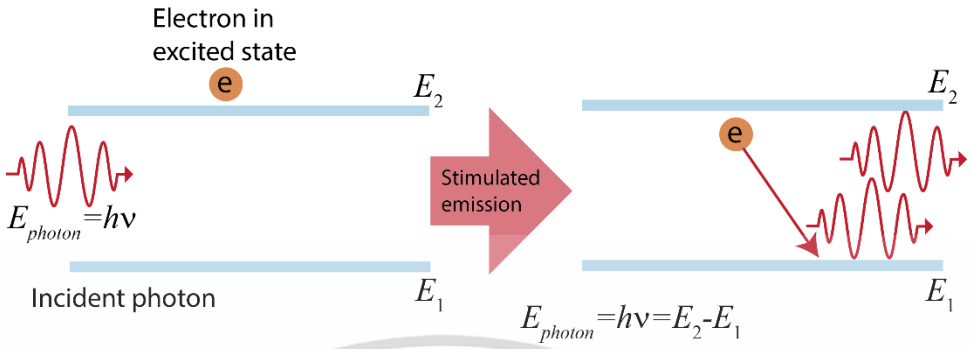

Figure 2.25 Stimulated emission.

2.6.4 Carrier Lifetime

Minority carrier lifetime (τ) or excess carriers in semiconductor mean the average time in which the excess carriers are reunified and evanescent after being injected to be approximately 0.368 times of the number of injections. For the accurate value of the carrier lifetime in each semiconductor, it is difficult to find the value due to its easily fluctuate and highly sensitive even though it is constructed with the same process. Therefore, it is difficult to control the Minority carrier's lifetime. In the semiconductor manufacturing process that wants to reduce the carrier's lifetime, this can be done by adding gold atoms into the semiconductor as well. Where the ratio of the carrier lifetime and the addition of the gold atom is approximately equal to 10 times the amount of gold atoms added to it. That is when adding 100 times the gold atom, and the carrier lifetime will be reduced by 1000 times [50]. In general, the carrier lifetime is minor, usually in the range of 10^{-6} s to 10^{-9} s. The purpose of reducing the carrier lifetime is to increase the speed of operation or the speed of the switching of semiconductor devices to make the device more responsive to high-frequency signals.

Chapter 3
RELATED RESEARCH AND ALL-OPTICAL SWITCHING SCHEME

Since the first proposal to use optical signal instead of electrical signal processing, the revolution of all-optical devices have been extremely developed to be smaller and higher performance. Several techniques of optical signal processing used in all-optical logic and arithmetic operations have been investigated. This is the roadmap to design a Photonic integrated circuit (PIC). Therefore, this thesis proposes the design system of all-optical full-adder and subtractor arithmetic operation using microring resonator for all-optical arithmetic and logic unit application based all-optical switching operation.

3.1 Technologies of All-optical Arithmetic and Logic Design

Technologies of all-optical logic and arithmetic designs can be divided into two categories, i.e., one is the architecture design without the use of a semiconductor optical amplifier (SOA), and another is the design with the use of SOA.

Table 3.1 Technologies of all-optical logic and arithmetic design

Architectures without SOA	Architectures with SOA
- Waveguide configuration	- SOA based MZI
- Sagnac interferometer	- Michelson interferometer
- Nonlinear optical loop mirror	- Ultra-fast nonlinear interferometer
- Optical intensity switch	- Terahertz optical asymmetric
- Phase shift based MZI	demultiplexer (TOAD)
	- SLALOM interferometer

3.2 Related Research

In optical data processing and computing, a variety of techniques have been proposed, and one of the essential methods and applications for optical arithmetic and logic operations is optical tree architecture [7]–[9], [51]–[54], which can be applied in various optical logic and arithmetic applications.

3.2.1 All-optical Logic and Arithmetic using SOA-based MZI

Mach-Zehnder interferometer (MZI) [9], [55], [56] is commonly used for optical logic building due to the simple structure and tolerance, making it favorable to design and to be applied. Building a logic gate with MZI using SOA, consists of SOAs installed on the two arms of the MZI, as shown in Figure 3.1. By operation, an MZI-based optical logic uses the XPM technique occurring in the SOA to induce the

phase difference between the two arms of the interferometer for establishing the logical state at the output ports.

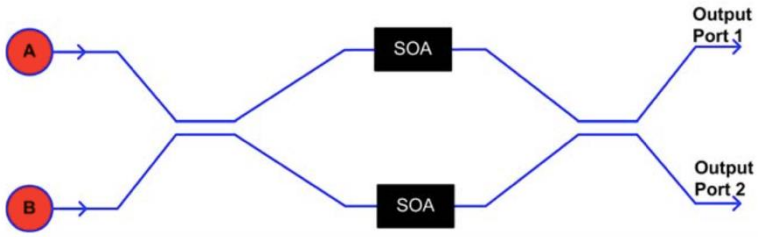

Figure 3.1 SOA based MZI configuration

The building of logical circuits and arithmetic circuits based on optical tree architecture using MZI relies on the nonlinear phenomena occurring within the SOA installed on both arms of the MZI [57] to perform all-optical switching as a path selection. This method has advantages and disadvantages as follows.

- Advantages: simple structure, control ability, operation in 40 Gb/s.
- Disadvantage: using SOA, large scale, difficulty in very-large-scale integration (VLSI) optics.

3.2.2 All-optical Logic and Arithmetic based on Tree-architecture using Nonlinear Materials

The building of logical circuits and arithmetic circuits based on optical tree architecture using nonlinear materials attached [7], as shown in Figure 3.2.

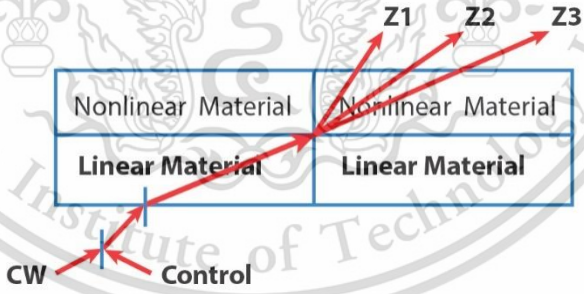

Figure 3.2 Nonlinear materials structure.

This method uses an attaching of linear and nonlinear semiconductor materials together, which has the following advantages and disadvantages:

- Advantages: simple structure, using a passive device.
- Disadvantages: limit in VLSI integration, difficulty in controllability.

3.2.3 All-optical Logic and Arithmetic Circuits using TOAD

A terahertz optical asymmetric demultiplexer (TOAD) device is used for the building of a logical and arithmetic circuit [8]. It functions as an optical switch to

choose the working path, as shown in Figure 3.3. This architecture has advantages and disadvantages as follows.

- Advantages: simple structure, control ability.
- Disadvantages: using SOA, large scale, difficulty in VLSI integration, low bitrate.

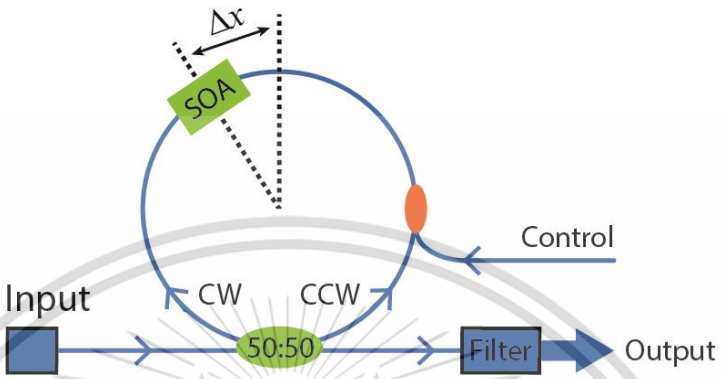

Figure 3.3 TOAD structure.

The operation of TOAD uses a nonlinear interferometer, which is applied to various optical data processing applications. The structure of the TOAD by using the Sagnac interferometer is shown in Figure 3.3 [58], [59]. From the figure, the input signal will be divided into two parts, moving in a loop in a clockwise and counterclockwise direction and will be combined at the coupler. The loop will be further connected with the control to enable and disable the switch, which will operate with SOA building from nonlinear materials to enable the phase shift of the input signal to cause the switching of a signal. The nonlinear value of SOA depends on the strength of the control signal.

3.2.4 Optical Channel Dropping Filter (OCDF)

OCDF is the access method to one of the channels in the wavelength division multiplexed (WDM) system without disturbing other channels, which is considered one of the critical components in photonic circuits and optical communication systems. Various schemes have been reported [60]–[63]. The schematic diagram of the optical channel filter is shown in Figure 3.4. It consists of two waveguides, the bus, and the drop. When the light signals pass through the waveguide, there is only one channel frequency can be exported to the drop.

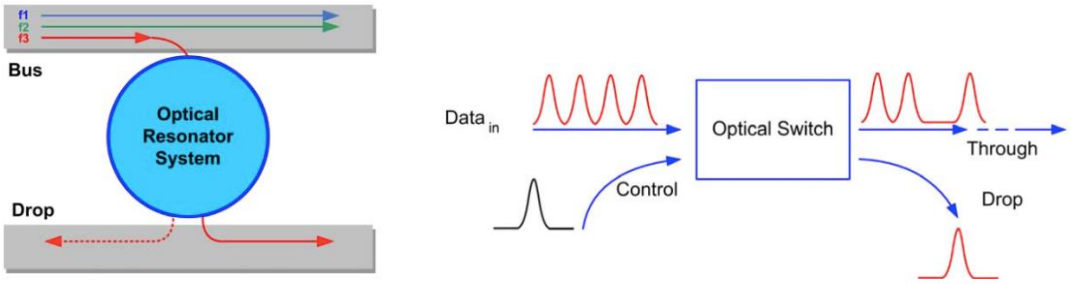

(a) (b)

Figure 3.4 Common structure of resonator-cavity channel dropping filter.

The efficiency of the OCDF is determined by the ability to transmit energy between the two waveguides. The maximum power transmission capacity is 100 %, both direct and backward, with no other channels appearing in the system.

3.2.5 Plasma Dispersion Effect

The change in the refractive index of the semiconductor optical material caused by the free carriers plasma dispersion effect will increase the absorption coefficient of the material while the refractive index of the material decreases. In which the refractive index of the material (Δn) and the light absorptive coefficient ($\Delta \alpha$) change when the device receives the power that is in the gap between the energy band of the optical semiconductor material that commonly used as shown in Table 3.2 [64]–[69].

Table 3.2 Bandgap energy for some specific semiconductor materials

Material	Formula	Bandgap energy	Wavelength
Aluminum Arsenide	AlAs	2.09 eV	550 nm
Aluminum Gallium Arsenide	AlGaAs	(1.42 to 1.61) eV	(770 to 870) nm
Gallium Arsenide	GaAs	1.42 eV	870 nm
Gallium Phosphide	GaP	2.24 eV	550 nm
Indium Gallium Arsenide Phosphide	InGaAsP	(0.74 to 1.13) eV	(1100 to 1670) nm
Indium Phosphide	InP	1.33 eV	930 nm

Annotation The bandgap energy of specific material may change depending on various parameters such as temperature, density, wavelength, the mixing ratio of the material, and mixing method, as well.

3.2.6 Carrier Injection for Electron-hole Pair Induction

The nonlinear method of the optical semiconductor materials used in this research is to inject carriers pumping light to induce electron-hole pairs, as shown in Figure 3.5. In which the injected carriers will change the gain-loss coefficient and the

index of refraction of the medium. The light pumping energy must not be less than the energy value of the substance used. The approximate wavelengths of each material that is universally applied are expressed in Table 3.2.

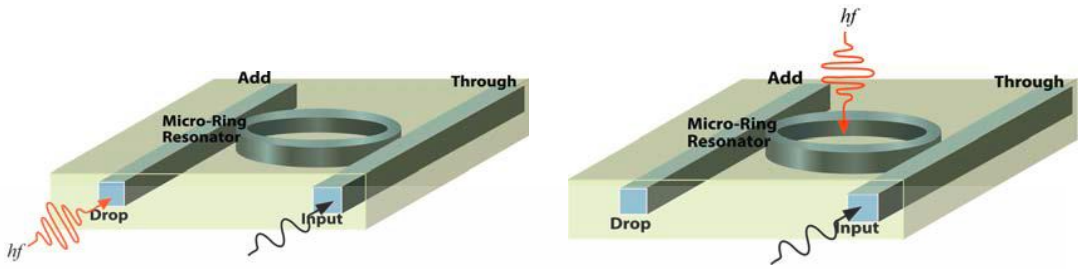

(a) (b)

Figure 3.5 The injection of induced carriers into the ring resonator (a) injection the induced carrier through the waveguide (b) direct injection of the carriers.

A semiconductor material can be changed the properties of a substance in various methods, such as using voltage, using heat, or adding energy to the material at an appropriate energy level until the substance can change its properties or specific responses. It also depends on other environmental factors, such as the shape and dimension of the material in each substrate layer, the methods of device fabrication, and more. The use of semiconductor materials for optical switching is generally based on the thermo-optic effect [70]–[72] and free carriers plasma dispersion effect (FCD) [73]–[75].

Although the Thermo-optic method is uncomplicated to operate, it is quite difficult to control heat emission, and the response time is slower [69], [76]. Even there are ongoing improvements to the methodology, and if compared to the free carrier plasma dispersion effect, it is still much slower. Therefore, this thesis proposes the design of all-optical logic circuits controlled by all-optical signals to improve the efficiency of the operation. The optical signal form used is the optical soliton, for both input and pumping to control the carrier induce effect [64], [77], [78] in order to change the refractive index in the optical semiconductor material. The semiconductor material that is universally used in optical applications could change the properties of the substance if the energy received is not less than the value of the bandgap energy. Carrier injection or signal import to induce changes in the refractive index of the nonlinear ring resonator can be achieved in two characteristics, as shown in Figure 3.5 [16], [79], [80].

This thesis discusses theoretical concepts and simulation results of the system used in the photonic circuit design to process all-optical arithmetic and logic operations using a nonlinear ring resonator, which is an exciting and continually evolving technologies. From the past to the present, the ring resonator has been

demonstrated [50] and fabricated [15] for various applications arranged from several massive to tiny radii, as concluded in Table 3.3.

Table 3.3 Ring resonator fabrication and application survey

Year	Proposed application	Radius	Type
2002 [81]	Switching, time-division demultiplexing, routing, four-wave mixing base on GaAs-AlGaAs	10 μm	Experiment
2003 [82]	InGaAsP-based passive ring coupler laser	20 μm	Simulation
2004 [83]	Third-order add-drop filters based on the series-coupled ring in silicon-rich silicon nitride	5 μm	Experiment
2006 [84]	Biosensor based on vertically coupled glass microring resonators	60 μm	Experiment
2006 [85]	Third-order microring filters fabricated in silicon-rich silicon nitride	8.004 μm	Experiment
2008 [15]	Demonstration of silicon ring resonator which minimizes spurious light scattering and increases critical dimensions of geometry	1.5 μm	Experiment
2008 [86]	The fabrication method for high-quality resonant photonic devices on SOI substrates	10 μm	Experiment
2010 [87]	Silicon-based asymmetrically coupled add-drop ring resonators	20 μm	Simulation, experiment
2013 [88]	The fabrication method is eliminating the surface roughness problem introduced during dry etching of waveguide sidewalls.	80 μm	Experiment
2014 [89]	Label-free biosensors	1.75 μm	Experiment
2015 [14]	Sub-wavelength grating (SWG) based rings realized on silicon on insulator (SOI) chips	(10 to 40) μm	Experiment
2016 [90]	Communication and sensing using microring resonator on the SOI platform	5 μm	Simulation, Experiment
2017 [91]	Integrated photonic structure of microring resonator based on As-deposited Si3N4 layer	100 μm	Experiment

The reports indicate that the smallest fabricated ring resonator size is 1.5 μm radius. Therefore, in order that makes the design system to fit the practical devices and to make the design circuit ultra-compact. This radius size is used for the circuits.

3.3 All-optical Switching Scheme within Nonlinear Ring Resonator

For telecommunications, an optical switch is a switch that enables the selective switching of the signal from one circuit to another in optical fibers or integrated optical circuits (IOC). An optical switch can be operated by mechanical means, such as physically shifting an optical fiber to drive one or more alternative fibers, fast optical switches, such as those with electro-optic or magneto-optic effects, can be used to perform logic operations, including semiconductor optical amplifiers (SOA) which are optoelectronic devices that can be used as optical amplifiers in this category.

This section describes how microring resonator (MRR) can perform the logic switching operation. Typically, the only particular wavelength is allowed to resonate in an MRR, when a resonant frequency is input into MRR via input-port with suitable coupling parameters, all output power appears at drop-port. Base on nonlinear Kerr effect, when the higher intensity input (control input) is applied into the MRR via add-port or pumping on the top of MRR, the intensity-dependent refractive index of the material changes and cause the change of resonant frequency. Thus, the optical power is wholly switched from drop-port to through-port.

The need to provide flexibility in optical network connectivity drives optical switching technology. Optical security, test systems, and wireless reconfigurable add-drop multiplexers are the primary applications. Possible future uses include remote optical supply and recovery.

Current applications for switching include passive safety switches for service restoration after the interruption, such as fiber cut. Remote Fiber Test Systems (RFTS) is a universal application for switches that can monitor and locate a fault on a fiber transmission line. Optical cross-connection is an emerging application of optical switches. The system uses optical switching fabrics to connect multiple optical inputs and outputs.

Nonlinear optical phenomena can be induced in semiconductors by free-carrier injection induced by single-photon absorption (SPA) [80], [92], [93]. The absorbed photons generate electron-hole pairs by pumping the semiconductor material optically above its bandgap energy. This carrier injection pumping would adjust the gain-loss ratio and the semiconductor material index of refraction. The results indicated that the switching was designed for ultrafast (25 ps) and low-power (25 mW) operation with high modulation depth (85 %) to enable logical operation at 40 Gb/s [93]. The advantages are compactness, cascade ability, high Q-factor, tunability, reversibility, and reconfigurability, making the designs favorable for practical applications.

In order to design an optical switch in the non-linear ring resonator, the control signal is applied to induce the refractive index in two ways: the control signal through the waveguide at add-port and the direct pump input to the ring resonator as shown in Figure 3.6. From a comparative study of the advantages and disadvantages of importing input signals to induce the refractive index of the resonant ring, it is found that the direct input method at the resonant ring is more flexible and more convenient in applications. Therefore, this thesis refers to the model of optical switching equipment fabrication that operates by inputting the input into the ring directly. In practice, the induction of the refractive index of the ring resonator by the light pump to change the coefficient of the medium may cause heat. This thesis does not consider the effect of changing the refractive index or the red-shift effect of a thermal medium.

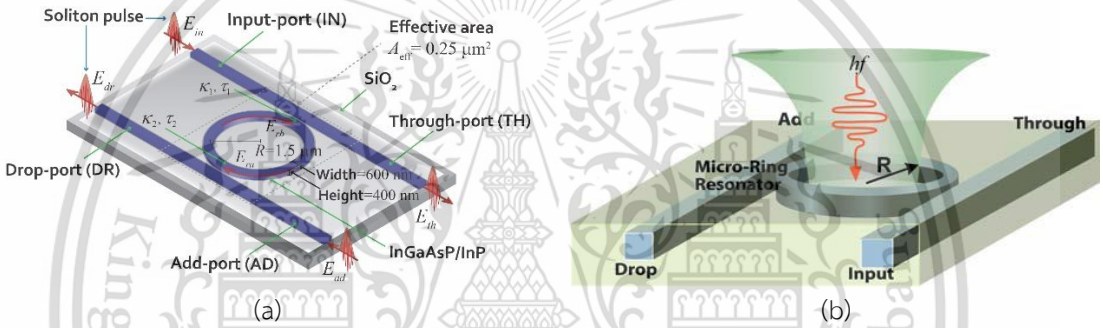

Figure 3.6 Applying a control signal to perform an optical switch from the ring resonator (a) Input via add-port of double coupling ring structure (b) Direct induction carrier injection on the ring resonator.

Based on the cross-phase modulation (XPM) caused by the nonlinear effect of the material, a modified add/drop ring resonator using for performing all-optical switching by carrier injection can be successfully operated with an optical pump beam on the top of microring (MRR) architecture as shown in Figure 3.6. In this scheme [94], the input and control field is generated by Gaussian pulses (or Soliton pulses). By using optical pulse for power controlling and for switching output signal, the input pulse (λ_1) is used for input, and the pumping pulse (or control pulse) at (λ_2) is used for controlling the all-optical switch (OSW).

3.3.1 Modified Add/Drop Ring Resonator (MARR)

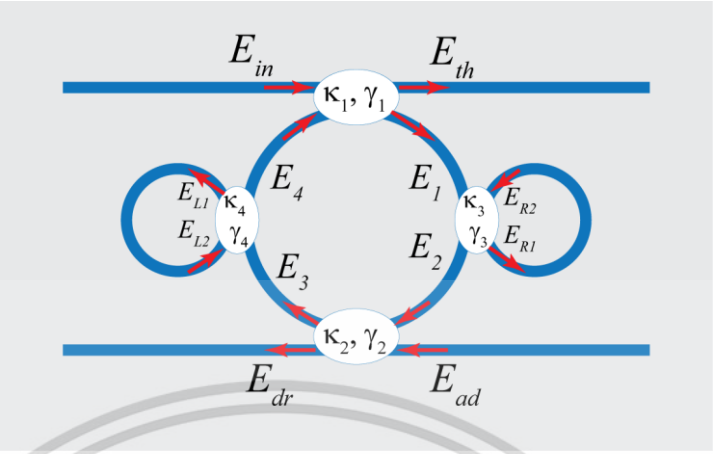

Figure 3.7 Modified add-drop ring resonator

In Figure 3.7, the modified add-drop multiplexer used for optical switching is illustrated. The coupling region is defined by the coupling factor (κ). The equations described the electric field coupling are given by $\sqrt{1-\kappa}$ for the bar section and $j\sqrt{\kappa}$ for the cross-section [44], [95], [96]. When the input light pulse is input and passed through the first optical coupler (C_1, See Figure 3.7) connected between the input waveguide and the center-ring resonator of the add-drop multiplexer, the transmitted (E_{th}) and circulated (E_1) optical fields can be expressed as in (3.1)–(3.2).

$$E_{th} = \sqrt{1-\gamma_1}\left(\sqrt{1-\kappa_1}E_{in} + j\sqrt{\kappa_1}e^{-\frac{\alpha}{8}L_{MAR}-\frac{jk_n}{4}L_{MAR}}E_4\right) \quad (3.1)$$

$$E_1 = \sqrt{1-\gamma_1}\left(\sqrt{1-\kappa_1}e^{-\frac{\alpha}{8}L_{MAR}-\frac{jk_n}{4}L_{MAR}}E_4 + j\sqrt{\kappa_1}E_{in}\right) \quad (3.2)$$

where κ_1 and γ_1 are the intensity coupling coefficient and the fractional coupler intensity loss of the first optical coupler, respectively, E_4 is the circulated optical field after passing through the fourth optical coupler (C_4) connected between the center ring resonator and the left-hand-side (LHS) ring resonator, k_{nR} is the wave propagation number of the center ring resonator, $L_{MAR}=2\pi R$ is the circumference of the center ring resonator, R is the ring radius of the center ring. Moreover, after the optical field (E_1) passed through the second coupler connected between the center ring resonator and the RHS ring resonator, the optical field coupled into the right ring resonator (E_{R1}) and the optical field transmitted to next optical coupler (E_2) are given by (3.3)–(3.5).

$$E_2 = \sqrt{1-\gamma_2}\left(j\sqrt{\kappa_2}E_{ad} + \sqrt{1-\kappa_2}e^{-\frac{\alpha}{8}L_{MAR}-\frac{jk_n}{4}L_{MAR}}E_3 \right) \tag{3.3}$$

$$E_R = \sqrt{1-\gamma_3}\left(j\sqrt{\kappa_3}e^{-\frac{\alpha}{8}L_{MAR}-\frac{jk_n}{4}L_{MAR}}E_1 + \sqrt{1-\kappa_3}e^{-\frac{\alpha}{2}L_R-jk_{nR}L_R}E_R \right)$$

$$E_R = \frac{j\sqrt{\kappa_3}\sqrt{1-\gamma_3}e^{-\frac{\alpha}{8}L_{MAR}-\frac{jk_n}{4}L_{MAR}}}{1-\sqrt{1-\gamma_3}\sqrt{1-\kappa_3}e^{-\frac{\alpha}{2}L_R-jk_{nR}L_R}}E_1 \tag{3.4}$$

Assume that $x_0 = \frac{j\sqrt{\kappa_3}\sqrt{1-\gamma_3}e^{-\frac{\alpha}{8}L_{MAR}-\frac{jk_n}{4}L_{MAR}}}{1-\sqrt{1-\gamma_3}\sqrt{1-\kappa_3}e^{-\frac{\alpha}{2}L_R-jk_{nR}L_R}}$, therefore

$$E_R = x_0 E_1 \tag{3.5}$$

where κ_2 and γ_2 are the intensity coupling coefficient and the partial coupler intensity loss of the second optical coupler (C_2), respectively. E_R is a round-trip circulated optical field inside the right-hand-side (RHS) ring resonator, α is the attenuation coefficient of the ring resonator (k_{nR}) is the wave propagation number of the RHS ring, λ is the optical wavelength, L_R=$2\pi r_R$ is the circumference of the RHS ring resonator, and r_R is the RHS ring radius.

Next step, when the light passed through the third optical coupler (C_3) connected between the center ring and the output waveguide, the optical field coupled into drop-port (E_{dr}) and the optical field circulated (E_3) into the fourth optical coupler is given by equations (3.6)–(3.7).

$$E_3 = \sqrt{1-\gamma_3}\left(\sqrt{1-\kappa_3}e^{-\frac{\alpha}{8}L_{MAR}-\frac{jk_n}{4}L_{MAR}}E_1 + j\sqrt{\kappa_3}e^{-\frac{\alpha}{2}L_R-jk_{nR}L_R}E_R \right) \tag{3.6}$$

$$E_{dr} = \sqrt{1-\gamma_2}\left(\sqrt{1-\kappa_2}E_{ad} + j\sqrt{\kappa_2}e^{-\frac{\alpha}{8}L_{MAR}-\frac{jk_n}{4}L_{MAR}}E_3 \right) \tag{3.7}$$

where κ_3 and γ_3 are the intensity coupling coefficient and the partial coupler intensity loss of the third optical coupler (C_3), respectively, E_{ad} is the added (control) optical field.

For the final step, when the light passed through the fourth optical coupler (C_4), the optical field coupled into the LHS ring resonator (E_L), and the optical field traveled back (E_4) to the first optical coupler is expressed in (3.8)–(3.10).

$$E_4 = \sqrt{1-\gamma_4}\left(\sqrt{1-\kappa_4}e^{-\frac{\alpha}{8}L_{MAR}-\frac{jk_n}{4}L_{MAR}}E_2 + j\sqrt{\kappa_4}e^{-\frac{\alpha}{2}L_L-jk_{nL}L_L}E_L \right) \tag{3.8}$$

$$E_L = \sqrt{1-\gamma_4}\left(j\sqrt{\kappa_4}e^{-\frac{\alpha}{8}L_{MAR}-\frac{jk_n}{4}L_{MAR}}E_2 + \sqrt{1-\kappa_4}e^{-\frac{\alpha}{2}L_L - jk_{nL}L_L}E_L \right)$$

$$E_L = \frac{j\sqrt{\kappa_4}\sqrt{1-\gamma_4}e^{-\frac{\alpha}{8}L_{MAR}-\frac{jk_n}{4}L_{MAR}}}{1-\sqrt{1-\gamma_4}\sqrt{1-\kappa_4}e^{-\frac{\alpha}{2}L_L - jk_{nL}L_L}}E_2 \quad (3.9)$$

Assume that $y_0 = \frac{j\sqrt{\kappa_4}\sqrt{1-\gamma_4}e^{-\frac{\alpha}{8}L_{mar}-\frac{jk_n}{4}L_{mar}}}{1-\sqrt{1-\gamma_4}\sqrt{1-\kappa_4}e^{-\frac{\alpha}{2}L_l - jk_{nl}L_l}}$, therefore

$$E_L = y_0 E_2 \quad (3.10)$$

where κ_4 and γ_4 are the intensity coupling coefficient and the partial coupler intensity loss of the fourth optical coupler (C_4), respectively. E_L is a round-trip circulated optical field inside the LHS ring resonator, $L_L=2\pi r_L$ is the circumference of the left-ring resonator, and the left-ring radius is r_L.

When substituting (3.5) to (3.6) and (3.10) to (3.8), therefore

$$E_3 = \sqrt{1-\gamma_3}\left(\sqrt{1-\kappa_3}e^{-\frac{\alpha}{8}L_{MAR}-\frac{jk_n}{4}L_{MAR}}E_1 + j\sqrt{\kappa_3}e^{-\frac{\alpha}{2}L_R - jk_{nR}L_R}x_0 E_1 \right) \quad (3.11)$$

$$E_4 = \sqrt{1-\gamma_4}\left(\sqrt{1-\kappa_4}e^{-\frac{\alpha}{8}L_{MAR}-\frac{jk_n}{4}L_{MAR}}E_2 + j\sqrt{\kappa_4}e^{-\frac{\alpha}{2}L_L - jk_{nL}L_L}y_0 E_2 \right) \quad (3.12)$$

Assume that $x_1 = \sqrt{1-\gamma_3}\left(\sqrt{1-\kappa_3}e^{-\frac{\alpha}{8}L_{MAR}-\frac{jk_n}{4}L_{MAR}} + j\sqrt{\kappa_3}e^{-\frac{\alpha}{2}L_R - jk_{nR}L_R}x_0 \right)$, therefore

$$E_3 = x_1 E_1 \quad (3.13)$$

and assume that $y_1 = \sqrt{1-\gamma_4}\left(\sqrt{1-\kappa_4}e^{-\frac{\alpha}{8}L_{MAR}-\frac{jk_n}{4}L_{MAR}} + j\sqrt{\kappa_4}e^{-\frac{\alpha}{2}L_L - jk_{nL}L_L}y_0 \right)$, therefore

$$E_4 = y_1 E_2 \quad (3.14)$$

When substituting (3.14) to (3.2) and (3.13) to (3.3), therefore

$$E_1 = \sqrt{1-\gamma_1}\left(\sqrt{1-\kappa_1}e^{-\frac{\alpha}{8}L_{MAR}-\frac{jk_n}{4}L_{MAR}}y_1 E_2 + j\sqrt{\kappa_1}E_{in} \right) \quad (3.15)$$

$$E_2 = \sqrt{1-\gamma_2}\left(j\sqrt{\kappa_2}E_{ad} + \sqrt{1-\kappa_2}e^{-\frac{\alpha}{8}L_{MAR}-\frac{jk_n}{4}L_{MAR}}x_1 E_1 \right) \quad (3.16)$$

Assume that $y_2 = \sqrt{1-\gamma_1}\sqrt{1-\kappa_1}e^{-\frac{\alpha}{8}L_{MAR}-\frac{jk_n}{4}L_{MAR}}y_1$, therefore

$$E_1 = \left(y_2 E_2 + j\sqrt{\kappa_1}\sqrt{1-\gamma_1}E_{in}\right) \tag{3.17}$$

Assume that $x_2 = \sqrt{1-\gamma_2}\sqrt{1-\kappa_2}e^{-\frac{\alpha}{8}L_{MAR}-\frac{jk_n}{4}L_{MAR}}x_1$, therefore

$$E_2 = \left(j\sqrt{\kappa_2}\sqrt{1-\gamma_2}E_{ad} + x_2 E_1\right) \tag{3.18}$$

When substituting (3.18) to (3.17), therefore

$$E_1 = \left(y_2\left(j\sqrt{\kappa_2}\sqrt{1-\gamma_2}E_{ad} + x_2 E_1\right) + j\sqrt{\kappa_1}\sqrt{1-\gamma_1}E_{in}\right)$$

$$E_1 = \frac{j\sqrt{\kappa_1}\sqrt{1-\gamma_1}}{1-x_2y_2}E_{in} + \frac{j\sqrt{\kappa_2}\sqrt{1-\gamma_2}y_2}{1-x_2y_2}E_{ad} \tag{3.19}$$

When substituting (3.19) to (3.18), therefore

$$E_2 = \left(j\sqrt{\kappa_2}\sqrt{1-\gamma_2}E_{ad} + x_2\left(\frac{j\sqrt{\kappa_1}\sqrt{1-\gamma_1}}{1-x_2y_2}E_{in} + \frac{j\sqrt{\kappa_2}\sqrt{1-\gamma_2}y_2}{1-x_2y_2}E_{ad}\right)\right)$$

$$E_2 = \frac{j\sqrt{\kappa_1}\sqrt{1-\gamma_1}x_2}{1-x_2y_2}E_{in} + j\sqrt{\kappa_2}\sqrt{1-\gamma_2}\left(1+\frac{x_2y_2}{1-x_2y_2}\right)E_{ad} \tag{3.20}$$

When substituting (3.20) to (3.14), therefore

$$E_4 = \left(\frac{j\sqrt{\kappa_1}\sqrt{1-\gamma_1}x_2y_1}{1-x_2y_2}E_{in} + j\sqrt{\kappa_2}\sqrt{1-\gamma_2}y_1\left(1+\frac{x_2y_2}{1-x_2y_2}\right)E_{ad}\right) \tag{3.21}$$

When substituting (3.19) to (3.13), therefore

$$E_3 = \left(\frac{j\sqrt{\kappa_1}\sqrt{1-\gamma_1}x_1}{1-x_2y_2}E_{in} + \frac{j\sqrt{\kappa_2}\sqrt{1-\gamma_2}x_1y_2}{1-x_2y_2}E_{ad}\right) \tag{3.22}$$

When substituting (3.21) to (3.1), therefore

$$E_{th}=\left(\sqrt{1-\gamma_1}\sqrt{1-\kappa_1}-\frac{\kappa_1(1-\gamma_1)x_2y_1e^{-\frac{\alpha}{8}L_{MAR}-\frac{jk_n}{4}L_{MAR}}}{1-x_2y_2}\right)E_{in}$$
$$-\sqrt{1-\gamma_1}\sqrt{1-\gamma_2}\sqrt{\kappa_1}\sqrt{\kappa_2}e^{-\frac{\alpha}{8}L_{MAR}-\frac{jk_n}{4}L_{MAR}}y_1\left(1+\frac{x_2y_2}{1-x_2y_2}\right)E_{ad} \quad (3.23)$$

When substituting (3.22) to (3.2), therefore

$$E_{dr}=\left(\sqrt{1-\gamma_2}\sqrt{1-\kappa_2}-\frac{\kappa_2(1-\gamma_2)x_1y_2e^{-\frac{\alpha}{8}L_{MAR}-\frac{jk_n}{4}L_{MAR}}}{1-x_2y_2}\right)E_{ad}$$
$$-\frac{\sqrt{\kappa_1}\sqrt{\kappa_2}\sqrt{1-\gamma_1}\sqrt{1-\gamma_2}x_1e^{-\frac{\alpha}{8}L_{MAR}-\frac{jk_n}{4}L_{MAR}}}{1-x_2y_2}E_{in} \quad (3.24)$$

The output intensities at through and drop ports are given by $I_{th}=|E_{th}|^2$ and $I_{dr}=|E_{dr}|^2$, respectively.

3.3.2 All-Optical Switching Scheme in Modified Add/drop Ring Resonator

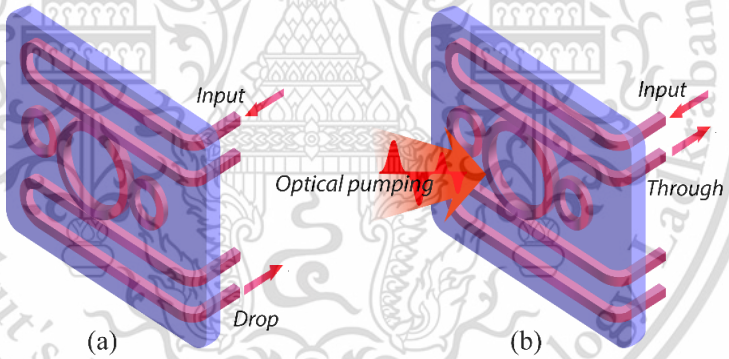

Figure 3.8 All-optical switching in modified add-drop ring resonator (MARR), where (a) no pumping signal, (b) with a pumping signal

In this scheme [94], the cross-phase modulation (XPM) is applied, which can be used to induce the decrease of the refractive index simultaneously. The optical signal output at through and drop ports can be controlled, which can make the optical switching signal at throughput port and drop port out of phase of π [97]. Regarding the plasma dispersive effect phenomena in nonlinear material, the optical logic switching at the output port of microring (throughput port and drop port) can be formed within InGaAsP/InP material based [46], [80], and represented the NOT gate, as shown in Figure 3.8. Results of the configuration by exciting on top of modified add/drop ring resonator are obtained simultaneously and seen at the drop and through ports, respectively, which can be functioned as the all-optical switch.

Since the bandgap wavelength of AlGaAs is around 800 nm, and InGaAsP's is around 1300 nm, hence $E_{g(InGaAsP)}=E_{g(AlGaAs)}$. In the microring waveguide, the pump pulse is almost completely absorbed, and high-density free carriers are produced. This carrier effectively results in a net decrease in the microring waveguide's refractive index and causes the resonance wavelength to temporarily blue shift [92]. The output probe signal would be modulated if the probe beam were adjusted to one of microring resonant wavelengths. The modulation depth depends on the resonance-wavelength shift magnitude. The steeper the resonant profile, i.e., the higher the finesse of the cavity, the greater the output signal modulation for a given shift in wavelength.

In the simulation [94], to perform the optical switching with an optimum result for the all-optical switch, the parameters of modified add/drop ring resonator are fixed to be $\kappa_1=0.5$, $\kappa_2=0.25$, $\kappa_3=0.5$, and $\kappa_4=0.25$, respectively. The ring radii $R_{ad}=5\ \mu m$ for microring resonator, $r_L=1.5\ \mu m$, and $r_R=1.5\ \mu m$ for left and right nanoring resonators. In order to make the system associate with the practical device [12], the selected parameters of the system are fixed to $n_0=3.34$ (refractive index of InGaAsP/InP), effective areas $A_{eff(MRR)}=0.5\ \mu m^2$, and $A_{eff\ (NRR)}=0.25\ \mu m^2$ for a microring resonator and nanoring resonator, respectively. Attenuation loss of light propagating within the system (i.e., waveguide) is $\alpha=0.5\ dB/mm$, and coupling loss $\gamma=0.1$. The nonlinear refractive index of the microring used is $n_2=2.2\times10^{-17}\ m^2/W$. The soliton input pulse has the wavelength at $\lambda_1=1.55\ \mu m$, peak power at $P_{IN}=1\ mW$, and the control signal with wavelength at $\lambda_2=1.25\ \mu m$, peak power at $P_P=1.6\ mW$, for pumping on top of microring. Both signals have a pulse width of 20 fs.

In the case of simulation, the author used two software to simulate the mathematical modeling and the physical modeling of the device such as MATLAB and Lumerical FDTD method. The simulation resulted from the FDTD method are shown in Figure 3.9 and Figure 3.10.

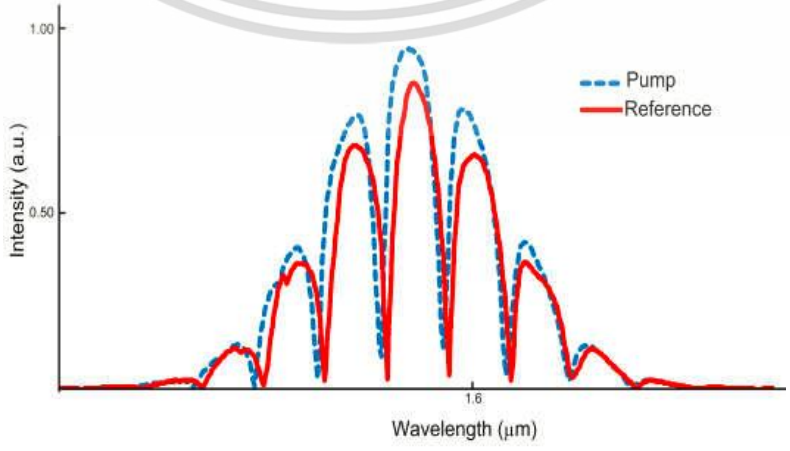

Figure 3.9 Simulation result of optical switching using the FDTD method

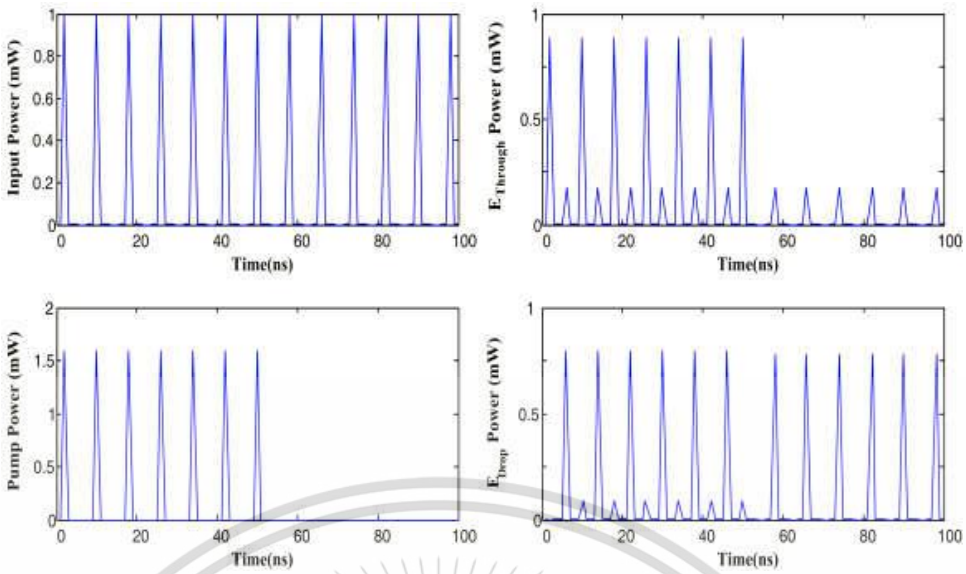

Figure 3.10 Simulation results with and without pumping signal

The optical logic switching for the simultaneous output is illustrated, which can be shown as follows in Table 3.4. This can be inferred that the input signal will be sent to the drop port (DR) if there is no control signal (the signal at the add port of a microring resonator). On the other hand, when the control signal is applied, the waveguide's refractive index is changed and causes the resonant wavelength to change. Hence the input signal is transmitted directly through port (TH).

Table 3.4 Modified add/drop ring resonator used as an optical switch

Input		Pumping		Output			
E_{IN}	P_{IN}(mW)	E_P	P_P(mW)	E_{TH}	P_{TH}(mW)	E_{DR}	P_{DR}(mW)
0	0	0	0	0	0	0	0
1	1	0	0	1	0.8	0	0.2
1	1	1	1.6	0	0.2	1	0.8

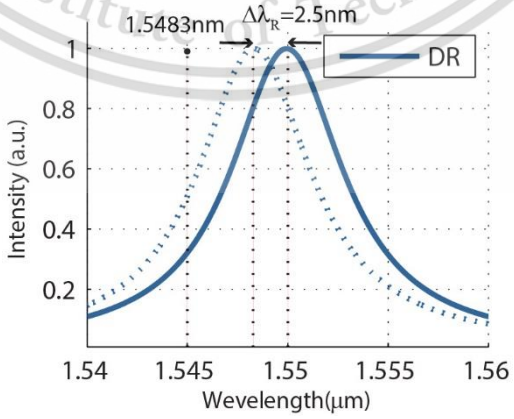

Figure 3.11 The pulse shift.

The all-optical switch base on modified add/drop ring resonator by using carrier injection control the switching at through and drop ports has been demonstrated, where the advantages of the system are the switching speed (τ_{sw}), low power consumption and each tunable channel can be operated independently. Therefore, the pumping energy is closed to the bandgap energy of material for refractive index changed due to the resonant wavelength of the microring changed. The all-optical switching operation can be replaced by the use of the electronic device, in order that increases the speed of communication. The proposed system is flexible and straightforward logic switching. Besides, this system can be expanded by proper integration of dark-bright soliton control-based optical switches, which can be required for more advanced applications, for a higher number of input digits implementation.

However, the modified add/drop ring resonator device remains not fabricated. Therefore, to make the work associated with the fabricated device, the practical parameters of the microring resonator is used in the design circuit and simulation to perform the arithmetic and logic operation all-optically.

3.4 All-Optical Half Adder/Subtractor based on Optical Switching

Half adder/subtractor circuit is a 2-bits binary addition or subtraction circuit which has two inputs and two outputs. From the tree-architecture circuit [7], the half adder and subtractor circuits can be built. As illustrated in Figure 3.13, all-optical half adder/subtractor based dark-bright soliton conversion control technique has been proposed [95]. This technique relied on dark-bright soliton behavior within the $\pi/2$ phase shift device (optical coupler) in which a beam combiner is integrated with the outputs T2-port ($\overline{X}Y$) and D3-port ($X\overline{Y}$) in order to represent the XOR logic operation where the arithmetic operations can be performed simultaneously at drop-port and through-port, respectively. Here the Carry and Borrow signals are represented by outputs T3-port and D3-port, respectively. The proposed half adder/subtractor circuit can be applied to design an all-optical full adder/subtractor circuit, which will be described in the next section.

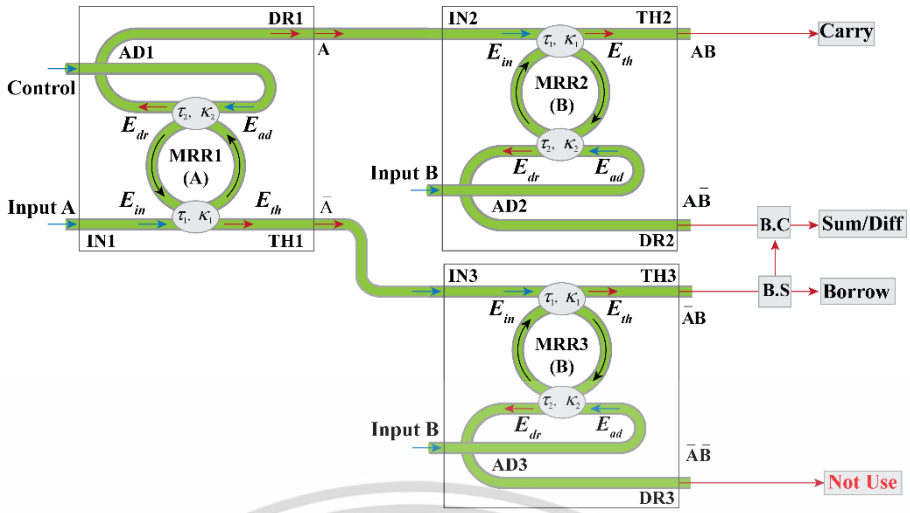

Figure 3.12 All-optical simultaneous half adder/subtractor circuit.

Table 3.5 The optimum parameters used in the simulation of half adder/subtractor.

Parameters	Value
Coupling coefficients of the center ring (κ_1=κ_2)	0.5
Resonant wavelength (λ_0)	1550 nm
Ring radius (R)	1500 nm
The effective area of the waveguide (A_{eff})	0.25 μm^2
Linear absorption coefficient (α)	0.05 dB/mm
Coupling loss (γ)	0.01
The effective refractive index of the waveguide (n_{eff})	3.34
Change of refractive index when the waveguide is induced (Δn)	3.5×10^{-3}
Resonant wavelength when the waveguide is induced by pumping (λ_1)	1.54 μm
Input power (P)	2.25 mW

From the simulation results of the system, as shown in Figure 3.13, the output is shown in Figure 3.14, where the Sum/Diff signal becomes logic "1" when the input signal is dark-bright (logic "01"), and bright-dark (logic "10"). In the same way, the Carry signal becomes logic "1" when the input signal is bright-bright (logic "11"), and the Borrow signal becomes logic "1" only when input is dark-bright (logic "01"). The figure illustrates the simulation results of the all-optical half adder/subtractor circuit when inputs are logic "00", "01", "10", and "11", respectively.

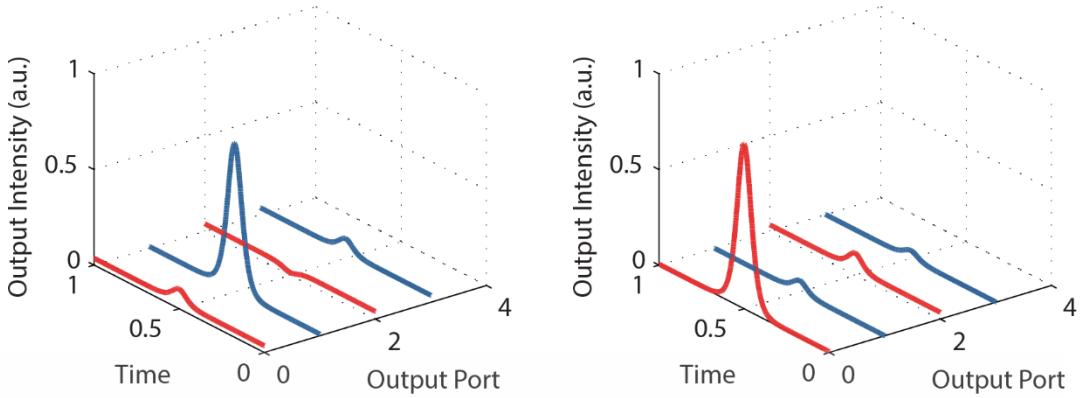

(a) when input logic 00 (b) when input logic 01

Figure 3.13 The simulation results when the input logic is (a) AB=00, (b) AB=01 [95].

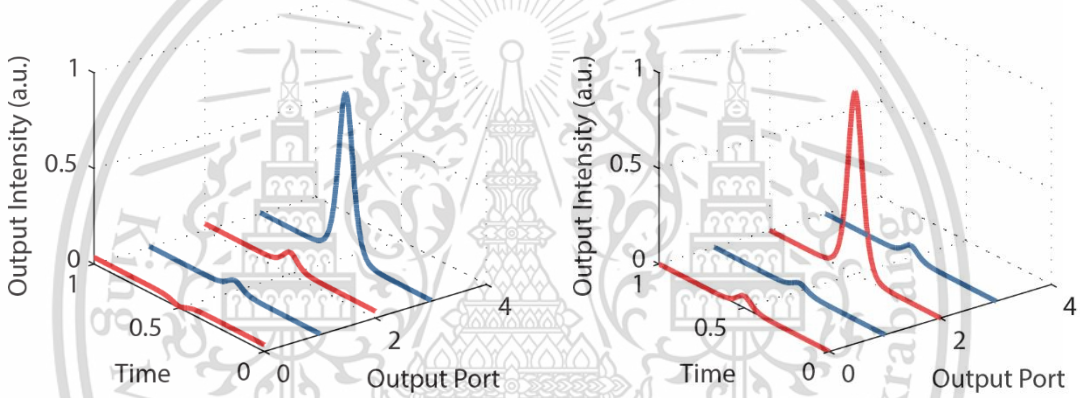

(a) when input logic 10 (b) when input logic 11

Figure 3.14 The simulation results when the input logic is (a) AB=10, (b) AB=11 [95].

From the obtained output signals, as illustrated in Figure (3.14 to 3.15), we can see that the ripple output energy is about 0.1. This ripple energy can be tuned and controlled by increasing or reducing the control signal (dark soliton) before inputting into the system. Moreover, from the simulation results using parameters, as shown in Table 3.5, we obtained new parameters, as illustrated in Table 3.6.

Table 3.6 The other parameters obtained from the simulation.

Parameters	Value
Maximum transmission at through-port ($TH_{\max}$)	1
Minimum transmission at through-port ($TH_{\min}$)	0.0243
On-Off ratio	41 dB
Free spectral range (FSR)	6 nm
The full width at half-maximum (FWHM)	0.56 nm
Quality factor (Q)	2767
Finesse (F)	10.71
Cavity time (τ_{cav})	2.276 ps
Switching time (τ_{sw})	0.14 ps

3.4.1 Performance Comparison

The proposed method uses the nonlinear pulse in all operations, which is an optical pulse that can keep its irregular pulse shape during the transmission. This optical pulse can further be travel for long distances with a slight loss, which is suitable for binary bit data communication. The limit in the performance of the proposed method depends on the free-carrier lifetime of the used material (for InP is about 100 ps) [64]–[66]. The control pulse width using for inducing the change of the refractive index of the medium must be higher than the value of τ_{cav} of the device.

From the simulation results, the value of τ_{cav} of the proposed method for different sizes of ring radius shown in Table 3.7. The bit-rate comparison of each technology shown in Table 3.8.

Table 3.7 The values of τ_{cav} resulted from different ring radii.

Sizes of ring radii	Values of τ_{cav}
5 μm	0.878 ps
10 μm	1.58 ps
20 μm	3.184 ps
50 μm	7.984 ps
100 μm	15.92 ps

Table 3.8 The bit-rate comparison with other techniques.

Technologies	Bit-rate
Ring resonator	40 Gbps
MZI	40 Gbps
TOAD	10-20 Gbps

Chapter 4
DESIGN CIRCUITS AND SIMULATION RESULTS

4.1 All-optical Full Adder/Subtractor based on Optical Switching

4.1.1 Propose Circuit

This section proposes the design of an all-optical circuit performing two arithmetic operations, i.e., full addition and full subtraction. The designed circuit has a continuous wave input (CW), three control inputs (X, Y, and Z), and tree outputs representing the results of summation or difference (SUM/DIFF), Carry, and Borrow.

The designed block diagram for all-optical full adder/subtractor is shown in Figure 4.1(a), and the designed circuit using six microring resonators is illustrated in Figure 4.1(b). The outputs of SUM or DIFF can simultaneously be obtained, in which input "S" is the selector for control the signal coming from Borrow or Carry to be transmitted to the output "C_0" to identify the operation of the circuit when will be full adder or full subtractor. The outputs of SUM and DIFF will always be the same logic in every case of "XYZ" logic inputs.

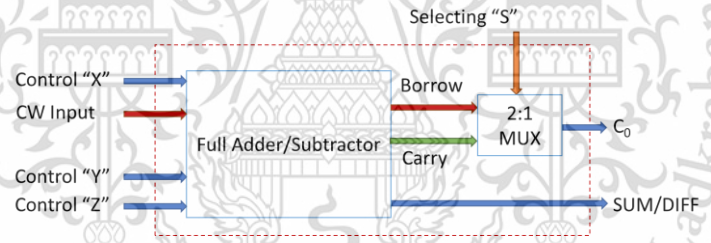

(a) Block diagram of all-optical full adder/subtractor

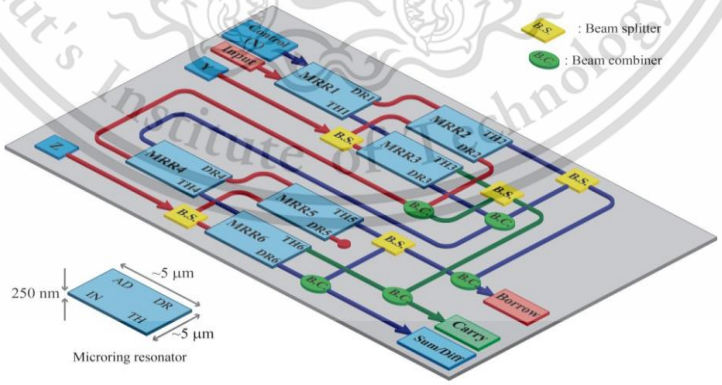

(b) all-optical full adder/subtractor circuit

Figure 4.1 Designed circuit of all-optical full adder/subtractor based on microring resonators, where input is a continuous wave (CW), X, Y and Z are control inputs, MRRs: microring resonators, IN IS input port, TH: throughput port, DR: drop port, and AD: add port.

The designed circuit consists of six microring resonators with four series stages, five beam splitters (BS), and five beam combiners (BC). Here the approximate physical size of a microring resonator (including bus waveguides) is 5 μm wide, 5 μm long, and 250 nm thick. The width of waveguides is approximately 290 nm to 440 nm, and the ring radius of ring resonators is 1.5 μm [15].

To perform full addition or full subtraction as illustrated in Figure 4.2, when the input and control pulses are initially inserted into first microring resonator (MRR1) using dark soliton (logic 0) or bright soliton (logic 1). The optical solitons converted to dark and bright solitons through MRR1, and the soliton outputs can be seen simultaneously at through and drop ports of MRR1 with π phase-shifted [80]. Therefore, MRR1 functions as an inverter gate-like at TH1 port and buffer gate-like for DR port. Consequently, outputs of MRR1 can be written as $TH1=\bar{X}$ for throughput port, and $DR1=X$ for drop port, as illustrated in Figure 4.2. The output signals from MRR1 applied to the next stage as the inputs of MRR2 and MRR3.

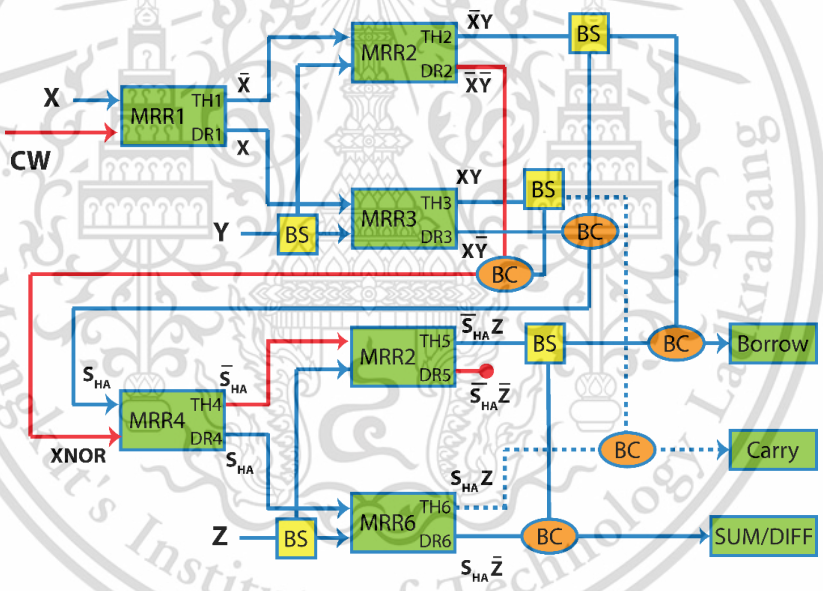

Figure 4.2 Algebraic expression of all-optical full adder/subtractor circuit

Next, logic 0 (dark soliton) or logic 1 (bright soliton) data input (Y) is applied to add ports of MRR2 and MRR3, the dark-bright soliton conversion with π phase shift is re-operated. The outputs are obtained simultaneously for all-optical logic operation at the output ports of MRR2 and MRR3. The outputs can be written as $TH2=\bar{X}Y$, $TH3=XY$ for throughput ports, and $DR2=\bar{X}\bar{Y}$, $DR3=X\bar{Y}$ for drop ports of MRR2 and MRR3, respectively. This method can be used to perform all-optical half adder (HA) and half-subtractor (HS) as following.

- Summation or Difference of HA/HS is the combined signal from TH2 and DR3 ports ($S_{HA}=D_{HA}=\bar{X}Y+X\bar{Y}$).

- Carry of HA is the signal from TH3 port ($C_{HA}=XY$).
- Borrow of HS is the signal from TH2 port ($B_{HA}=\overline{X}Y$).

To operate the all-optical HA and HS [95], it can be achieved simply by using beam splitters (BS) and beam combiners (BC), e.g., fiber couplers or optical Y-branches, where the beam splitters used in the designed circuit are not polarized, and the reflection-transmission ratio for all incident light is 50:50 (or 50 percent).

The outputs of the first HA/HS stage is obtained and is transmitted as the input signals (S_{HA}, D_{HA}, C_{HA}, B_{HA}) for the next HA/HS stage via input and add ports of MRR4. Consequently, the dark-bright soliton conversion is re-operated, and the outputs of MRR4 are $TH4=S_{HA}$ for throughput (TH4) port and $\mathrm{DR4}=\overline{S_{HA}}$ for drop port (DR4). Both output signals are then used as input signals of MRR5 and MRR6, respectively.

In this stage, the control input pulse "Z" with logic "0" or logic "1" is entered into both MRR5, and MRR6 via add ports (see Figure 4.2), then MRR5 and MRR6 are re-operated with the dark-bright conversion. The output is seen at the output ports simultaneously at output ports $TH5=\overline{S_{HA}}Z$, $\mathrm{DR5}=\overline{S_{HA}}\bar{Z}$, $TH6=S_{HA}Z$, and $DR6=S_{HA}\bar{Z}$. Therefore, all-optical full adder/subtractor can be finally performed by combining optical signals from output ports of MRR2, MRR3, MRR5, and MRR6 using beam combiners, where the algebraic expression of full addition and full subtraction are expressed by (4.1) – (4.4).

$$\mathrm{Sum}=\overline{S_{HA}}Z+S_{HA}\bar{Z}=TH5+DR6 \quad (4.1)$$

$$\mathrm{Carry}=XY+S_{HA}Z=TH3+TH6 \quad (4.2)$$

$$\mathrm{Diff}=\overline{D_{HA}}Z+D_{HA}\bar{Z}=TH5+DR6 \quad (4.3)$$

$$\mathrm{Borrow}=\overline{X}Y+\overline{S_{HA}}Z=TH2+TH5 \quad (4.4)$$

Based on optical switching methodology in the nonlinear device (MRR), the operations of all-optical arithmetic can be achieved. The simulation results and the discussion are provided in the next section.

4.1.2 Simulation Result

In the simulation, we assumed that the outputs from the first stage and second stage of HA/HS are synchronized in time when they are combined. The optimum parameters are expressed in Table 4.1. The parameters are fixed for all MRRs in the circuit. Wherein this case, the ring radius is set to respond to the resonant wavelength at 1.550 μm. The input is a continuous wave (CW), and the control inputs "XYZ" is formed by dark or bright soliton. Here, the width and the length of the waveguides connected between MRRs are not considered.

Table 4.1 Optimum parameters for all MRRs used in the simulation

Symbol	Definition	Value
R	Ring radius	1.551 μm
L	Diameter of	9.745 μm
A_{eff}	The effective mode core area	0.25 μm^2
α	Attenuation loss within the ring	0.05 dB/mm
κ	Coupling coefficient	0.25
γ	Coupling loss	0.01
n_{eff}	The effective refractive index of waveguide (InGaAsP/InP)	3.34
n_2	Nonlinear index of refraction of InGaAsP/InP	4.27×10^{-17} cm^2/W
P	Input power	1 mW
λ_R	Resonant wavelength	1.55

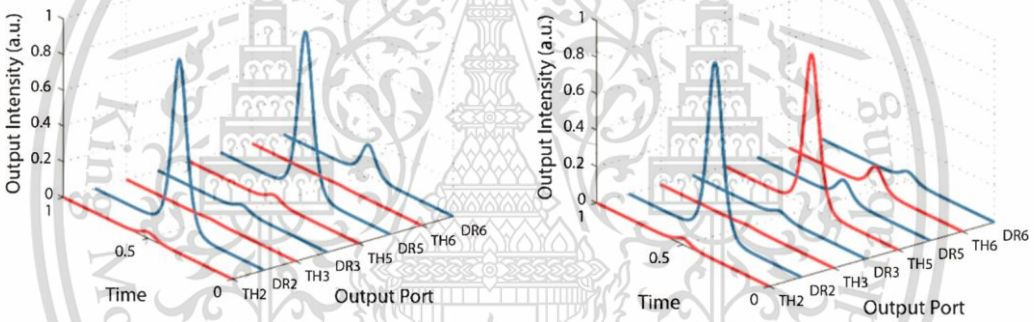

(a) output logic when input is 000 **(b)** output logic when input is 001

Figure 4.3 Output intensities at throughput and drop ports when inputs "XYZ" are logic (a) 000, (b) 001.

Figure 4.3(a) shows the signal transmitted at the full adder/subtractor output ports for the first state where XYZ control inputs are logic 000. Initially, the continuous input signal entered via the input port into MRR1, and there is no control signal (X=0), and therefore the optical signal is transmitted to the DR1-port due to the resonance state. The optical signal from DR1-port is immediately entered via an input port into MRR2, as there is no control input (Y=0) added to MRR2, such that the optical signal can exist at DR2-port and be defined as an optical data logic 1. The optical signal from the DR2 port is then used to input the MRR4 via the input port, and the output signal is appeared at the DR4-port due to the resonance condition. The signal is then fed into the MRR5 input port since no control input (Z=0) is added to MRR5, and so that the optical signal is again transmitted to DR5-port due to the

resonance condition and reflects the 01000100 optical logic at the TH2, DR2, TH3, DR3, TH5, DR5, TH6, and DR6 output ports respectively.

Figure 4.3(b) shows the signals transmitted when logic 001 is the XYZ inputs. In this situation, the initial state is the same as the earlier case where control inputs X and Y (XY=00) are not applied. The input signal is therefore transmitted to the DR2-port and DR4-port and then entered via the input port into the MRR5. The control input Z (Z=1) is used for this state, so the optical signal is transferred from DR5-port to TH5-port and presented at the output ports as optical logic 01001000.

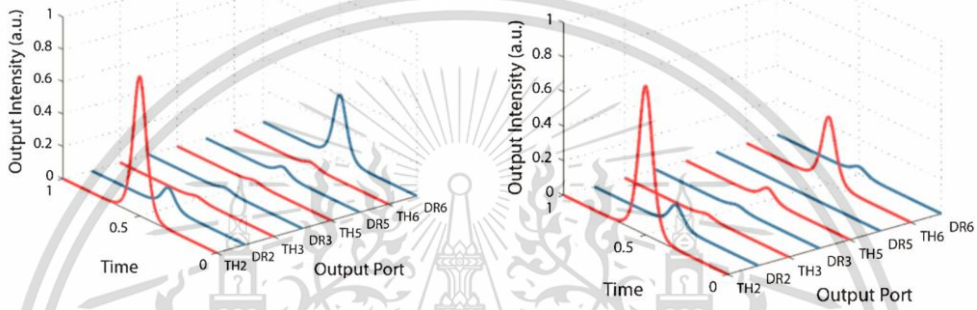

(a) the output logic is when input is 010 **(b)** output logic when input is 011

Figure 4.4 Output intensities at throughput and drop ports when inputs "XYZ" are logic (a) 010, (b) 011.

Figure 4.4(a) shows output signals at logic 010 inputs. There is no control input (X=0) applied to MRR1 in this case. Therefore, the input signal is again transmitted to the DR1-port. Next, the DR1-port signal is input to MRR2 via the input port, and the control input (Y=1) is applied to MRR2 via the add port, so the optical signal is switched from DR2-port to TH2-port as an optical logic 1. The TH2-port signal is then used as the MRR4 input signal via the add port and appears at the TH4-port caused by the resonance condition and then added to MRR6 via the input port. For this state, control input (Z=1) is applied via add port to MRR6, and therefore the optical signal is transmitted to the DR6 port and is defined as 10000001 optical logic at TH2, DR2, TH3, DR3, TH5, DR5, TH6, and DR6 output ports respectively.

Figure 4.4(b) shows the outputs when logic 011 is input XYZ. This case is the same as for the first and second states in which control signals are applied (XY=01), and the optical signal is transmitted to TH2-port and represented as optical logic 1. The TH2-port signal is then used as the MRR2 input signal via add port and appears at TH4-port due to resonance condition and is then applied to MRR6. Since the control input (Z=0) is applied in this state, the optical signal appears at the TH6 port and is represented at the output ports as optical logic 10000010, respectively.

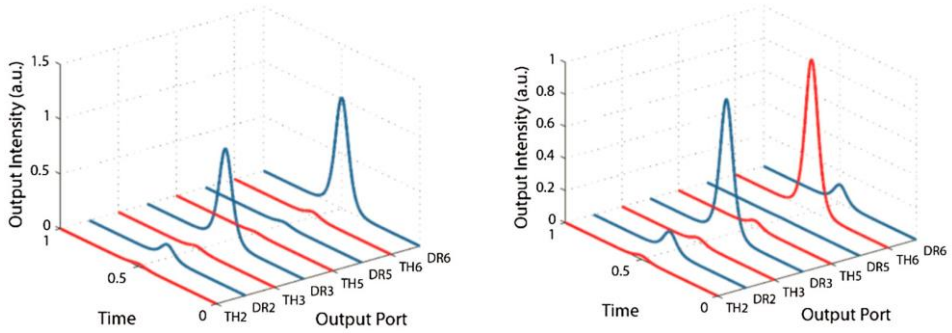

(a) output logic when input is 100 **(b)** output logic when input is 101

Figure 4.5 Output intensities at throughput and drop ports when inputs "XYZ" are logic (a) "100", (b) "101".

Figure 4.5(a) shows the outputs when the XYZ inputs are "100" logic. The control pulse is applied to MRR1 (X = "1") in this case, which transmits the input signal to TH1-port. Next, the TH1-port signal is entered via the input port into MRR3, and the control input (Y = "1") is applied to the AD2-port so that the optical signal appears as the optical logic "1" at the TH3-port. The TH3-port signal is then used as the MRR4 input signal via the input port and appears at the DR4-port due to the resonance condition, and the signal is then entered into MRR6. For this stage, no control input (Z = "0"), therefore, the optical signal appears at DR6-port, and the output logic at ports TH2, DR2, TH3, DR3, TH5, DR5, TH6, and DR4 are optical logic "00010001".

Figure 4.5(b) shows the outputs when logic "101" is the XYZ inputs. For the first and second states, since there are no control inputs (XY = "10"), this case is the same as the previous case, and the optical signal is transmitted as optical logic 1 to the DR3-port. The control input (Z = "1") is applied in this state. Therefore, the optical signal from MRR4 appears at the TH6-port and is represented at the output ports, respectively, as optical logic "10000010".

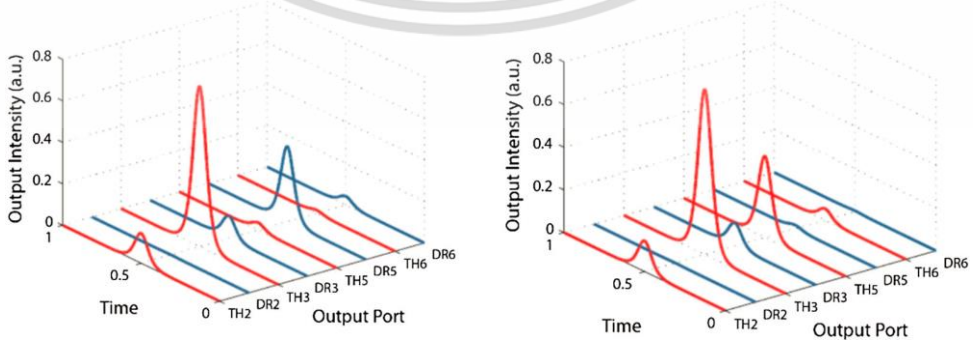

(a) output logic when input is 110 **(b)** when input is 111

Figure 4.6 Output intensities at throughput and drop ports when inputs "XYZ" are logic (a) "110", (b) "111".

Figure 4.6(a) illustrates the outputs, while XYZ inputs are logic “110”. In this case, the control signal is applied to MRR1 (input X = “1”), which caused the input signal to be transmitted to TH1-port. The control input (Y = “1”) is then added to MRR3, so the signal from MRR1 (TH1-port) is transmitted as an optical logic “1” to the TH3-port of MRR3. The signal from TH3-port is forwarded again as the MRR4 input signal via the input port and is then appeared at the DR4 port. The signal is then sent to MRR5. No control input (input Z = “0”) is used for this state. Therefore, the optical signal appears at the DR5-port and is shown as “00100100” optical logic at the TH2, DR2, TH3, DR3, TH5, DR5, TH5, and DR5, respectively.

Finally, the output logic is shown in Figure 4.6(b) when the XYZ input is logic “111”. This case is the same as the previous case for the first and second stages where two control signals (input XY = “11”) are applied, and the optical signal is then transmitted as an optical logic 1 to TH3-port. The control input (input Z = “1”) is applied to MRR5 in this state. Therefore, the optical signal from the DR4-port of MRR4 appears at the TH5-port of MRR5 and is transmitted to output ports as “00101000” optical logic output.

Table 4.2 Simulation result of all-optical full adder/subtractor

Input			Output Intensity								Output logic		
X	Y	Z	TH2	DR2	TH3	DR3	TH5	DR5	TH6	DR6	Carry	Sum/Diff	Borrow
0	0	0	0	0.9	0	0	0	0.8	0	0.1	0	0	0
0	0	1	0	0.9	0	0	0.7	0.1	0.1	0	0	1	1
0	1	0	0.8	0.1	0	0	0	0	0	0.3	0	1	1
0	1	1	0.8	0.1	0	0	0	0	0.3	0	1	0	1
1	0	0	0	0.1	0	0.8	0	0	0	0.9	0	1	0
1	0	1	0	0.1	0	0.8	0	0	0.8	0.1	1	0	0
1	1	0	0.1	0	0.7	0.1	0	0.1	0	0.3	1	0	0
1	1	1	0.1	0	0.7	0.1	0.3	0	0	0	1	1	1

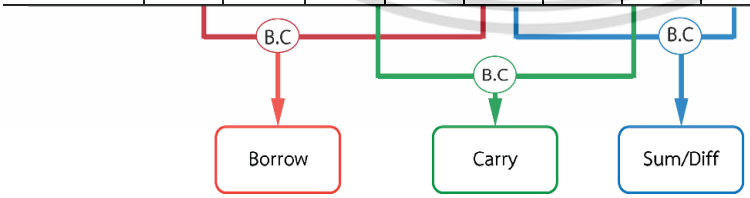

Note $TH2=\bar{X}Y$, $DR2=X\bar{Y}$, $TH3=XY$, $DR3=X\bar{Y}$, TH5=$\overline{S_{HA}}Z$, DR5=$\overline{S_{HA}}\bar{Z}$, $TH6=S_{HA}Z$, and $DR6=S_{HA}\bar{Z}$. The minimum intensity of logic “1” must higher than 0.2.

The description of the optical logic output states for the FA/FS circuit from the output ports are expressed in Table 4.2. Here, Summation or Difference can be performed using a beam splitter and beam combiner to split and combine the

output intensities transmitted to output ports of the circuit as the result of summation or difference, Carry, and Borrow, as expressed in (4.1) – (4.4). The Summation of FA is $Sum=TH5+DR6$, and Carry is $Carry=TH3+TH6$. The Difference of FS is $Diff=TH5+DR6$, and Borrow is $Borrow=TH2+TH5$.

The dark and bright soliton pulses represent the input signals and the control signal as logic "0" and logic "1", respectively. The input signal is input into the input port while the control signal is input into add port. In Figure 4.2(b), the DR2-port (red line) and TH3-port (green line) signals can either be the same or different depending on the resonant wavelengths of the control signals (X and Y). For the optical switching scheme, when both control signals X and Y are not applied to MRR1 and MRR2, most signal power from the input port is transmitted to DR2-port while the TH3-port signal is the remaining input power. In other words, when both control signals X and Y are applied to MRR1 and MRR3, most of the signal power from the input port is transmitted to TH3-port, whereas the signal at DR2-port is the tiny signal power remains. Moreover, all DR2-port and TH3-port signals are combined and used as the MRR4 input signal, while the MRR4 control signal is the TH2-port and DR3-port combination (blue lines) signal. Using additional Erbium-doped fiber amplifiers (EDFA) can manipulate this control signal and the input signal for the next stage.

4.1.3 Ring Resonator Parameter Analysis

The advantages of short output pulse generation, which is the purpose of this research, are light moving within the nonlinear material microring. In which ultra-short pulses will give the ultra-fast transmission [98]. The soliton equation is required to appear along with the result due to the more significant nonlinear effect caused by the Kerr effect that would affect the soliton pulse. The single soliton pulse is sliced to be multi-peaks, from which the single peak is shorter in time [99]. The scale of the device is within the current capacity of fabrication technology (the minimum size is 1.5 μm ring radius [15]). The adjustable input wavelength is 1.55 μm, which is necessary for math with the input solitons for witching identification. It is possible to calculate the initial estimated propagation time by $\tau_{pr}=OPL\times n_{eff}/c$, where OPL is the most extended optical path length along four microrings (MRR1 to MRR2 to MRR4 to MRR5) that the signal propagates from the MRR1 input port (IN-1) to the MRR5 drop port (DR-5), seen in Figure 4.1(b). Here, the length of the waveguides connected between four MRRs is not considered due to the connecting length depending on the fabrication technology.

$$\text{For through ports: } \tau_{pr}=\frac{(4\times 2\pi R)n_{eff}}{c} \tag{4.5}$$

$$\text{For drop ports: } \tau_{pr}=\frac{(4\times 3\pi R)n_{eff}}{c} \tag{4.6}$$

where n_{eff} is the effective refractive index of InGaAsP/InP (n_{eff}=3.34), and c is the speed of light in a vacuum.

The estimated time of propagation after inputting the signal is less than 1 ps and approximately equal to 0.42 ps at TH5-port and approximately equal to 0.62 ps at DR5 port. Therefore, the estimated operational speed of the circuit is about 40 Gb/s. It is higher compared with MZI (2.5 to 10 Gb/s) and TOAD (10 Gb/s) technologies. The coupling coefficient (κ) indicates the level of energy induced at the coupling length into the cross waveguide. This coefficient can be modified in practice by adjusting the gap between the input waveguide and a ring resonator.

In the simulation, it is a soliton pulse in which the high-level signal is retained because of the soliton pulse property called the self-phase modulation. In this design system, all input and control signal (XYZ) is an optical soliton. The controlled input wavelength is 1.55 μm. The required power to make the switching device activated is 2.25 mW. All devices are available through the existing fabrication technology in this model. The beam splitter and combiner can be replaced with the optical coupler, and a ring resonator with a small radius of 1.5 μm is already fabricated [15].

4.2 All-optical Logic AND Gate and OR Gate Circuit based on Microring resonators

4.2.1 Design circuit

The designed circuit of all-optical logic AND gate and OR gate [109] is shown in Figure 4.7. The circuit has a continuous wave input, which is divided into two pulse inputs into input ports of MRR2 and MRR3, and two control inputs "A" and "B" represent the inputs of AND gate and OR gate circuit. The output of the AND gate can be written seen at TH2 port of MRR2 (AB), and the output of the OR gate can be obtained from the combination of signals from output ports DR2 of MRR2 and TH3 of MRR3 ($A\overline{B}+B$), respectively.

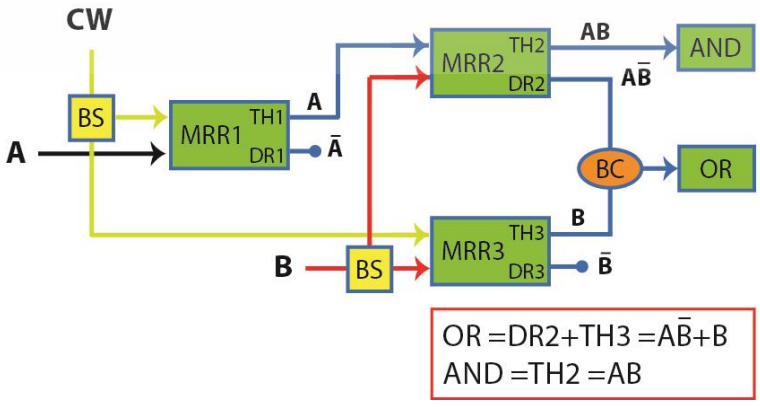

Figure 4.7 Design circuit of all-optical logic AND gate and OR gate.

4.2.2 Simulation Result

In a simulation, the parameters of all microring resonators are fixed as the same with the parameters in Table 4.1 in the previous section.

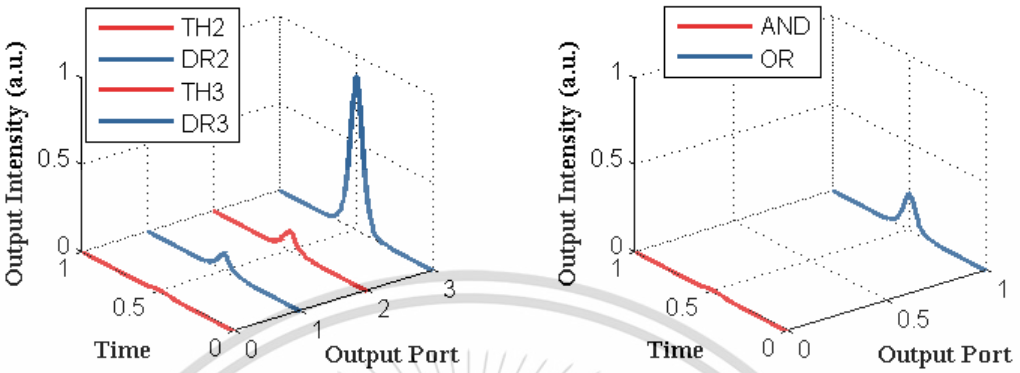

Figure 4.8 Simulation result when control input "AB" = "00", (a) output signal of MRR2 and MRR3, (b) AND gate and OR gate output.

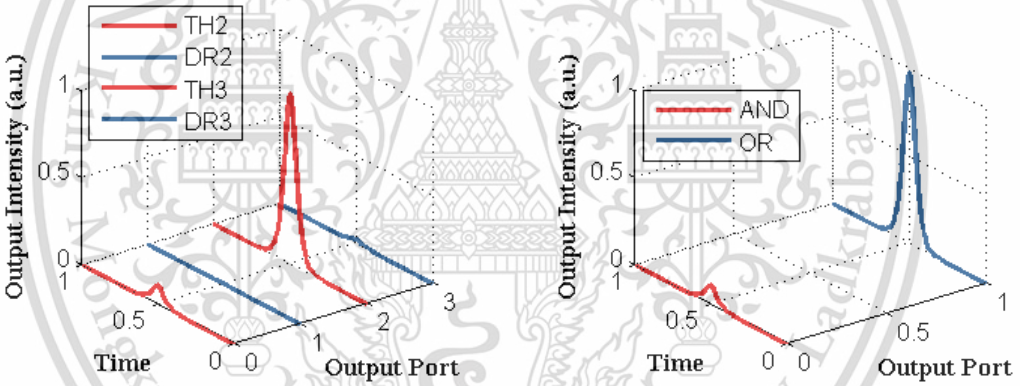

Figure 4.9 Simulation result when control input "AB" = "01", (a) output signal of MRR2 and MRR3, (b) AND gate and OR gate output.

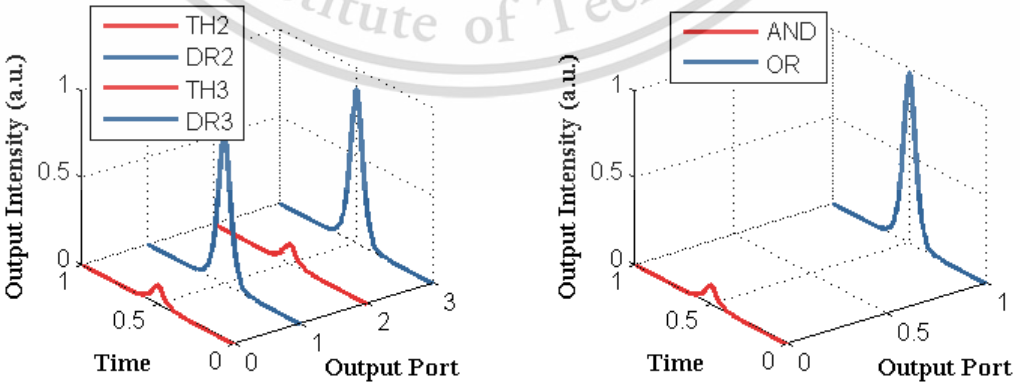

Figure 4.10 Simulation result when control input "AB" = "10", (a) output signal of MRR2 and MRR3, (b) AND gate and OR gate output.

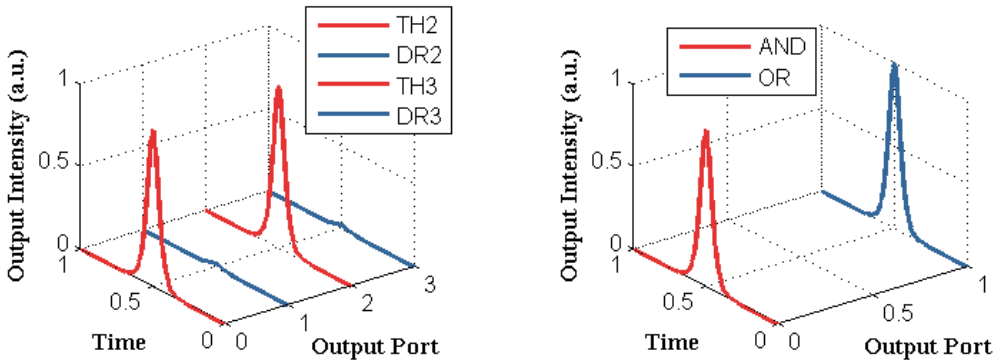

Figure 4.11 Simulation result when control input "AB" = "11", (a) output signal of MRR2 and MRR3, (b) AND gate and OR gate output.

Table 4.3 Output intensity of all-optical logic AND gate and OR gate

Input	Control inputs		Output intensity				Output logic gate	
CW	A	B	TH2	DR2	TH3	DR3	AND (TH2)	OR (DR2+TH3)
ON	OFF	OFF	0.01	0.09	0.1	0.8	0.01	0.2
ON	OFF	ON	0.1	0	0.9	0.02	0.1	0.9
ON	ON	OFF	0.1	0.8	0.1	0.8	0.1	0.9
ON	ON	ON	0.9	0.02	0.9	0.02	0.9	0.9

4.3 All-optical 2:1 Multiplexers based on Microring Resonators

An optical add-drop multiplexer (OADM) is an essential part of an optical fiber network in optical communication. A multiplexer combines two or more lower-bandwidth data streams or multiplexes into a single light beam. In electronics, a multiplexer (MUX), also known as a data selector, is a device that selects and transfers it to a single output line between several analogs or digital input signals. The optical fiber bandwidth properties are well known and make it the chosen medium for high-speed data. Nonetheless, this bandwidth requires different types of multiplexing. Optical-multiplexer and de-multiplexer are mostly passive optical filter systems that are designed to filter specific wavelengths (usually optical fiber) in and out of the transportation system. The process of filtering the wavelength can be performed using various techniques such as prisms, thin-film filters, dichroic filters, or interference filters. Microring resonator is used in this work in order to perform optical add-drop multiplexer, a device used in wavelength division multiplexing system for multiplexing and routing different channels of light into or out of a single-mode fiber (SMF) of microring resonator system as well.

The concept of using a microring resonator to perform an OADM has been proposed [83], [100]. A modified add-drop ring resonator is formed by an add-drop

filter, which modulated by two nonlinear side ring phase resonators [101]. When the input light fed into the system, the nonlinear effect is induced by the two side rings into the center ring, which has a few benefits in various applications as follows. Firstly, the nonlinear effect coupled into the center ring and the faster switching output pulse obtained [102], which can apply for a higher transmission bit rate than the add-drop filter. However, the energy conservation maintained while the power increased due to the shorter pulse width. Secondly, the self-pumping of the system obtained using the suitable control of the two side ring parameters and input power, where the signal amplification obtained [103]. Thirdly, the whispering gallery mode of the system is obtained by controlling the two side ring parameters, which can be applied for a wireless transmission link [104], [105].

Lastly, the space-time function can apply to form the space-time function-controlled system, which can use in various applications [106]–[108].

In Figure 4.12 2:1 multiplexer can be designed based on an optical switching scheme in MARR, where IN: input port, TH: throughput port, AD: add port, and DR: drop port. Figure 4.12(a), when the pump signal is not injected (selected input S=0), the signal coming from IN-port is dropped at DR-port, while the signal coming from AD-port is transmitted into TH-port of MARR. Figure 4.12(b), when the pumping signal is injected, which causes the change of the refractive index of MARR, therefore, the signal coming from IN-port is switched to TH-port, and the signal coming from AD-port is transmitted to DR-port, respectively.

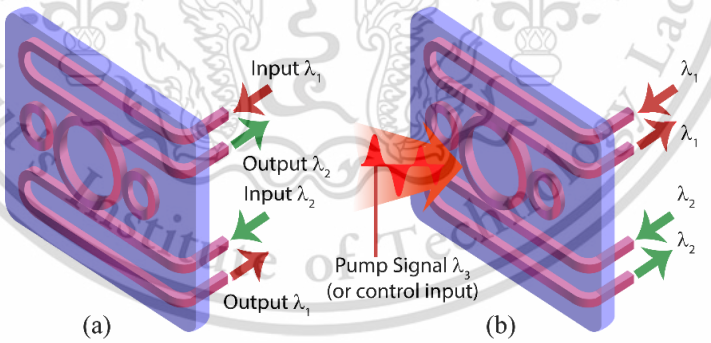

Figure 4.12 All-optical 2:1 multiplexer based on nonlinear ring resonator; λ_1 and λ_2 are resonant wavelengths, λ_3 is the wavelength of pumping signal.

When considering the transfer function of the modified add-drop ring resonator (MARR) [94], the mathematical model is the same with section 3.3.1. In this case, the input port is used for the first input, and the add port is used for the second input. The summary of the optimum parameters of 2:1 add/drop MUX used in the simulation is expressed in Table 4.4. The left and right MRRs radii are 1.551

μm, in order to make the device response for center wavelength 1.55 μm and associate with the practical device.

Table 4.4 Parameters of modified add/drop multiplexer used in the simulation

Symbol	Definition	Value
R	Center ring radius	5 μm
rL, rR	Left and right ring radii	1.5 μm
A_{eff1}	The effective mode core area for the center ring	0.5 μ m^2
A_{eff}	The effective mode core area for left and right ring	0.25 μm^2
α	Attenuation loss within the ring	0.05 dB/mm
κ_1, κ_2	Coupling coefficients between ring resonators	0.25
κ_3, κ_3	Coupling coefficients between ring and waveguides	0.5
γ	Coupling loss	0.01
n_{eff}	The effective refractive index of MRRs (InGaAsP/InP)	3.34
n_2	Nonlinear index of refraction of InGaAsP/InP	4.27×10^{-17} cm^2/W
Δn	Change of refractive index when applying control	3.5×10^{-3}
λ_R	Resonant wavelength	1.55
$\Delta\lambda_R$	Changed resonant wavelength	1.54

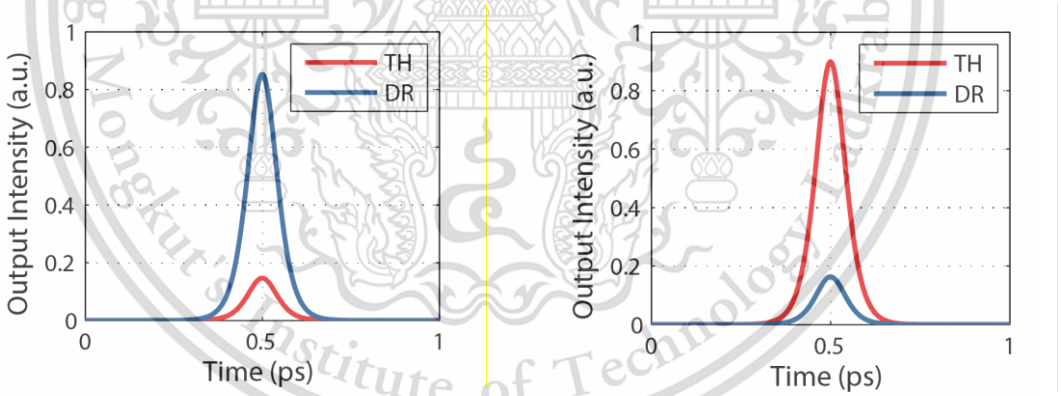

(a) Input= λ_1 (1 mW), no control (resonant wavelength is 1550 nm)

(b) input= λ_1 (1 mW), control= λ_2 (2.25 mW) (resonant wavelength changed)

Figure 4.13 Output intensity of 2:1 MUX

4.4 Design of All-optical Arithmetic and Logic Unit

Base on the proposed method and the designed circuits in previous sections, all-optical 1-bit ALU can be integrated and performed two logical and two arithmetic operations. In Figure 4.14, the design circuit of all-optical logic OR gate and AND gate [109], and all-optical ultra-fast multiplexing [94] have been reported. The beam splitters are used to divide the input signal into both separated AU and LU parts. The operations of 1-bit ALU is expressed in Table 4.5.

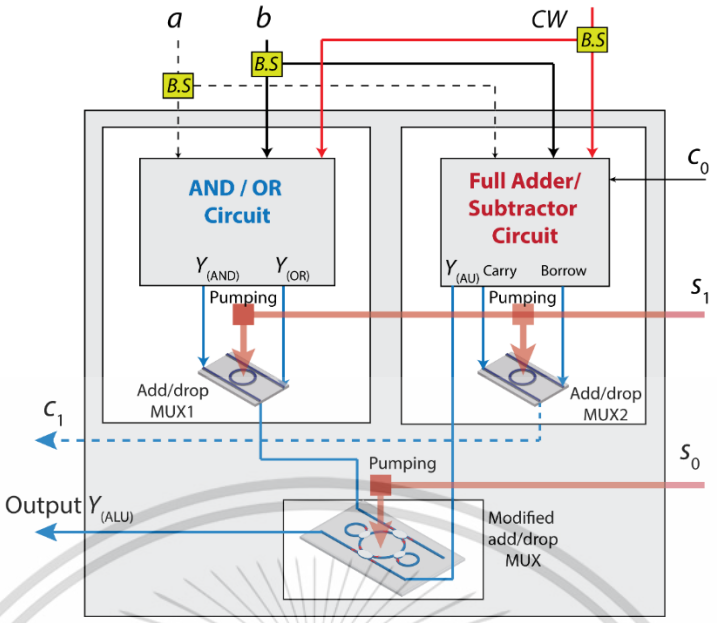

Figure 4.14 All-optical arithmetic and logic unit, where a and b are inputs, c_0 is carried input, S_1 and S_0 are selecting inputs, and c_1 is Carry/Borrow output.

Table 4.5 Operation of all-optical AU block and LU block

Pumping		Input			Output Operations		Output	
S_1	S_0	a	b	c_0	Y_{LU}	Y_{AU}	c_1	Y_{ALU}
OFF	OFF	x	y	z	a OR b	Ignored	Ignored	OR
OFF	ON	x	y	z	a OR b	Ignored	Ignored	AND
ON	OFF	x	y	z	Ignored	SUM/DIFF	Borrow	DIFF
ON	ON	y	y	z	Ignored	SUM/DIFF	Carry	SUM

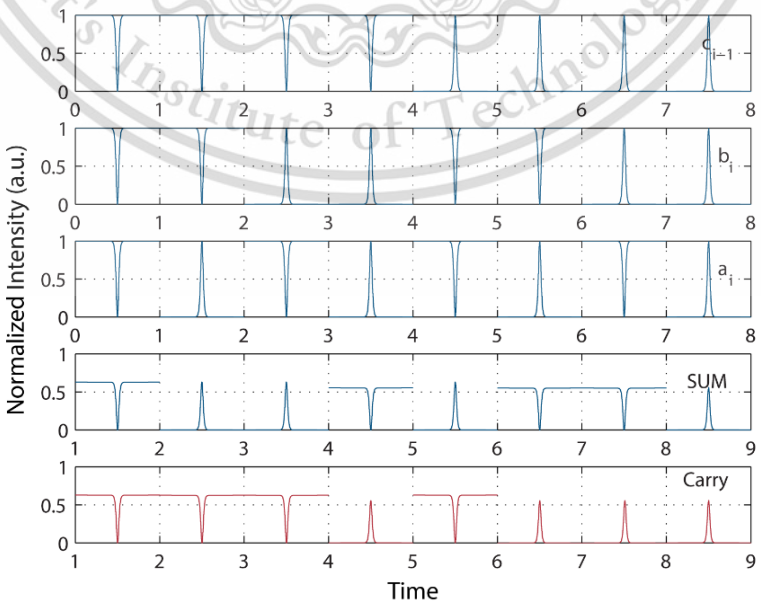

Figure 4.15 The simulation result of the full addition of ALU.

When selecting input S_0S_1 is logic 00, the output from logic OR gate is transmitted to the drop port of add-drop multiplexer. When selecting input S_0S_1 is logic 01, the selecting input S_1 is pumped onto the left hand-hand-side add-drop filter, and output from logic AND gate is selected to be transmitted into the multiplexer and dropped at the drop port. When selecting input S_0S_1 is logic 10, the selecting input S_1 is not pumped onto the add-drop filter, and the borrow output is directly transmitted to c_1. Hence, the output from the add-drop multiplexer is the output of the full-subtractor. Lastly, when selecting input S_0S_1 is logic 11, the selecting input S_1 is pumped onto the add-drop filter, and carry output is transmitted to c_1 port. Hence, the output from the add-drop multiplexer is the output of the full-adder. Therefore, when selecting input S_0 is logic 0, the output of ALU is from the output of the LU part when selecting input S_0 is logic 1, the output of ALU is from AU part. The simulation result of ALU when selecting inputs S_1S_0 is logic "11" is shown in Figure 4.15, and the output intensity of ALU circuit when in some cases of inputs are expressed in Table 4.6.

Table 4.6 Output intensity of optical ALU

Selecting		Input			Output Y				Output C_0	
S_0	S_1	c_0	b	a	$a \vee b$	$a \wedge b$	DIFF	SUM	Borrow	Carry
OFF	OFF	0	0	0	0.2	0	0.1	0.1	0	0
OFF	ON	0	0	1	0.9	0.1	0.9	0.9	0.7	0.1
ON	OFF	0	1	0	0.9	0.1	0.8	0.3	0	0.3
ON	ON	0	1	1	0.9	0.9	0.1	0.1	0.7	0.3
OFF	OFF	1	0	0	0.2	0	0.9	0.9	0	0
OFF	ON	1	0	1	0.9	0.1	0.2	0.2	0	0.7
ON	OFF	1	1	0	0.9	0.1	0.1	0.1	0	0.8
ON	ON	1	1	1	0.9	0.9	0.3	0.3	0.7	0.7

Note The minimum intensity the define the output logic "1" of the circuit must not be lower than 0.3. The intensity which is lower than 0.3 is defined as logic "0".

Figure 4.6 shows the simulation results when we input the signal in two condition. In Figure 4.6(a), shows the output signal when a dark soliton is represented as logic "0", and Figure 4.6(b) shows the results when input logic "0" is represented by no pumping power.

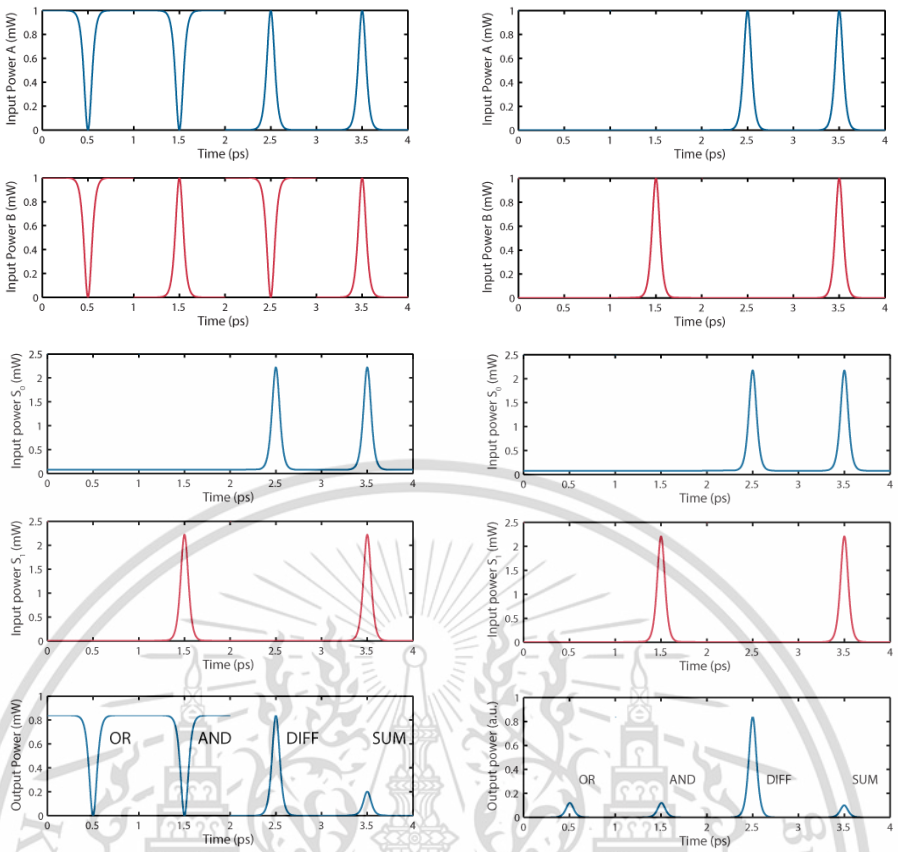

Figure 4.16 Simulation result of ALU when selecting inputs S_0S_1 are logic, 00, 01, 10, and 11; (a) logic "0" is dark soliton and logic "1" is bright soliton; (b) logic "0" is minimal signal and logic "1" is bright soliton.

4.5 Performance Analysis of Ring Resonator and Comparison

In order to design an optical logic and arithmetic operation using a nonlinear ring resonator to increase system performance to be in line with the intended use, there are important parameters that should be taken into consideration when determining the efficiency of the system. Consists of essential parameters such as quality factor (Q), free spectral range (FSR), Finesse (F), and photon lifetime (τ_{cav}). Each parameter has detail and effect when applied to the design of an optical ALU using a nonlinear ring resonator, in which specifies the parameters of the ring resonator to be the same value. From the simulation results of the all-optical ALU structure, the parameters have been varied as follows. Figure 4.17 shows the transmission characteristic of MRRs when ring radius is 1.5 μm. coupling coefficient (κ) is 0.25, and the input power at 1 mW. The output free spectral range is 36 nm, FWHM is 4 nm, and the high ON-OFF ratio of 41 dB.

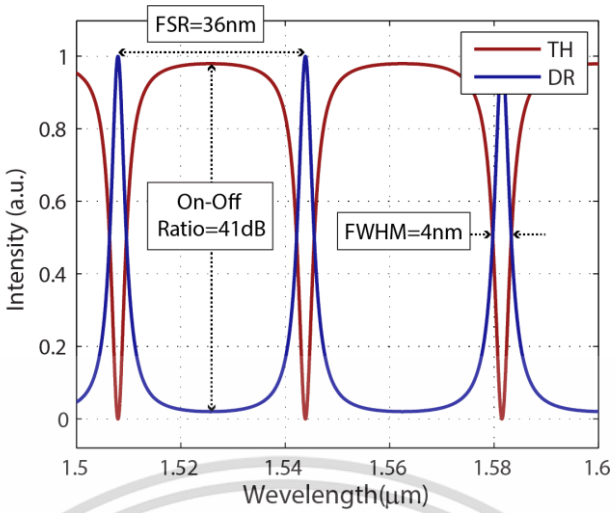

Figure 4.17 Simulation result of the transmission characteristic

4.5.1 Full-Width at Half-Maximum

The value of the FWHM of the resonant frequency in the simulation result of the ring resonator is shown in Figure 4.18. According to the relation graph, when the coupling coefficient (κ) value is fixed, it illustrates that the FWHM of the resonant frequency, according to (4.7), will increase when the radius of the nonlinear ring resonator decreases. When the radius of the ring resonator is fixed, when the κ value increases significantly, this will result in full-width half of the resonant frequency increases. The full-width at half-maximum (FWHM) is given for this configuration by (4.7)

$$FWHM = \frac{\kappa^2 \lambda_0}{\pi L n_{eff}} \tag{4.7}$$

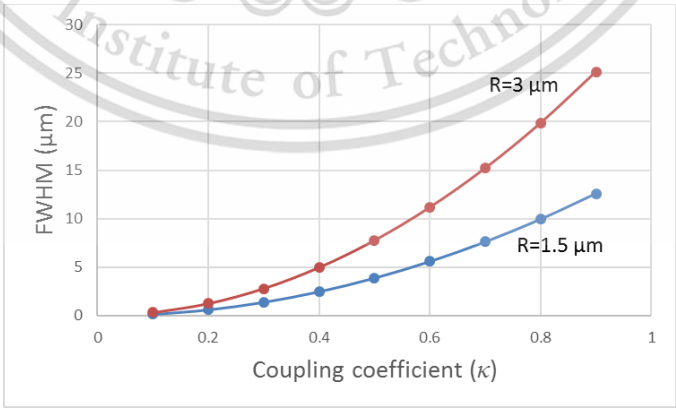

Figure 4.18 The ratio between FWHM of resonant wavelength and coupling coefficient.

4.5.2 Free Spectral Range

Free spectral range (FSR) is a parameter that indicates the distance between resonance peaks. The simulation results of the FSR in nonlinear ring resonator according to (4.8) is shown in Figure 4.19 and Figure 4.20 From the relation graph, when giving a constant refractive index (n) of the medium, the value of FSR decreases as the ring size increases. The value of FSR increases accordingly as the wavelength increases.

$$FSR = \frac{\lambda^2}{n_{eff}L} = \frac{2\pi c}{n_{eff}2\pi R} = \frac{c}{n_{eff}R} \tag{4.8}$$

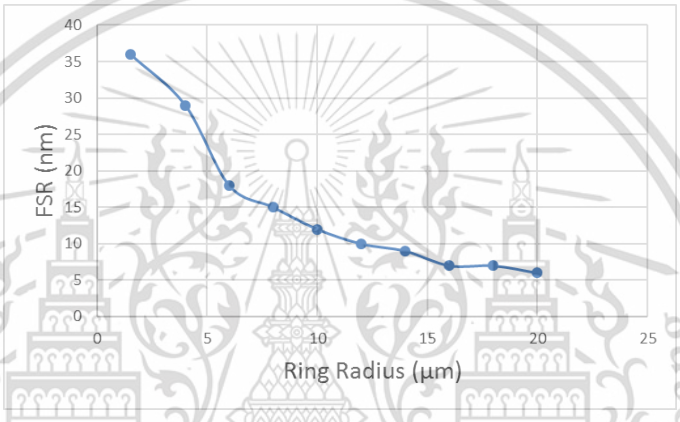

Figure 4.19 Relation between free spectral range and ring radius when n_{eff}=3.34

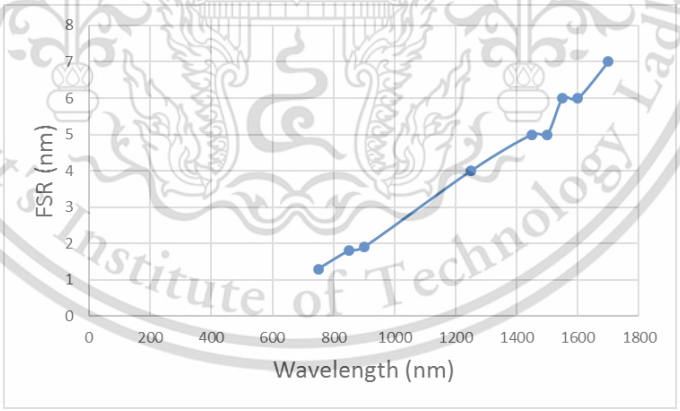

Figure 4.20 The relation between wavelength and FSR.

4.5.3 Quality Factor

The quality factor (Q) is one of the essential parameters, in which the quantity value will indicate the period of energy accumulation and energy loss within a ring resonator in each cycle. The simulation results show the changing ratio of Q value compared with the change of coupling coefficients (κ) value in the nonlinear ring resonators according to the equation $Q=2\pi n_{eff}/\lambda\kappa^2$ is shown in Figure 4.21. From

the figure, the relationship between the Q value and the κ value shows that when the κ value increases, it causes the Q value to decrease. From the simulation result, it is found that when the Q value is high, it will cause the change of the logic output status to have more delay.

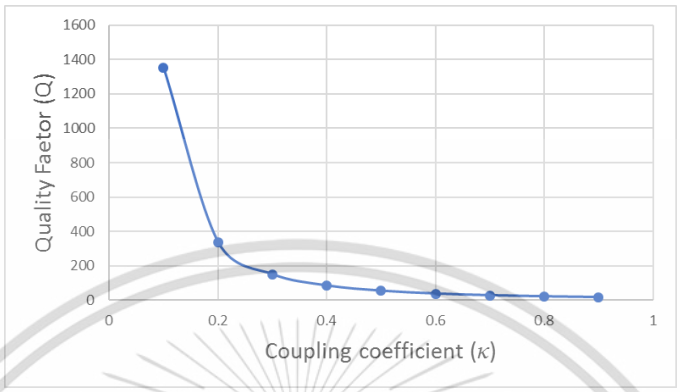

Figure 4.21 The ratio between quality factor and coupling coefficient.

4.5.4 Finesse

The Finesse (F) of the ring resonator is determined by the ratio of the free spectral range and the full-width at half-maximum (FWHM) of the resonant frequency. The finesse value can be calculated by equation $F=2\pi/\alpha L$, in the case of that does not consider the loss within the ring resonator and coupling loss ($\alpha=0$), and the coupling coefficient value is symmetrical ($\kappa_1=\kappa_2=\kappa$ "1), the finesse (F) can be estimated according to the equation $F=\pi/\kappa^2$ as shown in Figure 4.22 which can be seen that the value F increases when coupling coefficient decreases.

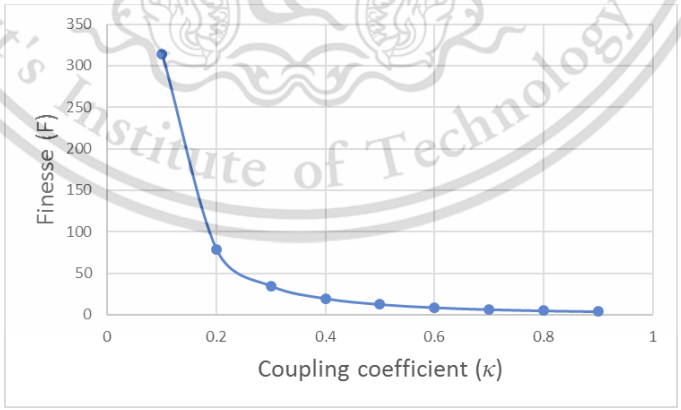

Figure 4.22 The relationship between finesse and coupling coefficient.

4.5.5 Propagation Time

Propagation time (T) or propagation delay, in networking, is the amount of time it takes for the head of the signal to travel from the sender (input port) to the receiver (output port). It can be computed as the ratio between the optical path

length (OPL), of the circuit, and the propagation speed (velocity of light) over a specific medium. The propagation time in a nonlinear ring resonator is defined by (4.9) and (4.10). The simulation results of the propagation time from the inputs to the output port (Y_1) is shown in Figure 4.23. In this case, the length of the connecting line between ring resonators is not taken into consideration.

$$T_{TH}=\frac{Ln_{eff}}{c}=\frac{10\pi Rn_{eff}}{c} \tag{4.9}$$

$$T_{DR}=\frac{(L+\frac{L}{2})n_{eff}}{c}=\frac{15\pi Rn_{eff}}{c} \tag{4.10}$$

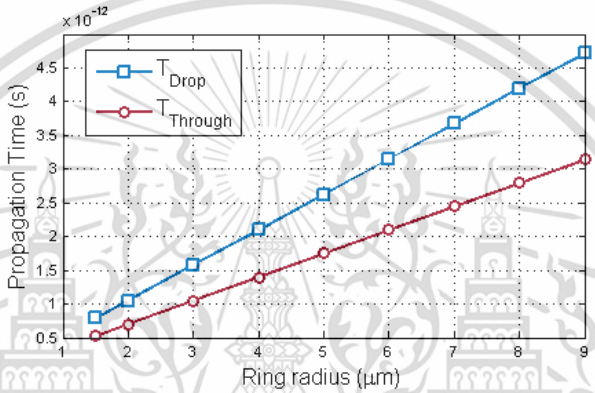

Figure 4.23 The ratio between propagation time and ring radius.

4.5.6 Photon Lifetime

The photon lifetime (τ_{cav}) is related to the coupling between waveguide and ring resonator, as well as the losses that occur within the ring. The existence of the photons within the nonlinear ring resonator in comparison with the Q value according to equation $\tau_{cav}=Q\lambda/2\pi c$. The relationship can be seen in Figure 4.24. The figure shows that when the Q value increases, the result will increase the photon lifetime, which results in a change in the logic state of the circuit (delay) increases.

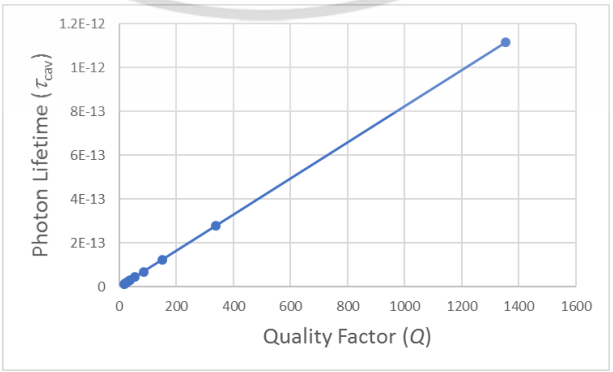

Figure 4.24 The ratio between photon lifetime and quality factor.

4.6 Simulation Results of Varying Some Parameters

4.6.1 Simulation Result when Varying Coupling Coefficient

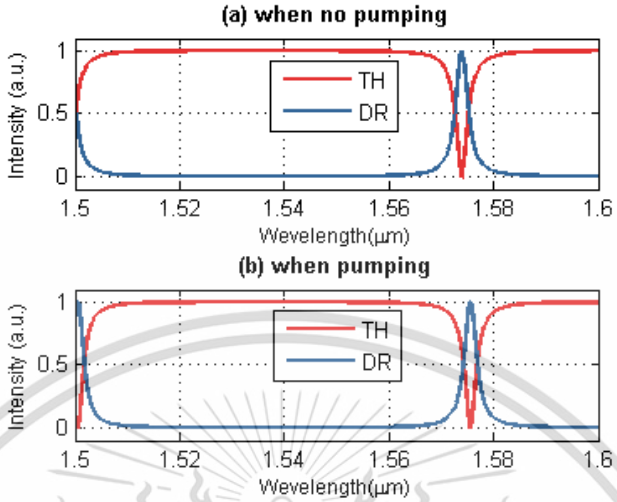

Figure 4.25 Simulation result when the ring radius is 1.5 μm and coupling coefficients are 0.1

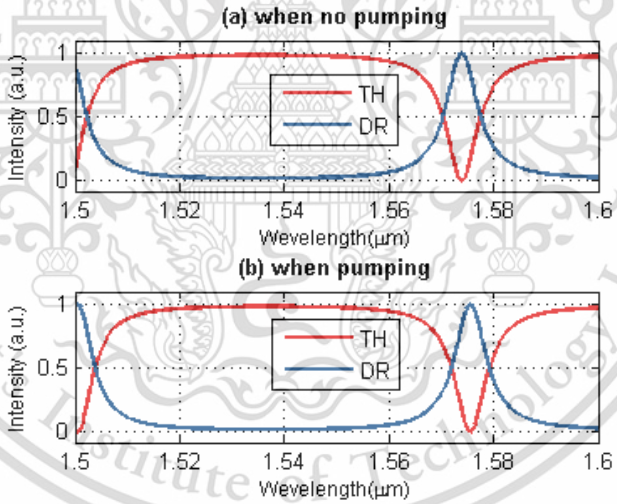

Figure 4.26 Result when ring radius is 1.5 μm, and coupling coefficients are 0.25.

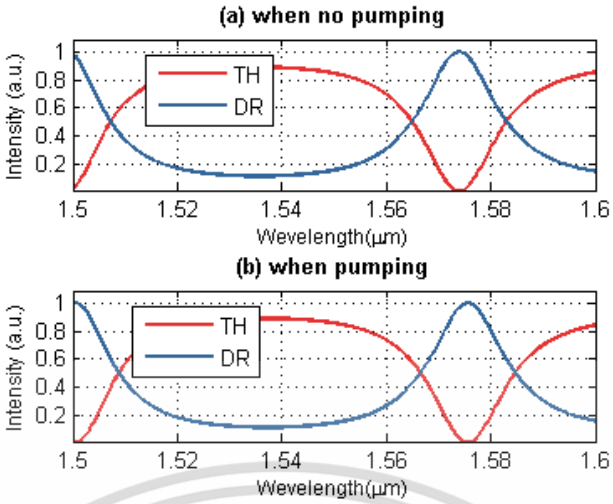

Figure 4.27 Result when ring radius is 1.5 μm, and coupling coefficients are 0.5.

From Figures 4.25 to Figure 4.27, the figures illustrate that the coupling coefficient influences the pulse shape of the transmitted signals. When the coupling coefficient increases, this affects the full width at half-maximum (FWHM) to be increased.

4.6.2 Simulation Result when Varying Ring Radius

From Figures 4.28 to 4.30, the figures illustrate that the ring radius influences the mode number of the transmitted signals. When the ring radius increases, this affects the change of resonant wavelength and the amount of resonant wavelength, while the free spectral range (FSR) decreases as well.

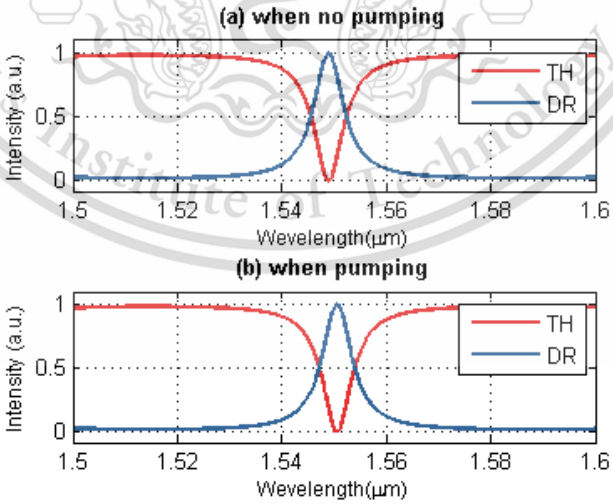

Figure 4.28 Result when coupling coefficients are 0.25 and ring radius is 1.55 μm.

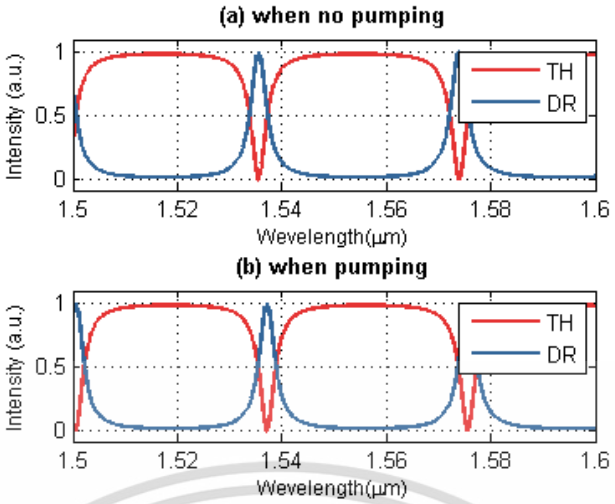

Figure 4.29 Result when coupling coefficients are 0.25 and ring radius is 3 μm.

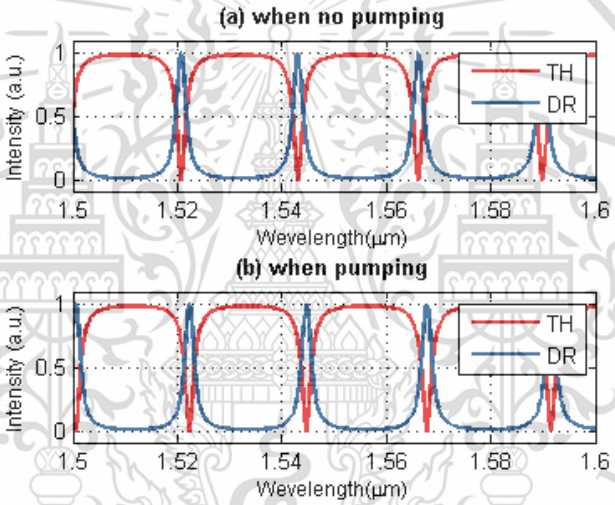

Figure 4.30 Result when coupling coefficients are 0.25 and ring radius is 5 μm.

4.6.3 Simulation Result when Coupling Coefficients are Different

From Figures 4.31 to 4.32, the figures illustrate that the difference of the coupling coefficients signal intensity coupled into the ring and the transmitted output. This affects the change in the ON-OFF ratio of the devices.

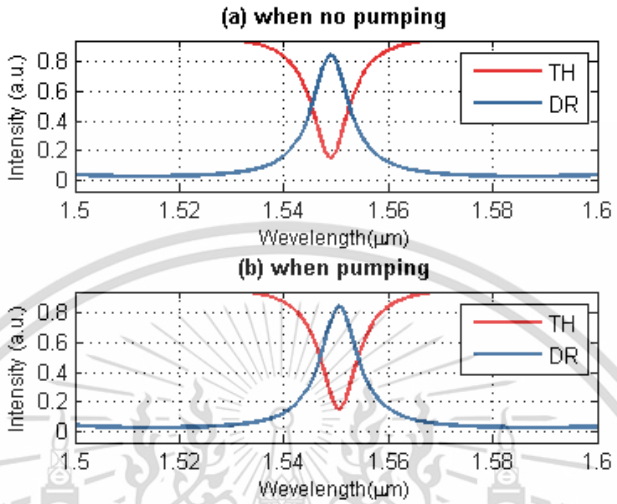

Figure 4.31 Result when ring radius is 1.55 μm, coupling coefficient κ_1=0.2, κ_2=0.4

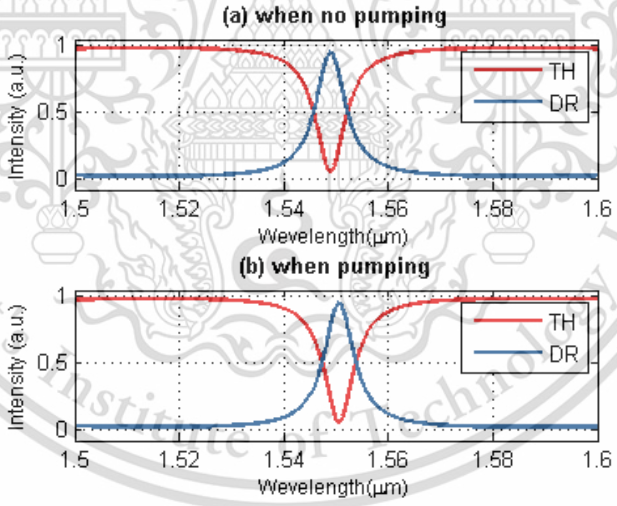

Figure 4.32 Result when ring radius is 1.55 μm, coupling coefficient κ_1=0.2, κ_2=0.3

Chapter 5
CONCLUSION

This thesis proposes an all-optical adder/subtractor and other logical circuits based on optical switching in nonlinear microring resonators. The method of switching can be performed by external pumping input with the power just above the bandgap energy of the specific material used for microring resonators (2.25 mW for InGaAsP/InP) [110]. The pumping induced the change of refractive index and causes the resonant wavelength shifted, i.e., MRRs are set up to respond to some resonant wavelengths when MRR is on resonant state, the output is dropped at drop port, and when the optical pumping is applied, the signal is therefore transmitted to the throughput port due to the resonant wavelength shifted. The proposed method and circuit can be used to design 1-bit optical ALU performing two arithmetic operations and two logic gates, i.e., full addition, full subtraction, logic OR gate, and logic AND gate, respectively. The input of the circuits is bright soliton pulse (logic "1") or dark soliton pulse (logic "0"). This soliton pulses can be controlled and applied for high-security long-distance communication using the dark-bright conversion principle [111], [112]. the optical switching is therefore performed using carrier injection technique by pumping input to induce the change of refractive index

The simulation result shows the ultrafast switching time of only 0.14 ps, and the ultrafast response time of approximately 0.78 ps at drop port of a modified add/drop multiplexer.

The proposed circuit is a microscopic scale just smaller than 100 μm^2 compared to the Mach-Zehnder interferometer structure (MZI) with a total length of 6 mm [108], and terahertz optical-asymmetric demultiplexer (TOAD) structure with the SOA structure of 500 μm [119]. However, TOAD structure has a lower operating speed of up to 20 Gbps [120], it makes it more difficult to be integrated with photonic circuits. In many pieces of research, SOA is applied to the operation, resulting in a smaller device structure; however, this increases the complexity of designing and fabricating more sophisticated devices as well.

Ring resonator has attracted a lot of research and development of new devices to replace electronic devices continuously, since many of the advantages such as robustness, ultra-fast switching speed, and high bitrate (up to 40 Gbps). This results in a smaller device scale (just 1.5 μm of radius) [15], and increased operating efficiency. Since the circuit uses a nonlinear ring resonator with a small radius, it makes it favorable to be considered for fabrication, and flexible to demonstrate in the more considerable amount of bits integration. New materials, such as the Silicon

on Insulator (SOI), have been introduced for use in the fabrication of stable quality devices for better integration with other technologies in the future. The comparison of the advantages between ring resonator are expressed in Table 5.1.

Table 5.1 The comparison of the advantage and disadvantages of each architecture.

Technologies	Bitrate	Advantage	Disadvantage
- Ring Resonator structure	40 Gb/s	+ Simple and compact structure, low loss, low power consumption	- Need additional amplifier (e.g., EDFA) when integrated with a larger circuit
- TOAD [51]	10 Gb/s	+ High stability	- Low operation speed
SOA-MZI [55]	(2.5 to 10) Gb/s	+ Stable, small scale	- limited operation speed, using SOA
- Nonlinear optical loop mirror [113]	40 Gb/s	+ Simple structure, high bitrate	- Difficult to be applied with other devices
- Intensity switch [114]	13 Gb/s	+ Simple structure	- High loss, limited operation speed
- SLALOM [115]	(1 to 2.5) Gb/s	+ Small scale, low energy consumption	- Ultra-low operation speed
- Nonlinear Interferometer [116]	40 Gb/s	+ Can be serially connected	- Sensitive for polarization, large scale, using SOA
- Semiconductor Optical Amplifier [117]	40 Gb/s	+ Small scale, low energy consumption, can be applied with other devices	- large scale, using SOA, difficult to be integrated into a photonic circuit

5.1 Future Work

However, this research, based on simulation, the output obtained from the AU block, and the LU block were assumed to be synchronized in time. Therefore, time taken in bus waveguides is not considered due to this parameter is depending on the suitable length of the connection line, and material used. In a further experiment, this parameter might be compensated by specific devices, e.g., optical clock. The circuit is designed based on a series-connection between microring resonators; therefore, the intensity loss occurs when light travels along with each microring. The additional amplifier (e.g., EDFA) might be necessary in order to integrate with a larger circuit.

Based on the proposed method, some more logical operations can be designed, such as 4:1 multiplexer; as illustrated in Figure 5.1, the circuit combines or multiplexes four input channels into one output, which is the same method with 2:1 multiplexer. The design circuit is essential in design more complicated logical circuits, and ALU circuit that has eight functions, or higher as well. Furthermore, the design circuit of 1-bit ALU can be improved by adjusting suitable parameters in order to integrate with higher bits of ALU.

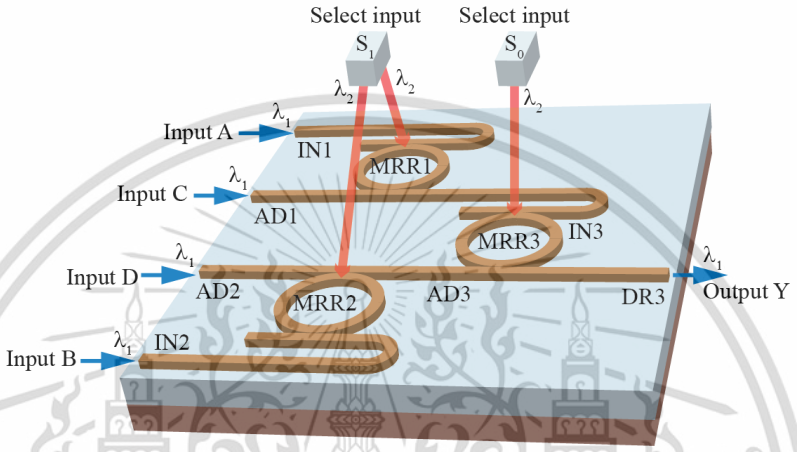

Figure 5.1 Design of all-optical 4:1 multiplexer using microring resonator.

REFERENCE

[1] Reed G. T., Mashanovich G., Gardes F. Y. and Thomson D. J. “Silicon Optical Modulators.”, **Nat. Photonics.,** vol. 4, no. 8, Aug. 2010. pp. 518–526

[2] Tucker R. S., Hinton K. and Raskutti G. “Energy Consumption Limits in High-speed Optical and Electronic Signal Processing.”, **Electron. Lett.,** vol. 43, no. 17, Aug. 2007. pp. 906–908

[3] Tucker R. S., Eisenstein G. and Korotky S. K. “Optical Time-division Multiplexing for Very High Bit-rate Transmission.”, **J. Light. Technol.,** vol. 6, no. 11, Nov. 1988. pp. 1737–1749

[4] Rashed A. N. Z. “Optical Add Drop Multiplexer (OADM) Based on Dense Wavelength Division Multiplexing Technology in Next Generation Optical Networks.”, **Electr. Electron. Eng.,** vol. 1, no. 1, 2011. pp. 24–32

[5] Yoo S. J. B. and Yang H. “Petabit-per-Second Routers: Case for All-Optical over Electronic Implementation.”, **OFC/NFOEC 2007 - 2007 Conference on Optical Fiber Communication and the National Fiber Optic Engineers Conference,** 2007. pp. 1–3

[6] Reed G. T. “Device Physics: the Optical Age of Silicon.”, **Nature.,** vol. 427, no. 6975, Feb. 2004. pp. 595–596

[7] Roy J. N., Maiti A. K., Samanta D. and Mukhopadhyay S. “Tree-net Architecture for Integrated All-optical Arithmetic Operations and Data Comparison Scheme with Optical Nonlinear Material.”, **Opt. Switch. Netw.,** vol. 4, no. 3, Nov. 2007. pp. 231–237

[8] Gayen D. K. and Roy J. N. “All-optical Arithmetic Unit with the Help of Terahertz-optical-asymmetric-demultiplexer-based Tree Architecture.”, **Appl. Opt.,** vol. 47, no. 7, Mar. 2008. pp. 933–943

[9] Roy J. N. “Mach–Zehnder Interferometer-based Tree Architecture for All-optical Logic and Arithmetic Operations.”, **Optik.,** vol. 120, no. 7, Mar. 2009. pp. 318–324

[10] Garai S. K. “A Novel All-optical Frequency-encoded Method to Develop Arithmetic and Logic Unit (ALU) Using Semiconductor Optical Amplifiers.”, **J. Light. Technol.,** vol. 29, no. 23, Dec. 2011. pp. 3506–3514

[11] Rakshit J. K., Chattopadhyay T. and Roy J. N. “Design of Ring Resonator Based All Optical Switch for Logic and Arithmetic Operations – A Theoretical Study.”, **Optik.,** vol. 124, no. 23, Dec. 2013. pp. 6048–6057

[12] Kokubun Y., Hatakeyama Y., Ogata M., Suzuki S. and Zaizen N. “Fabrication Technologies for Vertically Coupled Microring Resonator with Multilevel Crossing Busline and Ultracompact-ring Radius.”, **IEEE J. Sel. Top. Quantum Electron.,** vol. 11, no. 1, Jan. 2005. pp. 4–10

[13] Madani A., Azarinia H. and Latifi H. “Design and Fabrication of a Polymer Micro Ring Resonator with Novel Optical Material at Add/Drop Geometry Using Laser Beam Direct Write Lithography Technique.”, **Optik.,** vol. 124, no. 14, pp. Jul. 2013. 1746–1748

[14] Donzella V., Sherwali A., Flueckiger J., Grist S. M., Fard S. T. and Chrostowski L. “Design and Fabrication of SOI Micro-ring Resonators Based on Sub-wavelength Grating Waveguides.”, **Opt. Express.,** vol. 23, no. 4, Feb. 2015. pp. 4791–4803

[15] Xu Q., Fattal D. and Beausoleil R. G. “Silicon Microring Resonators with 1.5-μm Radius.”, **Opt. Express.,** vol. 16, no. 6, Mar. 2008. pp. 4309–4315

[16] Lin S., Ishikawa Y. and Wada K. “Demonstration of Optical Computing Logics Based on Binary Decision Diagram.”, **Opt. Express.,** vol. 20, no. 2, Jan. 2012. pp. 1378–1384

[17] Nair N., Kaur S. and Goyal R. “All-optical Integrated Parity Generator and Checker Using an SOA-based Optical Tree Architecture.”, **Curr. Opt. Photonics.,** vol. 2, no. 5, Oct. 2018. pp. 400–406

[18] Wang F., Fan J. W., Han X. G. and Sun Q. L. “Discussion About Maxwell Equation Based on Monopole.”, **2013 IEEE International Conference on Applied Superconductivity and Electromagnetic Devices,** 2013. pp. 434–436

[19] Poon T.-C. and Banerjee P. P. **Contemporary Optical Image Processing with MATLAB**. Elsevier. 2001.

[20] Franken P. A., Hill A. E., Peters C. W. and Weinreich G. “Generation of Optical Harmonics.”, **Phys. Rev. Lett.,** vol. 7, no. 4, Aug. 1961. pp. 118–119

[21] Kapron F. P., Keck D. B. and Maurer R. D. “Radiation Losses in Glass Optical Waveguides.”, **Appl. Phys. Lett.,** vol. 17, no. 10, Nov. 1970. pp. 423–425

[22] Stolen R. H., Ippen E. P. and Tynes A. R. “Raman Oscillation in Glass Optical Waveguide.”, **Appl. Phys. Lett.,** vol. 20, no. 2, Jan. 1972. pp. 62–64

[23] Ippen E. p. and Stolen R. h. “Stimulated Brillouin Scattering in Optical Fibers.”, **Appl. Phys. Lett.,** vol. 21, no. 11, Dec. 1972. pp. 539–541

[24] Stolen R. H. “Nonlinearity in Fiber Transmission.”, **Proc. IEEE.,** vol. 68, no. 10, 1980. pp. 1232–1236

[25] Agrawal G P. **Nonlinear Fiber Optics.** 2nd Edition. Missouri : Academic Pr. 1995.

[26] Newell A. C. and Moloney J. V. **Nonlinear optics.** Redwood City : Addison-Wesley. 1992.

[27] Shen Y. R. **The Principles of Nonlinear Optics.** California. 2002.

[28] Kippenberg T. J. A. “**Nonlinear Optics in Ultra-high Q Whispering-gallery Optical Microcavities.**” Ph.D. Thesis of California Institute of Technology. 2004.

[29] Silberhorn C., Lam P. K., Weiss O., König F., Korolkova N. and Leuchs G. “Generation of Continuous Variable Einstein-podolsky-rosen Entanglement Via

the Kerr Nonlinearity in a Optical Fiber.", **Phys. Rev. Lett.,** vol. 86, no. 19, May. 2001. pp. 4267–4270

[30] Agrawal G. P. "Nonlinear Fiber Optics.", **Nonlinear Science at the Dawn of the 21st Century,** 2000. pp. 195–211

[31] Agrawal G. P. and Olsson N. A. "Self-phase Modulation and Spectral Broadening of Optical Pulses in Semiconductor Laser Amplifiers.", **IEEE J. Quantum Electron.,** vol. 25, no. 11, Nov. 1989. pp. 2297–2306

[32] Chen Y. "**Nonlinear Optical Process Enhancement by Artificial Resonant Structures.**" Ph.D. Thesis of The University of Utah, United States. 2004.

[33] Li C. **Nonlinear Optics: Principles and Applications**. Singapore: Springer Singapore. 2017. pp. 215–250.

[34] Tong X. C. **Advanced Materials for Integrated Optical Waveguides.** Springer. 2013.

[35] Otsuka K. "Pitchfork Bifurcation and all-Optical Digital Signal Processing with a Coupled-element Bistable System.", **Opt. Lett.,** vol. 14, no. 1, Jan. 1989. pp. 72–74

[36] Zhao L. M., Tang D. Y., Lin F. and Zhao B. "Observation of Period-doubling Bifurcations in a Femtosecond Fiber Soliton Laser with Dispersion Management Cavity.", **Opt. Express.,** vol. 12, no. 19, Sep. 2004. pp. 4573–4578

[37] Lynch S. **Dynamical Systems with Applications using MATLAB®**. 2nd ed. Birkhäuser Basel. 2014.

[38] Jayawardena A. W. **Environmental and Hydrological Systems Modelling.** Florida : Taylor & Francis. 2014.

[39] Drazin P. G., Johnson R. S. **Solitons Introduction.** 2nd edition. Cambridge : Cambridge University Press. 1989.

[40] Allen J. E. "The Early History of Solitons (Solitary Waves).", **Phys. Scr.,** vol. 57, no. 3, Mar. 1998. pp. 436–441

[41] Duarte F. J. **Coherence and Ultrashort Pulse Laser Emission.** Croatia : Intech. 2010.

[42] Gabriela S., Philippe R. **Optical Generation and Control of Quantum Coherence in Semiconductor Nanostructures**. Springer. 2010.

[43] Ávila G. M. R., Guisset J. L. and Deneubourg J. L. "Synchronization in Chains of Light-Controlled Oscillators.", **J. Phys. Conf. Ser.,** vol. 23, Jan. 2005. pp. 252–258

[44] Yariv A. "Universal Relations for Coupling of Optical Power Between Microresonators and Dielectric Waveguides.", **Electron. Lett.,** vol. 36, no. 4, Feb. 2000. pp. 321–322

[45] Okamoto K. **Fundamentals of Optical Waveguides.** 2nd Edition. Elsevier Science. 2006.

[46] Mookherjea S. and M. A. Schneider M. A. “The Nonlinear Microring Add-drop Filter.”, **Opt. Express.,** vol. 16, no. 19, Sep. 2008. pp. 15130–15136

[47] Gulde S., Jebali A. and Moll N. “Optimization of Ultrafast All-optical Resonator Switching.”, **Opt. Express.,** vol. 13, no. 23, Nov. 2005. pp. 9502–9515

[48] Wen Y. H., Kuzucu O., Hou T., Lipson M. and Gaeta A. L. “All-optical Switching of a Single Resonance in Silicon Ring Resonators.”, **Opt. Lett.,** vol. 36, no. 8, Apr. 2011. pp. 1413–1415

[49] Nozaki K., Shinya A., Matsuo S., Sato T., Kuramochi E. and Notomi M. “Ultralow-energy and High-contrast All-optical Switch Involving Fano Resonance Based on Coupled Photonic Crystal Nanocavities.”, **Opt. Express.,** vol. 21, no. 10, May. 2013. pp. 11877

[50] Kokubun Y. “Vertically Coupled Microring Resonator Filter for Integrated Add/Drop Node.”, **IEICE Trans. Electron.,** vol. E88-C, no. 3, Mar. 2005. pp. 349–362

[51] Roy J. N., Maity G. K., Gayen D. K. and Chattopadhyay T. “Terahertz Optical Asymmetric Demultiplexer Based Tree-net Architecture for All-optical Conversion Scheme from Binary to Its Other 2n Radix Based Form.”, **Chin. Opt. Lett.,** vol. 6, no. 7, Jul. 2008. pp. 536–540

[52] Dutta S. and Mukhopadhyay S. “All Optical Frequency Encoding Method for Converting a Decimal Number to Its Equivalent Binary Number Using Tree Architecture.”, **Optik.,** vol. 122, no. 2, Jan. 2011. pp. 125–127

[53] Mukhopadhyay S. “An Optical Conversion System: From Binary to Decimal and Decimal to Binary.”, **Opt. Commun.,** vol. 76, no. 5, May. 1990. pp. 309–312

[54] Das M. K., Roy J. N. and Chattopadhyay T. “Passive All-optical Tree Architecture-based Scheme for Conversion of 2n Radix-based Number to Its Binary Form.”, **IET Optoelectron.,** vol. 6, no. 5, Oct. 2012. pp. 223–229

[55] Kim J. Y., Kang J. M., Kim T. Y. and Han S. K. “All-optical Multiple Logic Gates with XOR, NOR, OR, and NAND Functions Using Parallel SOA-MZI Structures: Theory and Experiment.”, **J. Light. Technol.,** vol. 24, no. 9, Sep. 2006. pp. 3392–3399

[56] Kaur S. “All Optical Integrated Full Adder-subtractor and Demultiplexer Using SOA-Based Mach-zehnder Interferometer.”, **International Journal of Engineering Science and Technology (IJEST).,** Vol. 4, No. 01, Jan. 2012.

[57] Stubkjaer K. E. “Semiconductor Optical Amplifier-based All-optical Gates for High-speed Optical Processing.”, **IEEE J. Sel. Top. Quantum Electron.,** vol. 6, no. 6, Nov. 2000. pp. 1428–1435

[58] Glesk I., Sokoloff J. P. and Prucnal P. R. “Demonstration of All-optical Demultiplexing of TDM Data at 250 Gbit/s.”, **Electron. Lett.,** vol. 30, no. 4, Feb. 1994. pp. 339–341

[59] Wang B. C., Xu L., Baby V., Zhou D., Runser R. J, Glesk I. and Prucnal P R. "Experimental Study on the Regeneration Capability of the Terahertz Optical Asymmetric Demultiplexer.", **Opt. Commun.,** vol. 199, no. 1, Nov. 2001. pp. 83–88

[60] Haus H. A. and Lai Y. "Narrow-band Optical Channel-dropping Filter.", **J. Light. Technol.,** vol. 10, no. 1, Jan. 1992. pp. 57–62

[61] Adar R., Henry C. H., Dragone C., Kistler R. C. and Milbrodt, M. A. "Broad-band Array Multiplexers Made with Silica Waveguides on Silicon.", **J. Light. Technol.,** vol. 11, no. 2, Feb. 1993. pp. 212–219

[62] Little B. E., Chu S. T., Haus H. A., Foresi J. and Laine J.-P. "Microring Resonator Channel Dropping Filters.", **J. Light. Technol.,** vol. 15, no. 6, Jun. 1997. pp. 998–1005

[63] Little B.E., Foresi J.S., Steinmeyer G., Thoen E.R., Chu S.T., Haus H.A., Ippen E.P., Kimerling L.C. and Greene W. "Ultra-compact Si-SiO2 Microring Resonator Optical Channel Dropping Filters.", **IEEE Photonics Technol. Lett.,** vol. 10, no. 4, Apr. 1998. pp. 549–551

[64] Soref R. and Bennett B. "Electrooptical Effects in Silicon.", **IEEE J. Quantum Electron.,** vol. 23, no. 1, Jan. 1987. pp. 123–129

[65] Soref R. A. and Bennett B. R. "Kramers-kronig Analysis of Electro-optical Switching in Silicon.", **presented at the Proc.SPIE.,** vol. 0704, Mar. 1987.

[66] Giguere S. R., Friedman L., Soref R. A. and Lorenzo J. P. "Simulation Studies of Silicon Electro-optic Waveguide Devices.", **J. Appl. Phys.,** vol. 68, no. 10, Nov. 1990. pp. 4964–4970

[67] Soref R. A. "Silicon-based Optoelectronics.", **Proc. IEEE.,** vol. 81, no. 12, Dec. 1993. pp. 1687–1706

[68] Cutolo A., Iodice M., Spirito P. and Zeni L. "Silicon Electro-optic Modulator Based on a Three Terminal Device Integrated in a Low-loss Single-mode SOI Waveguide.", **J. Light. Technol.,** vol. 15, no. 3, Mar. 1997. pp. 505–518

[69] Fei S., Jin-zhong Y. and Shao-wu C. "High Speed 2×2 Optical Switch in Silicon-on-Insulator Based on Plasma Dispersion Effect.", **Chinese Physics Letters.,** vol. 22, no. 12, 2005.

[70] Fischer U., Zinke T., Schuppert B. and Petermann K. "Singlemode Optical Switches Based on SOI Waveguides with Large Cross-section.", **Electron. Lett.,** vol. 30, no. 5, Mar. 1994. pp. 406–408

[71] Espinola R. L., Tsai M. C., Yardley J. T. and Osgood R. M. "Fast and Low-power Thermooptic Switch on Thin Silicon-on-insulator.", **IEEE Photonics Technol. Lett.,** vol. 15, no. 10, Oct. 2003. pp. 1366–1368

[72] Liu J., Yu J., Chen S. and Xia J. “Fabrication and Analysis of 2×2 Thermo-optic SOI Waveguide Switch with Low Power Consumption and Fast Response by Anisotropy Chemical Etching.”, **Opt. Commun.,** vol. 245, no. 1, Jan. 2005. pp. 137–144

[73] Png C. E., Chan S. P., Lim S. T. and Reed G. T. “Optical Phase Modulators for MHz and GHz Modulation in Silicon-on-insulator (SOI).”, **J. Light. Technol.,** vol. 22, no. 6, Jun. 2004. pp. 1573–1582

[74] Liu A., Liao L., Jones R. and Rubio D. S. “A high-speed Silicon Optical Modulator Based on a Metal–oxide–semiconductor Capacitor.”, **Nature.,** vol. 427, no. 6975, Feb. 2004. pp. 615–618

[75] Xu Q., Schmidt B., Pradhan S. and Lipson M. “Micrometre-scale Silicon Electro-optic Modulator.”, **Nature.,** vol. 435, no. 7040, May. 2005. pp. 325–327

[76] Lloret J., Kumar R., Sales S., Ramos F., Morthier G., Mechet P., Spuesens T., Van Thourhout D., Olivier N., Fédéli J. M. and Capmany J. “Ultracompact Electro-optic Phase Modulator Based on III-V-on-silicon Microdisk Resonator.”, **Opt. Lett.,** vol. 37, no. 12, Jun. 2012. pp. 2379–2381

[77] Bennett B. R., Soref R. A. and Del Alamo J. A. “Carrier-induced Change in Refractive Index of InP, GaAs and InGaAsP.”, **IEEE J. Quantum Electron.,** vol. 26, no. 1, Jan. 1990. pp. 113–122

[78] Treyz G. V., May P. G. and Halbout J. “Silicon Mach–Zehnder Waveguide Interferometers Based on the Plasma Dispersion Effect.”, **Appl. Phys. Lett.,** vol. 59, no. 7, Aug. 1991. pp. 771–773

[79] Manolatou C. and Lipson M. “All-optical Silicon Modulators Based on Carrier Injection by Two-photon Absorption.”, **J. Light. Technol.,** vol. 24, no. 3, Mar. 2006. pp. 1433–1439

[80] Hwang I., Kim M. and Lee Y. “All-Optical Switching in InGaAsP–InP Photonic Crystal Resonator Coupled with Microfiber.”, **IEEE Photonics Technol. Lett.,** vol. 19, no. 19, Oct. 2007. pp. 1535–1537

[81] Van V., Ibrahim T. A., Absil P. P., Johnson F. G., Grover R. and Ho P. “Optical Signal Processing Using Nonlinear Semiconductor Microring Resonators.”, **IEEE J. Sel. Top. Quantum Electron.,** vol. 8, no. 3, May. 2002. pp. 705–713

[82] Bian Z., Liu B. and Shakouri A. “InP-based Passive Ring-resonator-coupled Lasers.”, **IEEE J. Quantum Electron.,** vol. 39, no. 7, Jul. 2003. pp. 859–865

[83] Barwicz T., Popovic M. A., Rakich P. T., Watts M. R., Haus H. A., Ippen E. P. and Smith H. I. “Microring-resonator-based Add-drop Filters in SiN: Fabrication and Analysis.”, **Opt. Express.,** vol. 12, no. 7, Apr. 2004. pp. 1437–1442

[84] Yalçin A., Popat K. C., Aldridge J.C. and Desai T. “Optical Sensing of Biomolecules Using Microring Resonators.”, **IEEE J. Sel. Top. Quantum Electron.,** vol. 12, no. 1, Jan. 2006. pp. 148–154

[85] Barwicz T., Popović M. A., Watts M. R., Rakich P. T., Ippen E. P. and Smith H. I. “Fabrication of Add-Drop Filters Based on Frequency-Matched Microring Resonators.”, **J. Light. Technol.,** vol. 24, no. 5, May 2006. pp. 2207

[86] Plachetka U., Koo N., Wahlbrink T. and Bolten J. “Fabrication of Photonic Ring Resonator Device in Silicon Waveguide Technology Using Soft UV-Nanoimprint Lithography.”, **IEEE Photonics Technol. Lett.,** vol. 20, no. 7, Apr. 2008. pp. 490–492

[87] Xiao C. X., Li Y., Yu Y. and Yu J. “Silicon-based Asymmetric Add-drop Microring Resonators with Ultra-large Through-port Extinctions.”, **Chin. Phys. Lett.,** vol. 27, no. 5, Apr. 2010. pp. 54208–054208

[88] Rabiei P., Ma J., Khan S., Chiles J. and Fathpour S. “Submicron Optical Waveguides and Microring Resonators Fabricated by Selective Oxidation of Tantalum.”, **Opt. Express.,** vol. 21, no. 6, Mar. 2013. pp. 6967–6972

[89] Lee J., Song J., Sung G. Y. and Shin J. H. “Plasmonic Waveguide Ring Resonators with 4 nm Air Gap and $\lambda_0^2/15000$ Mode-area Fabricated Using Photolithography.”, **Nano Lett.,** vol. 14, no. 10, Oct. 2014. pp. 5533–5538

[90] Kolli V. R., Yadunath T.R., Resmi R. K., Hegde G., Badrinarayana T., Das P. P. and Srinivas T. “Design, Fabrication and Characterization of 5 μm Ring Resonator.”, **13th International Conference on Fiber Optics and Photonics (2016),** Dec, 2016. pp. Tu3F.4

[91] Cheng X., Hong J., Spring A. M. and Yokoyama S. “Fabrication of a High-Q Factor Ring Resonator Using LSCVD Deposited Si_3N_4 Film.”, **Opt. Mater. Express.,** vol. 7, no. 7, Jul. 2017. pp. 2182–2187

[92] Ibrahim T. A., Cao W., Kim Y. W., Li J., Goldhar J., Ho P. E. and Lee C. H. “All-optical Switching in a Laterally Coupled Microring Resonator by Carrier Injection.”, **IEEE Photonics Technol. Lett.,** vol. 15, no. 1, Jan. 2003. pp. 36–38

[93] Sethi P. and Roy S. “All-optical Ultrafast Switching in 2 × 2 Silicon Microring Resonators and Its Application to Reconfigurable DEMUX/MUX and Reversible Logic Gates.”, **J. Light. Technol.,** vol. 32, no. 12, Jun. 2014. pp. 2173–2180

[94] Soysouvanh S., Luangxaysana K., Phongsanam P., Mitatha S., Fukuhara M. and Yupapin P.P. “All-optical Switching in PANDA Ring Resonator by Carrier Injection.”, **The 34th JSST Annual Concerence: International Conference on Simulation Technology (JSST2015), At Toyama, Japan,** Oct, 2015.

[95] Phongsanam P., Mitatha S., Teeka C. and Yupapin P.P. "All Optical Half Adder/subtractor Using Dark-bright Soliton Conversion Control.", **Microw. Opt. Technol. Lett.,** vol. 53, no. 7, 2011. pp. 1541–1544

[96] Rabus D. G., Hamacher M. and Heidrich H. "Resonance Frequency Tuning of a Double Ring Resonator in GaInAsP/InP: Experiment and Simulation.", **Jpn. J. Appl. Phys.,** vol. 41, no. 2S, Feb. 2002. pp. 1186

[97] Wang J., Sun Q. and Sun J. "All-optical 40 Gbit/s CSRZ-DPSK Logic XOR Gate and Format Conversion Using Four-wave Mixing.", **Opt. Express.,** vol. 17, no. 15, Jul. 2009. pp. 12555–12563

[98] Soysouvanh S., Phongsanam P., Mitatha S., Ali J., Yupapin P.P., Amiri I. S., Grattan K. T. V. and Yoshida M. "Ultrafast All-optical ALU Operation Using a Soliton Control within the Cascaded InGaAsP/InP Microring Circuits.", **Microsyst. Technol.,** vol. 25, no. 2, Feb. 2019. pp. 431–440

[99] Yupapin P.P., Pornsuwancharoen N. and Chaiyasoonthorn S. "Attosecond Pulse Generation Using the Multistage Nonlinear Microring Resonators.", **Microwave and Optical Technology Letters - Wiley Online Library**, 2008.

[100] Kumar H., Janyani V., Oleh B., Serhij U., Dmytro S. and Singh G. "Ring Resonator Based Optical Add Drop Multiplexer Using Lithium Niobate on Insulator Channel Waveguides.", **13th International Conference on Fiber Optics and Photonics,** 2016. pp. W3A.15

[101] Songmuang S., Punthawanunt S., Mitatha S. and Yupapin P. P. "Multi Light Sources Enhancement Using Double PANDA Ring Resonators.", **2nd Int. Sci. Soc. Sci. Eng. Energy Conf. 2010 - SEEC 2010.,** vol. 8, Jan. 2011. pp. 451–458

[102] Soysouvanh S., Jalil M. A., Amiri I. S., Ali j., Singh G., Mitatha S., Yupapin P.P., Kenneth T V Grattan K. T. V. and Yoshida M. "Ultra-fast Electro-optic Switching Control Using a Soliton Pulse within a Modified Add-drop Multiplexer,". **Microsyst. Technol.,** vol. 24, no. 9, Sep. 2018. pp. 3777–3782

[103] Jalil M. A., Abdolkarim A., Saktioto T., Ong C. T. and Yupapin P. P. "Generation of THz Frequency Using PANDA Ring Resonator for THz Imaging.", **Int. J. Nanomedicine.,** vol. 7, 2012. pp. 773–779

[104] Amiri I. S., Alavi S. E., Idrus S. M., Nikoukar A. and Ali J. "IEEE 802.15.3c WPAN Standard Using Millimeter Optical Soliton Pulse Generated by a Panda Ring Resonator.", **IEEE Photonics J.,** vol. 5, no. 5, Oct. 2013. pp. 7901912–7901912

[105] Pornsuwancharoen N., Amiri I. S., Suhailin F. and Aziz M. S. “Micro-Current Source Generated by a WGM of Light Within a Stacked Silicon-Graphene-Au Waveguide.”, **IEEE Photonics Technol. Lett.,** vol. 29, 2017. pp. 1768–1771

[106] Ranjan S. and Mandal S. “Performance Analysis of Triple Asymmetrical Optical Multiple Ring Resonator with a 1 × 3 Input-output Waveguide for Application as an Optical Filter.”, **Appl. Opt.,** vol. 57, no. 9, Mar. 2018. pp. 2040–2049

[107] Bunruangses M., Youplao P., Amiri I. S., Pornsuwancharoen N. and Yupapin P.P. “Double Vision Model Using Space-Time Function Control within Silicon Microring System.”, **Silicon.,** Dec. 2019.

[108] Bunruangses M., Youplao P., Amiri I. S., Pornsuwancharoen N., Punthawanunt S., Singh G., Senior Member., IEEE. and Yupapin P. P. “Microring Distributed Sensors Using Space-Time Function Control.”, **IEEE Sens. J.,** vol. 20, no. 2, Jan. 2020. pp. 799–805

[109] Phongsanam P., Teeka C., Jomtarak R., Mitatha S. and Yupapin P.P. “All-optical Logic AND and OR Gates Generated by Dark–bright Soliton Conversion.”, **Opt. - Int. J. Light Electron Opt.,** vol. 124, Mar. 2013. pp. 406–410

[110] Yamazoe Y., Nishino T., Hamakawa Y. and Kariya T. “Bandgap Energy of InGaAsP Quaternary Alloy.”, **Jpn. J. Appl. Phys.,** vol. 19, no. 8, Aug. 1980. pp. 1473–1479

[111] Amiri I. S. “Dark-bright Solitons Conversion System for Secured and Long Distance Optical Communication.”, **IOSR J. Appl. Phys.,** vol. 2, no. 1, 2012. pp. 43–48

[112] Phatharaworamet T., Teeka C., Jomtarak R., Mitatha S. and Yupapin P.P. “Random Binary Code Generation Using Dark-bright Soliton Conversion Control within a PANDA Ring Resonator.”, **J. Light. Technol.,** vol. 28, no. 19, Oct. 2010. pp. 2804–2809

[113] Miyoshi Y., Ikeda K., Tobioka H., Inoue T., Namiki S. and Kitayama K. “Ultrafast All-optical Logic Gate Using a Nonlinear Optical Loop Mirror Based Multi-periodic Transfer Function.”, **Opt. Express.,** vol. 16, no. 4, Feb. 2008. pp. 2570–2577

[114] Threepak T., Mitatha S. and Yupapin P.P. “Novel All-optical Logic Gate Using an Add-drop Filter and Intensity Switch.”, **2010 3rd International Nanoelectronics Conference (INEC),** 2010. pp. 248–249

[115] Eiselt M., Pieper W. and Weber H. G. “SLALOM: Semiconductor Laser Amplifier in a Loop Mirror.”, **J. Light. Technol.,** vol. 13, no. 10, Oct. 1995. pp. 2099–2112

[116] Webb R. P., Yang X., Manning R. J. and Giller R. “All-optical 40 Gbit/s XOR Gate with Dual Ultrafast Nonlinear Interferometer.”, **Electron. Lett.,** vol. 41, no. 25, Dec. 2005. pp. 1396–1397

[117] Dong J., Zhang X., Xu J. and Huang D. “40Gb/s All-optical Logic NOR and OR Gates Using a Semiconductor Optical Amplifier: Experimental Demonstration and Theoretical Analysis.”, **Opt. Commun.,** vol. 281, no. 6, Mar. 2008. pp. 1710–1715

[118] Sobu Y., Shoji Y., Sakurai K. and Mizumoto T. “GaInAsP/InP MZI Waveguide Optical Isolator Integrated with Spot Size Converter.”, **Opt. Express**, vol. 21, 2013, pp. 15373-15381

[119] Le Minh Hoa, Ng Wai & Ngah R., “Terahertz Optical Asymmetric Demultiplexer Switch with a Symmetrical Switching Window”, **London Communications Symposium**., 2004.

[120] Bhattacharyya A., Gayen D. K. and Chattopadhyay T., “Design of 2-to-4 All-Optical Decoder with the Help of Terahertz Optical Asymmetric Demultiplexer”, **International Journal of Modern Nonlinear Theory and Application**, vol. 5, no. 1, Mar. 2016, pp. 67–72

Appendix A
LIST OF SYMBOLS

Symbol	Definition
α	Attenuation loss in fiber (dB/km)
β_1	Linear term coefficient of the propagation constant
β_2	Second-order terms coefficient of Taylor expansion of the propagation constant
χ^3	Third-order susceptibility
δ	Resonance bandwidth (FWHM)
ε_0	Vacuum permittivity
$\Phi(\phi)$	Phase contribution
Γ	Scale over which nonlinear effects make the beam becomes wider or narrower
γ	Coupling loss
κ	Coupling coefficient
λ_R	Resonant wavelength
τ_{sw}	Switching time
τ_{cav}	Photon lift time
τ	Soliton phase shift time
$f_R(v_R)$	Resonant frequency
ω_0	Soliton frequency shift

Appendix B
LIST OF PARAMETERS

Parameter	Definition
A	Soliton amplitude in one round trip
A_{eff}	Effective mode core area
c	Speed of light in vacuum (3×10^8 km/s)
E	Electric field
I	Optical intensity
k_n	Propagation number
m	Mode number
n_0	Linear refractive index
n_2	Nonlinear refractive index
n_{eff}	Effective refractive index
P	Optical power
R	Microring radius
r	Nanoring radius
L	Ring circumference
T	Propagation time in a round trip
T_0	Initial soliton pulse width

Appendix C
LIST OF PARAMETERS AND FORMULAS

Parameter	Formula
ON-OFF ratio	$ON - OFF\ ratio = \frac{T_{\max\,(Through)}}{T_{\min\,(Drop)}}$
Extinction Ratio	$ER(dB) = 10log\left(\frac{T^1_{min}}{T^0_{max}}\right)$
Contrast Ratio	$CR(dB) = 10log\left(\frac{T^1_{mean}}{T^0_{mean}}\right)$
Loss factor	$20log\left(\frac{I_{Output}}{I_{Input}}\right)$
Group refractive index	$n_{gr}=n_{eff}-\lambda\frac{dn_{eff}}{d\lambda}$
Full width at half maximum	$FWHM=\frac{\lambda^2}{Fn_{gr}L}$
Quality factor	$Q=\frac{f_c}{\Delta f}=\frac{\lambda_0}{\Delta\lambda}$
Finesse	$F=\frac{FSR}{\Delta\lambda}\approx\frac{2\pi}{\alpha L}$
Frequency	$f=\nu=\frac{1}{T}$
Wave propagation constant	$k_n=\frac{2\pi n_{eff}}{\lambda}$
Effective refractive index	$n_{eff}=n_0+n_2I=n_0+n_2\frac{P}{A_{eff}}$
Optical power	$P = \mathrm{A}_{eff}I$
Free spectral range of wavelength	$FSR_\lambda = \Delta\lambda\left\lvert-\frac{\lambda^2}{n_{gr}L}\right\rvert$
Free spectral range of frequency	$FSR_f = \Delta f\left\lvert\frac{c}{n_{gr}L}\right\rvert$
Propagation time (TH-port)	$T_{TH} = \frac{Ln_{eff}}{c}$
Propagation time (DR-port)	$T_{DR} = \frac{\left(L+\frac{L}{2}\right)n_{eff}}{c}$

Appendix D
LIST OF PUBLICATION

1. Soysouvanh S., Luangxaysana K., Phongsanam P., Mitatha S., Fukuhara M. and Yupapin P.P. “All-optical Switching in PANDA Ring Resonator by Carrier Injection.”, **The 34th JSST Annual Concerence: International Conference on Simulation Technology (JSST2015), At Toyama, Japan,** Oct, 2015.
2. Soysouvanh S., Mitatha S. and Juleang P. “Highly Secured Tunnel by Optical Crypto Carrier Transmission Using Ring Resonator System.”, **2017 14th International Conference on Electrical Engineering/Electronics, Computer, Tele-communications and Information Technology (ECTI-CON)**, 2017. pp. 198–201
3. Soysouvanh S., Phongsanam P., Mitatha S., Ali J., Yupapin P.P., Amiri I. S., Grattan K. T. V. and Yoshida M. “Ultrafast All-optical ALU Operation Using a Soliton Control within the Cascaded InGaAsP/InP Microring Circuits.”, **Microsyst. Technol.,** vol. 25, no. 2, Feb. 2019. pp. 431–440
4. Soysouvanh S., Jalil M. A., Amiri I. S., Ali J., Singh G., Mitatha S., Yupapin P. P., Grattan K. T. V. and Yoshida M. “Ultra-fast electro-optic switching control using a soliton pulse within a modified add-drop multiplexer”, **Microsyst. Technol.**, vol. 24, no. 9, Sep, 2018. pp. 3777-3782

BIOGRAPHY

Name	Mr. Saysamone Soysouvanh
Date of Birth	08 October 1989
Born	Vientiane, LAO PDR
Current Address	Faculty of Engineering, National University of Lao, Vientiane, Lao PDR
Education	- Bachelor's degree in computer engineering, Faculty of Engineering, National University of Lao, Vientiane, Lao PDR in 2010 - Master's degree in computer and information engineering, International College, King Mongkut's Institute of Technology Ladkabang, Thailand, in 2012
Skilled Works	- Digital signal processing - Optical logic and arithmetic